Adaptive Filtering and Control for an ASVC

Devon Veronica Evelyn Yates

Kongens Lyngby 2005
IMM-MSC-68

IMM

Technical University of Denmark
Informatics and Mathematical Modelling
Building 321, DK-2800 Kongens Lyngby, Denmark
Phone +45 45253351, Fax +45 45882673
reception@imm.dtu.dk
www.imm.dtu.dk

Acknowledgements

Dedicated to my dearest Morten, who has taught me, inspired me, and supported me throughout my time in Denmark. Thanks to my three parents, who have made my life possible and continue to fill it with possibility. To my advisor Niels Kjœlstad Poulsen who's clear insight and guidance have been indispensable to me. To my other advisor, Tonny Rasmussen, whose encyclopedic knowledge of ASVC's and help in setting up the measurements were integral to the project. Also thanks to Henrik Madsen, Knud Ole Helgesen Pedersen, Kurt Hansen, John Eli Nielsen and all of my colleagues and professors the wind energy department of DTU. Finally, thank you to Denmark, for making this education accessible for people all over the world, and for having such nice police officers.

Devon Yates,
IMM, September 5, 2005.

Abstract

Stability and efficiency in the electrical grid is very dependent on fluctuations in reactive power which may be caused by wind turbines, transformers, generators, motors, and capacitor-reactor banks. Control of these variations can be accomplished by using advanced static var compensators(ASVC). ASVC are capable of compensating for variation in the reactive power load, but are disrupted when harmonics are present in the system. Filtering to remove these harmonics, but introduce a lag into the control system. Suboptimal control of compensation can result in high losses and voltage fluctuations, and may cause the ASVC to go offline during disturbances.

A description of the noise in the grid has been determined using time series analysis methods with measured data from the grid. This model has been used to design a stochastic adaptive filtering system which can quickly recognize and react to actual phase shifts, thereby improving the quality and speed of the compensation, while remaining impervious to harmonic distortion. This adaptive filter has been implemented in a integral control system with gain scheduling. A mean model of an ASVC is developed, as well as a switched model, and the control strategy is tested upon it.

KEYWORDS: ASVC, STATCOM, FACTS,Reactive Power, Harmonic Filter, Adaptive Estimation, Stochastic Estimation, Harmonic Estimation, Wind Turbine, Synchronization, Symmetrical Components.

Contents

List of Symbols

PCC	Point of Common Coupling
C	Inverter capacitor
L	Inverter inductor
R_c	Copper and core losses in inductor
R_s	Switching losses in inverter
R_l	Equivalent grid resistance
L_l	Equivalent grid impedance
L_m	Impedance used in lab measurements
R_p	Switched resistance in lab measurements
C_{nl}	Capacitor in nonlinear load in lab measurements
R_{nl}	Resistance in nonlinear load in lab measurements
ϕ	Power factor
E	Voltage across inverter capacitor
I	Current in inverter capacitor and resistor
e_a, e_b, e_c	Phase voltages of the grid at the PCC
v_a, v_b, v_c	Phase voltages at inverter output
$\theta_a, \theta_b, \theta_c$	Angles between the three grid voltage phases
θ	Phase angle of the grid voltage
ϕ	Angle between the current and voltage at the PCC
V	Voltage across ASVC inductance
i_a, i_b, i_c	Phase current through the inverter inductors
i_α,i_β	Single phase representation of current through inverter inductors
i_d, i_q	Direct and quadrature current through the inverter inductors
e_d, e_q	Direct and quadrature voltage at PCC
v_d, v_q	Direct and quadrature voltage at inverter output
i_G	Current from the grid source
i_L	Current into the consumer load
ω	Measured grid frequency
$\hat{x}$	unit vector
S	Logical state of inverter switches
y	Estimated Grid Voltage
y_0	Filtered grid voltage
θ_0	Filtered grid voltage phase angle
ω_0	Estimated grid frequency
k_{dq}	dq Current in reference to filtered voltage

Chapter 1

Introduction

Reactive power occurs when reactive elements, such as capacitors, inductors, transformers and motors, are connected to the grid. These elements cause current to flow which is out of phase with the fundamental grid current. Reactive current is a concern, because it increases losses in transmission lines without increasing the usable power. It also is a source of instability in the grid, and if the percentage of reactive power become too large, it can lead to instability and even black outs.

In Figure 1.1, the voltage variations for different loading of the system modelled in this project are plotted. This is done for different power factors, ϕ, which correspond to the reactive component in the lines. The maximum power reached by the curve is known as the critical point, because after this point, the voltage drops. Thus it is seen that the power factor is a clear indicator of the strength of the grid. Also, with increasing ϕ, the gradient of the PV curve increases, causing power fluctuations to create larger voltage fluctuations.

Reactive power is a relevant topic for the wind power industry because wind turbines consume reactive power, while also producing variable amounts of active power. This combination could easily lead to fluctuation of the voltage near wind parks, particularly since wind parks tend to be located in areas where the grid is not particularly stiff. However, this potential problem has been confronted by the wind industry by installation of reactive power compensation and the development of asynchronous generators, which can actively compensate reactive power. This has lead to a situation where wind parks are actually becoming a stabilizing force in weak areas of the grid, rather than a disturbance. At this point, utilities which have significant wind power production are considering requirements that wind plants should be able to ride through significant

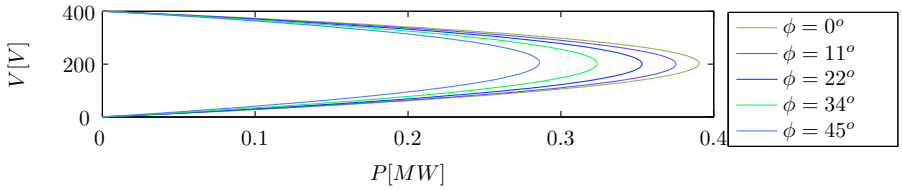

Figure 1.1: *PV curve at different power factors*

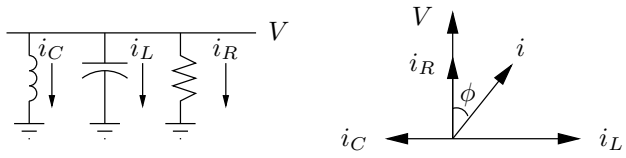

Figure 1.2: *Phasor Diagram of active and reactive currents*

power events, and even act in island mode to help reinstate the grid in the case of failure. Both of these requirements will depend on the ability of reactive power controllers to act quickly and effectively, while remaining insensitive to disturbances in the grid.

1.1 Controlling Reactive Power

Reactive elements are an integral part of the electrical system, so it is not reasonable to remove them. In order to control the amount of reactive power in the lines, it is necessary to compensate the reactive power near the site of the source. Switched capacitor banks are often used for this purpose, because they produce reactive power, while transformers and motors are said to consume reactive power. In some cases, switched inductor banks are used to compensate for the reactive power produced by the capacitance resulting from underground cables.

Capacitor and reactor banks only produce a constant step value of reactive power, and thus power electronics systems have been developed to dynamically compensate for the variation in the grid. Basically, these compensators use an inverter to control the phase of the current which the compensator injects into the grid. This current is controlled by controlling the voltage across a leakage inductance between the compensator and the grid. In this way, it is possible to cancel out the reactive current flowing in the lines. These systems are known as STATCOMs, static compensators, or VSC, (Var Static Compensators).

The voltage source used to provide the reactive current, is usually either a DC link capacitor, or a HVDC (High Voltage Direct Current) voltage source inverter. For this project, only systems using a DC link capacitor are considered. The capacitor is charged by the rectified current from the grid, and this DC voltage is then output using PWM (Pulse Width Modulation), to create the output voltage.

When IGBT's (Insulated Gate Bipolar Transistors) are used as switching elements, a STATCOM is called an ASVC, or Advanced Static Var Compensator. IGBT's are high power switching elements, which have the capability of turning on and off much quicker than previously used high power switching technology. This allows the possibility of controlling the reactive power relatively quickly, as well as both providing and consuming reactive power.

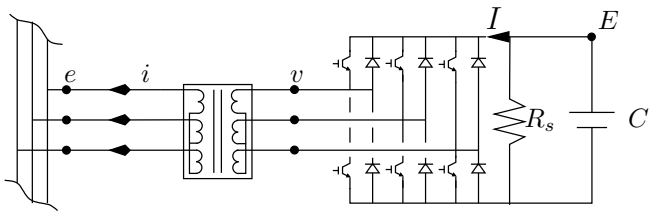

Figure 1.3: *ASVC topography*

However, there are a few challenges to be overcome in control of reactive power compensators. The first comes as a result of the use of a capacitor as the DC source. This introduces a nonlinearity into the system, which will be discussed in more detail later in the report. Another nonlinearity is caused by the switching elements, specifically for control of the capacitor voltage. For slow control of the ASVC, this can be neglected, and a mean model of the system can be used, but for faster control, it can be problematic.

Another problem is caused by what is effectively measurement noise in the grid. There are many harmonics present in the grid, which are carried through in the calculation of the required reactive power compensation. It is possible to use a filter to remove these harmonics, but this causes a phase delay in voltage. This delay is particularly notable during phase shifts, when the information about the phase change can cause incorrect calculation of the current references, and can take half a cycle to recover from. It is difficult to compensate for this because the the frequency of the grid is varying. In the classical control of SVC, the presence of harmonic components in the reference signal can lead to problematic oscillations in the capacitor voltage, which can cause the lights to flicker at nearby power outlets.

In this report, state space control is used to develop a controller which approaches optimal control of the nonlinear system of an ASVC. Measurements of the electrical grid in Denmark are taken, to provide information about the harmonic distortion. A system to estimate the fundamental frequency, phase, and harmonic components dynamically with time is used as a filter for measurement of voltage magnitude and phase at the point of common coupling (PCC). A simulation of the implementation of the control system into an electrical grid is developed using Matlab©Simulink and SimPowerSystems.

Chapter 2

Simulation

2.1 Single Phase

If we look at a single phase of the ASVC, as shown in figure 2.1, we can try to understand the fundamental characteristics of the system. First we can look at the situation where switch s_1 is closed. In this case, $v = E$, and Ohms law across the inductor and resistor gives,

$$\frac{di}{dt} = \frac{1}{L}(e - E - iR_c) \tag{2.1}$$

Across the capacitor and switching resistance, the voltage is described by,

$$\frac{dE}{dt} = \frac{i}{C} - \frac{E}{R_s C} \tag{2.2}$$

When s_1 goes open, and s_2 closes, the current, i initially remains the same, because of the inductance, while the inverter voltage, v is changed to, $-E$. If a logical vector S is chosen so that $S = 1$ when s_1 is closed, and $S = -1$ when s_2 is closed, the system can be represented in state space form as,

$$\begin{bmatrix} \dot{i} \\ \dot{E} \end{bmatrix} = \begin{bmatrix} -\frac{R_c}{L} & \frac{S}{L_S} \\ \frac{1}{C} & -\frac{S}{R_s C} \end{bmatrix} \begin{bmatrix} i \\ E \end{bmatrix} + \begin{bmatrix} \frac{1}{L} \\ 0 \end{bmatrix} e \tag{2.3}$$

Thus, for one phase, switching allows the output voltage to be set to $\pm E$ or zero. The capacitor is charged by the current through the inductor, which is in turn controlled by the switched voltage.

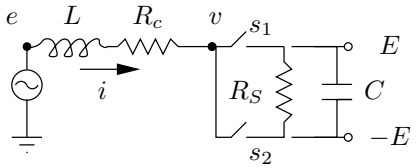

Figure 2.1: *A single phase of the system*

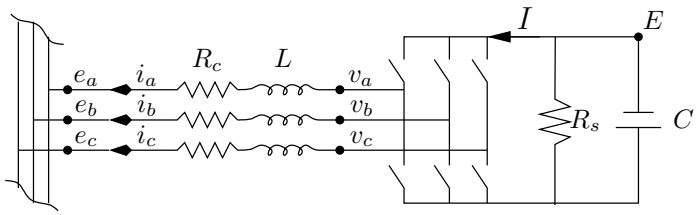

Figure 2.2: *Equivalent Circuit for STATCOM*

2.2 Three Phase Analysis

In order to analyze three phase systems, several transformations are used to simplify the system, discussed in detail in appendix A. The Clark transformation is used to express a three phase variable, X_{abc}, as a two dimensional rotating vector with a zero component, $X_{\alpha\beta 0}$. The Park transformation is composed of a two dimensional frame, which rotates at the same speed as the vector, $X_{\alpha\beta 0}$, resulting in a constant direct and quadrature vector, X_{dq0}. The phase of the rotating axis is determined using a PLL (Phase Lock Loop) on the voltage at the PCC. If the phase is defined as,

$$\theta = \arctan\left(\frac{e_\beta}{e_\alpha}\right), \tag{2.4}$$

then the reference frame has been chosen such that the quadrature voltage, e_q, becomes zero[1].

For a given voltage, u, and current, i, the definitions of active and reactive power are, respectively,

$$P = \frac{3}{2}(u_d i_d + u_q i_q) \tag{2.5}$$

$$Q = \frac{3}{2}(u_d i_q + u_q i_d) \tag{2.6}$$

If the reference frame has been chosen such that e_q is zero, the active and reactive power are a function of e_d and the active and reactive current, respectively. However, for the ASVC, the output v_q is not zero, in most cases, so the active and reactive power will be functions of both i_d and i_q.

2.3 Mean Model

An equivalent circuit for the STATCOM is shown in Figure 2.2. The PWM and IGBTs are replaced by ideal switches, where the switching losses are modelled

[1]The function for arctan should be one which determines the angle quadrant using the signs of the two input voltages, in Matlab, atan2

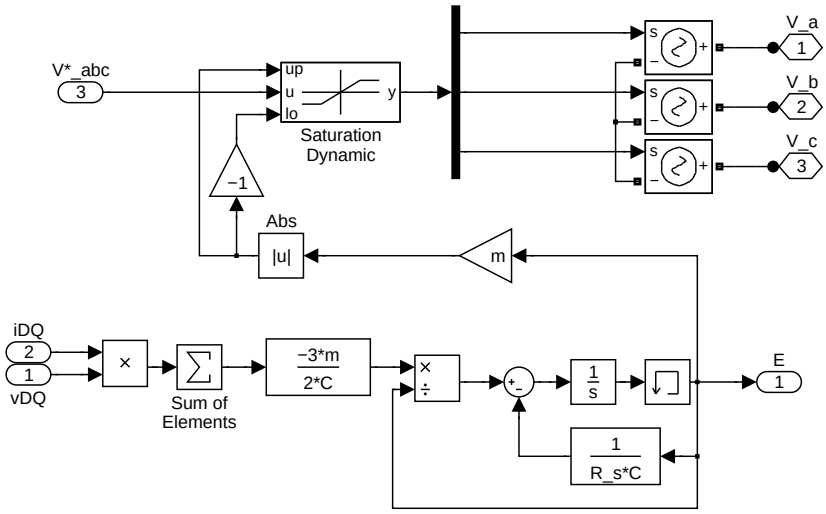

Figure 2.3: *Simulink mean model of ASVC*

by a resistor, R_s, parallel to the switching elements. The conducting losses are modelled by another resistor, R_c, at the output of the inverter.

In order to create a simulation which can run quickly, a mean model has been used to develop the control. The Simulink diagram is shown in Figure 2.3. Essentially, the PWM of the inverter is modelled as a voltage source, thereby avoiding the nonlinearities involved in switching. The capacitor is modelled by an integrator, with an equivalent modulation factor, m, and a parallel average resistance, R_s.

$$\frac{dE}{dt} = -\frac{3m}{2CE}\left(v_d i_d + v_q i_q\right) - \frac{E}{R_s C} \tag{2.7}$$

This equation is derived in section 3.2. In reality, the values that the output voltage, v, can attain, are limited by the value of the dc link voltage,E, multiplied by the modulation factor, E, so a dynamic limiter is included. This is generally not an issue, except for when the system is already in trouble. Additionally, a memory block is included for the inverter voltage output, to remove algebraic loops.

2.4 Disturbance Model

The reactive current characteristics of a site are assumed to be described sufficiently by a 400V voltage source with an equivalent impedance and variable reactive load, as shown in figure 2.4 on the following page. A reactive load, rather than impedance, is chosen because many consumer elements will use switching

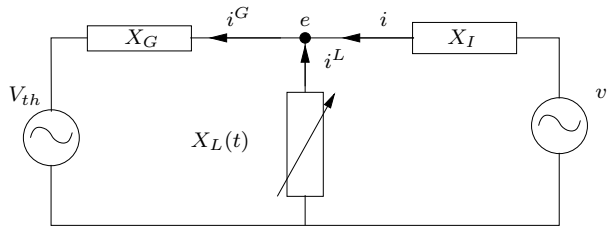

Figure 2.4: *Equivalent diagram of transmission network*

to maintain a constant power consumption, regardless of voltage at the source. Unless otherwise noted, the consumer reactive power disturbance given is a step change in the reactive power consumption from $Q = 0$ to $Q = 50kVar$ at 0.05s, to $Q = -50kVar$ at 0.1 s, and back to $Q = 0$ at 0.15s. This is a step of half of the rated reactive power for this system. The active consumer load is a constant, $P = 500$ kW. The line impedance is 10 mH, and the line resistance is 0.01 Ω.

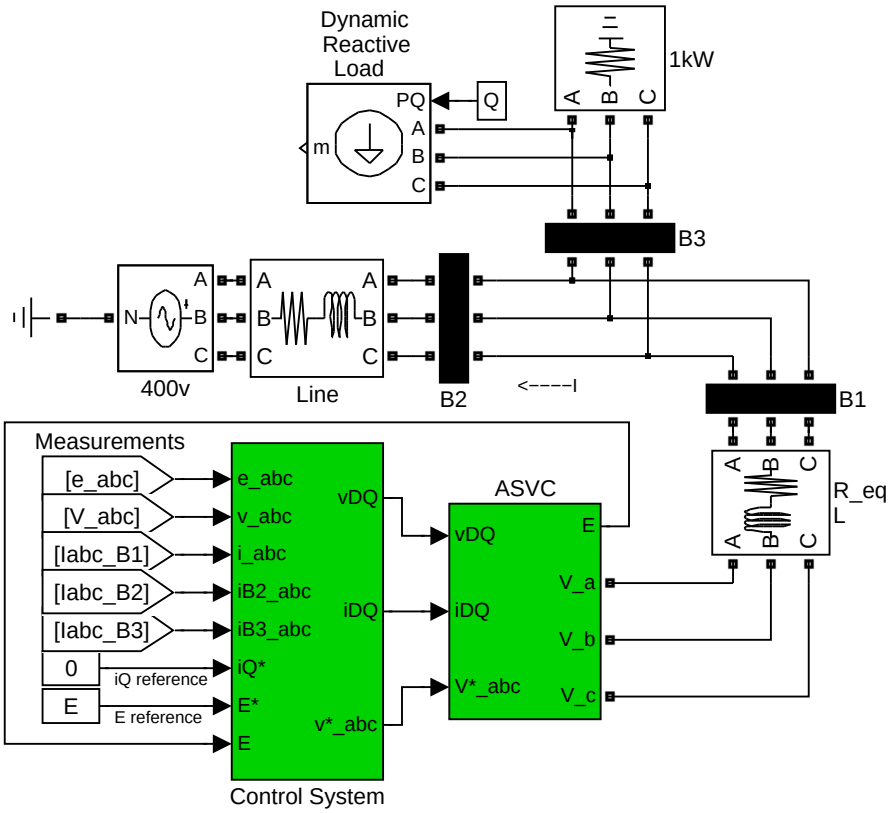

Figure 2.5: *Simulink Model of Grid*

Chapter 3

Control

3.1 Vector Control

Vector control is a standard method of controlling ASVC's. The vector control system consists of two loops, one of which controls the reactive current, while the other controls the DC capacitor voltage. This is done by creating a linear mean model of the inverter, and neglecting harmonics, switching losses and losses in the inductor. This system works surprisingly well, generally reacting to a step input within one 50 Hz cycle. The layout of the control is shown in Figure 3.1 on the next page. The system has effectively been reduced to two separate PI loops, which don't disturb each other too much, though there is some interdependence. The voltage of the capacitor is actually a nonlinear function, as seen in (2.7), but in this control method, it is linearized by assuming that the power in the capacitor is only a function of the direct voltage at the grid and direct current out of the inverter. The quadrature terms have disappeared in this equation, because the grid voltage is the reference for the transformation.

$$EI = \frac{3}{2} v_d i_d \tag{3.1}$$

The ratio of the capacitor and output voltages are expressed in the literature as a function of an average modulation factor, m, and are phase to phase values, leading to an expression for the current entering the capacitor [13].

$$v_d = \frac{m}{2\sqrt{2}} E \tag{3.2}$$

$$I = \frac{3m}{2\sqrt{2}} i_d \tag{3.3}$$

The differential equation for the capacitor is,

$$I = -C\frac{dE}{dt} \tag{3.4}$$

Therefore, in terms of the phase and quadrature components, the transfer function for the mean capacitor voltage can be found by combining equations (3.4) and (3.3).

$$\frac{E}{i_d} = -\frac{3m}{2\sqrt{2}Cs} \tag{3.5}$$

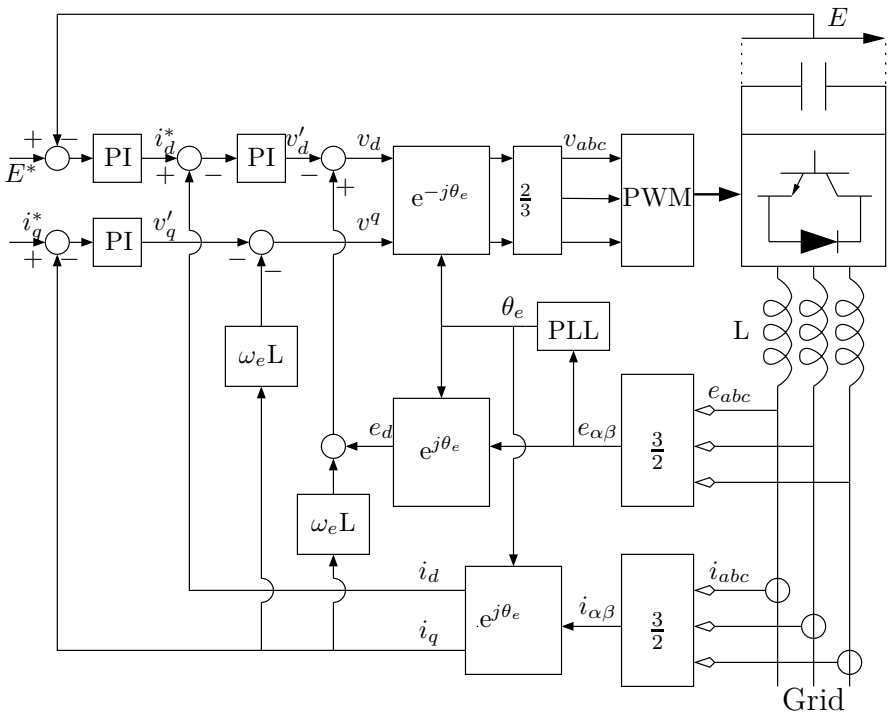

Figure 3.1: *Classical control diagram*

For the direct and quadrature current control, the transfer functions are,

$$\mathrm{F(s)} = \frac{i_d(\mathrm{s})}{e_d'(\mathrm{s})} \tag{3.6}$$

$$= \frac{i_q(\mathrm{s})}{e_q'(\mathrm{s})} \tag{3.7}$$

$$= \frac{1}{L\mathrm{s} + R} \tag{3.8}$$

The reference values for the inverter, are then determined by including the offset of the voltage at the point of common coupling, and the frequency terms resulting from the park transform.

$$v_d^* = -e_d' + \omega L i_q + e_d \tag{3.9}$$

$$v_d^* = -e_q' - \omega L i_d \tag{3.10}$$

As a baseline, a mean model of the the classical control system has been simulated using Matlab Simulink with the Power Systems toolbox. The control parameters are shown in Table 3.1 on page 14. The state response to a step

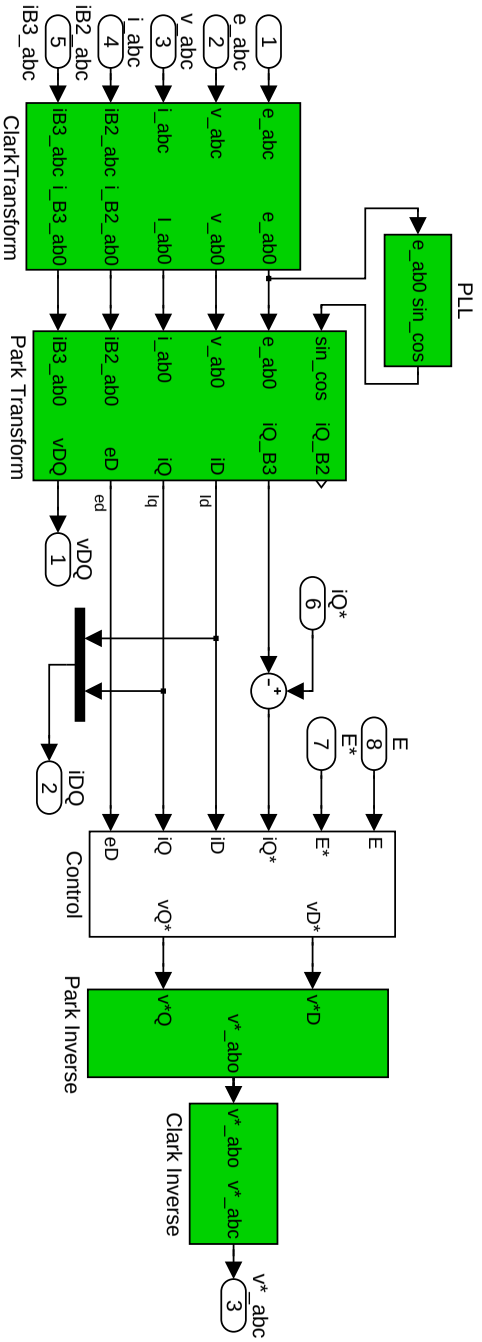

Figure 3.2: *Control block of Simulink model*

Current Control				DC Voltage Control			
ξ	ω	K	a	ξ	ω	K	a
0.7	500	-1.8	319.7	0.7	100	71.42	-0.064

Table 3.1: *Control Parameters for Vector Control*

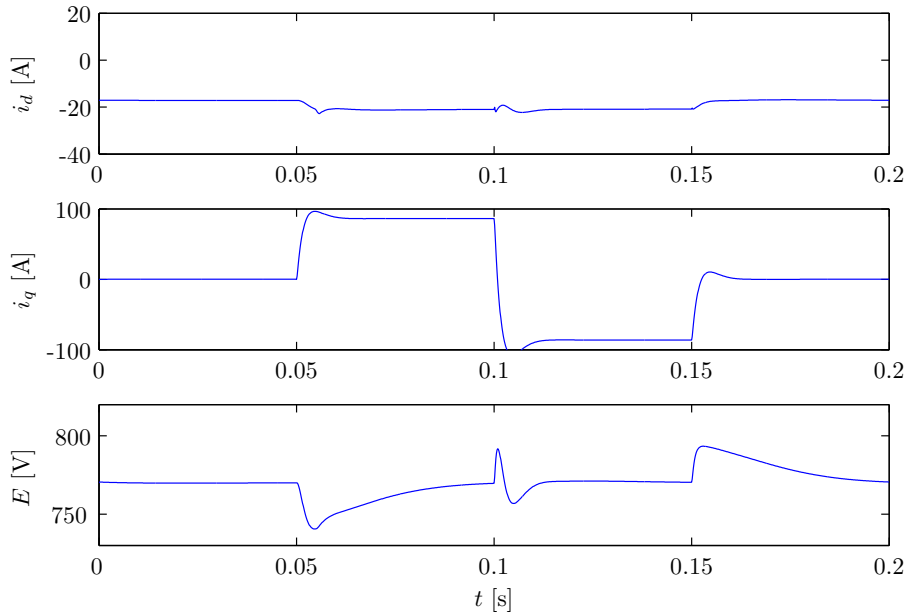

Figure 3.3: *State variation for vector control*

input in reactive load is shown in Figure 3.3. The inverter set-point voltages are shown in Figure 3.4 on the facing page. The grid voltage, reactive current into the grid, and comparison of inverter and load reactive current are shown in Figure 3.5 on the next page.

Additionally, the AC current and voltage across the inductor are shown in Figure 3.6 on page 16. This is useful for understanding how the ASVC works, as the inverter voltage chances in relation to the grid voltage, depending on the reactive load. Looking at the current through the inductor, it can be seen that the current changes its amplitude during the reactive power step changes. Note that the current is not zero when the reactive load is zero, due to losses in the converter, this also contributes to some phase change in the current during step inputs.

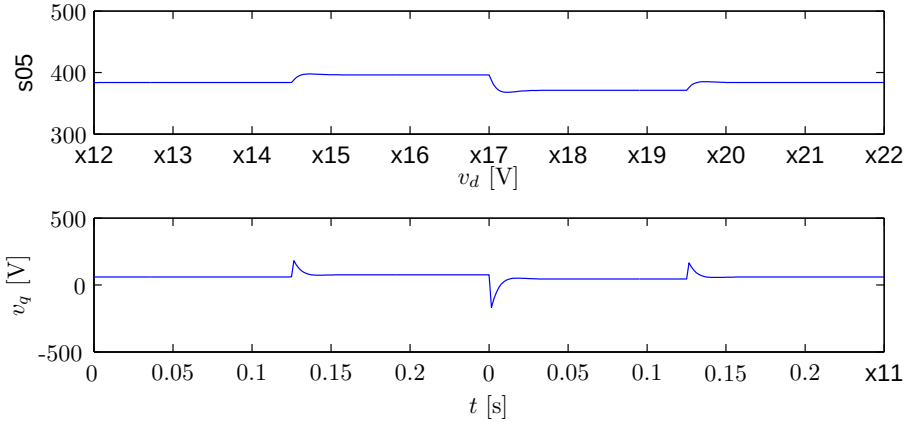

Figure 3.4: *Output voltage for vector control*

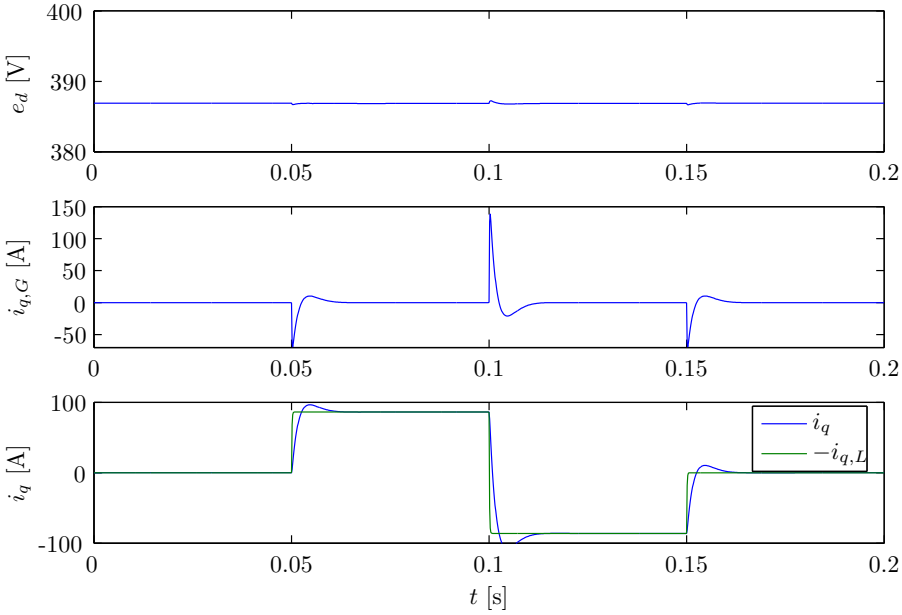

Figure 3.5: *Grid voltage and reactive currents for vector control*

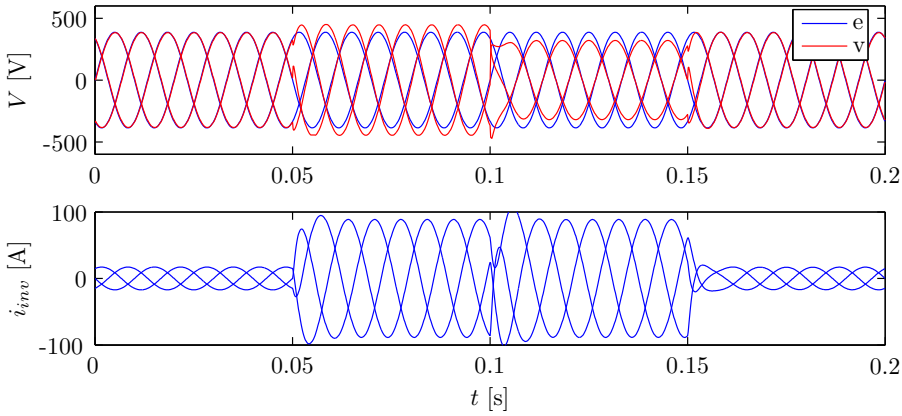

Figure 3.6: *AC voltage and current for vector control*

3.2 State Space Control

In order to design advanced control algorithms for a STATCOM, it is useful to formulate the system as a state space model. This allows the designer to maintain a holistic view over the system, rather than the classical approach of using two separate loops. It also facilitates the use of optimization algorithms in control design. This method formulates the system as a set of matrices, $\boldsymbol{A}$, $\boldsymbol{B}$, $\boldsymbol{C}$, and $\boldsymbol{D}$, such that,

$$\dot{\boldsymbol{x}} = \boldsymbol{A}\boldsymbol{x} + \boldsymbol{B}\boldsymbol{u} \tag{3.11}$$

$$\dot{\boldsymbol{y}} = \boldsymbol{C}\boldsymbol{x} + \boldsymbol{D}\boldsymbol{u} \tag{3.12}$$

Where $\boldsymbol{x}$ is the state vector, $\boldsymbol{u}$ is the input, or control, vector, and $\boldsymbol{y}$ is the output.

The voltage equation at the output of the inverter reactors is:

$$\frac{d}{dt}\begin{bmatrix} i_a \\ i_b \\ i_c \end{bmatrix} = -\frac{R_c}{L}\begin{bmatrix} i_a \\ i_b \\ i_c \end{bmatrix} + \frac{1}{L}\begin{bmatrix} v_a - e_a \\ v_b - e_b \\ v_c - e_c \end{bmatrix} \tag{3.13}$$

The system can be transformed into the d-q reference frame,

$$\frac{d}{dt}\begin{bmatrix} i_d \\ i_q \end{bmatrix} = \begin{bmatrix} -\frac{R_c}{L} & -\omega \\ \omega & -\frac{R_c}{L} \end{bmatrix}\begin{bmatrix} i_d \\ i_q \end{bmatrix} + \frac{1}{L}\begin{bmatrix} v_d - e_d \\ v_q - e_q \end{bmatrix} \tag{3.14}$$

The frequency, ω, is the rate at which the d-q frame is rotating. This is generally equal to the fundamental frequency of the grid but may differ when the PLL is not locked in. When the PLL is correctly locked in, the quadrature voltage at the grid should be zero, by definition, but without that assumption it is possible that there will be a quadrature component.

The inverter voltages are a nonlinear function of the angle, ϕ, by which the inverter voltage is required to lead the line voltage. The relative magnitude of the inverter voltages is given by the modulation factor, m. A simple way to express this is demonstrated in [17],

$$\begin{aligned} v_d &= mE\cos\phi \\ v_q &= mE\sin\phi \end{aligned} \tag{3.15}$$

The dc voltage in the capacitor is determined by,

$$\frac{dE}{dt} = -\frac{1}{C}\left(I + \frac{E}{R_s}\right) \tag{3.16}$$

Where I can be determined by using the inverter voltage description (3.2), and the instantaneous power equation,

$$P = EI = \frac{3}{2}(v_d i_d + v_q i_q) \tag{3.17}$$

A state space representation can be formulated by defining the state, input, and disturbance vectors below, and using equations, (3.14),(3.2), and (3.17).

$$\boldsymbol{x} = \begin{bmatrix} i_d \\ i_q \\ E \end{bmatrix} \quad \boldsymbol{u} = \begin{bmatrix} v_d \\ v_q \end{bmatrix} \quad \boldsymbol{v} = \begin{bmatrix} e_d \\ e_q \end{bmatrix} \tag{3.18}$$

The system can be represented as,

$$\dot{\boldsymbol{x}} = f(x,u,v) = \begin{bmatrix} -\frac{R_c}{L} i_d - \omega i_q + \frac{1}{L} v_d \\ +\omega i_d - \frac{R_c}{L} i_q + \frac{1}{L} v_q \\ -\frac{3}{2CE}\left(v_d i_d + v_q i_q\right) - \frac{E}{R_s C} \end{bmatrix} + \begin{bmatrix} -\frac{1}{L} & 0 \\ 0 & -\frac{1}{L} \\ 0 & 0 \end{bmatrix} \begin{bmatrix} e_d \\ e_q \end{bmatrix} \tag{3.19}$$

The third row in the system matrix is not linear, so a linearization must be performed, resulting in,

$$\begin{aligned} \frac{d}{dt}\begin{bmatrix} \Delta i_d \\ \Delta i_q \\ \Delta E \end{bmatrix} = &\begin{bmatrix} \frac{-R_c}{L} & -\omega_0 & 0 \\ \omega_0 & \frac{-R_c}{L} & 0 \\ -\frac{3v_{d0}}{2CE_0} & -\frac{3v_{q0}}{2CE_0} & \frac{3}{2CE_0^2}\left(v_{d0}i_{d0} + v_{q0}i_{q0}\right) - \frac{1}{R_s C} \end{bmatrix} \begin{bmatrix} \Delta i_d \\ \Delta i_q \\ \Delta E \end{bmatrix} \\ &+ \begin{bmatrix} \frac{1}{L} & 0 \\ 0 & \frac{1}{L} \\ -\frac{3i_{d0}}{2CE_0} & -\frac{3i_{q0}}{2CE_0} \end{bmatrix} \begin{bmatrix} \Delta v_d \\ \Delta v_q \end{bmatrix} + \begin{bmatrix} -\frac{1}{L} & 0 \\ 0 & -\frac{1}{L} \\ 0 & 0 \end{bmatrix} \begin{bmatrix} \Delta e_d \\ \Delta e_q \end{bmatrix} \end{aligned} \tag{3.20}$$

For a linearized system, the states are observed as perturbations from the steady state values at the point of linearization. This results in,

$$\delta\dot{\boldsymbol{x}} = \boldsymbol{F}\delta\boldsymbol{x} + \boldsymbol{G}\delta\boldsymbol{u} \tag{3.21}$$

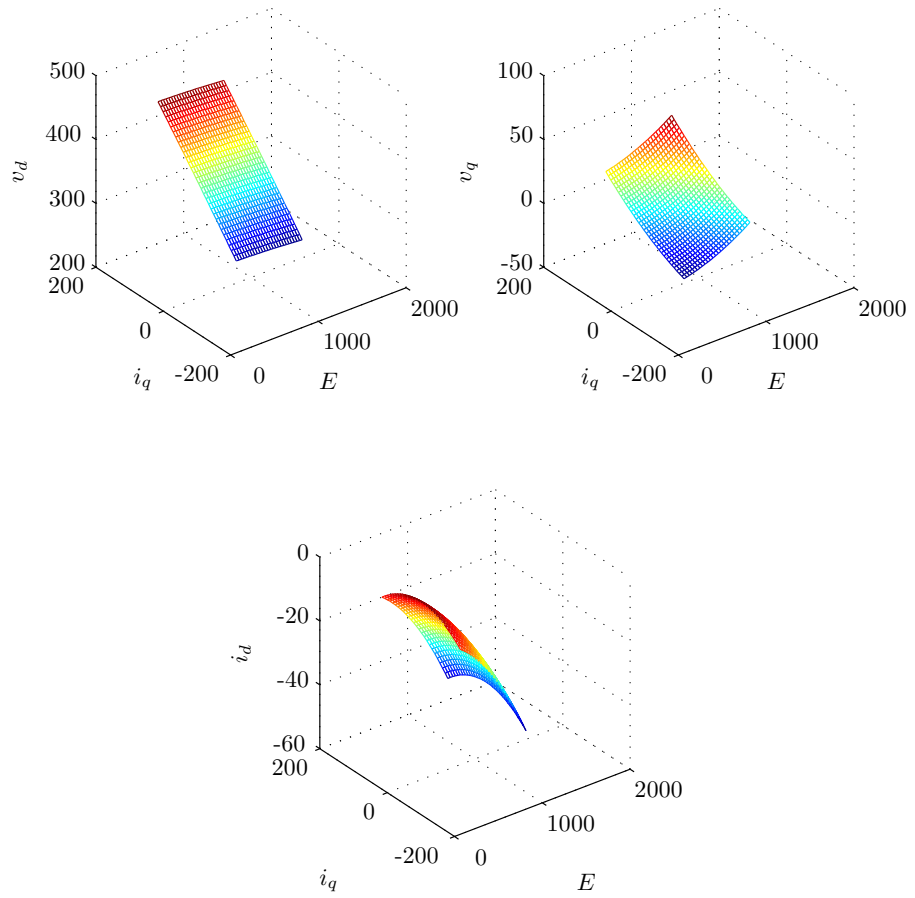

Figure 3.7: *Variation of steady state conditions with changing i_Q and E*

Where F and G are the matrices from equation (3.20). The steady state values can be determined by solving equation (3.19) for $\dot{\boldsymbol{X}} = 0$, for a given e_d, e_q, E, and i_q. This can be accomplished numerically using the Newton-Raphson method, where

$$x_{i+1} = x_i - H^{-1} f \tag{3.22}$$

$$x = \begin{bmatrix} v_d \\ v_q \\ i_d \end{bmatrix}, \; H = \frac{\delta f}{\delta x} = \begin{bmatrix} \frac{1}{L} & 0 & -\frac{R_c}{L} \\ 0 & \frac{1}{L} & \omega \\ -\frac{3i_d}{2CE} & -\frac{3i_q}{2CE} & -\frac{3v_d}{2CE} \end{bmatrix}$$

Now, for a required $\boldsymbol{y}$, we can determine an optimal feedback gain, $\boldsymbol{K}$, which modifies the steady state control input, r_0, keeping in mind that the states are

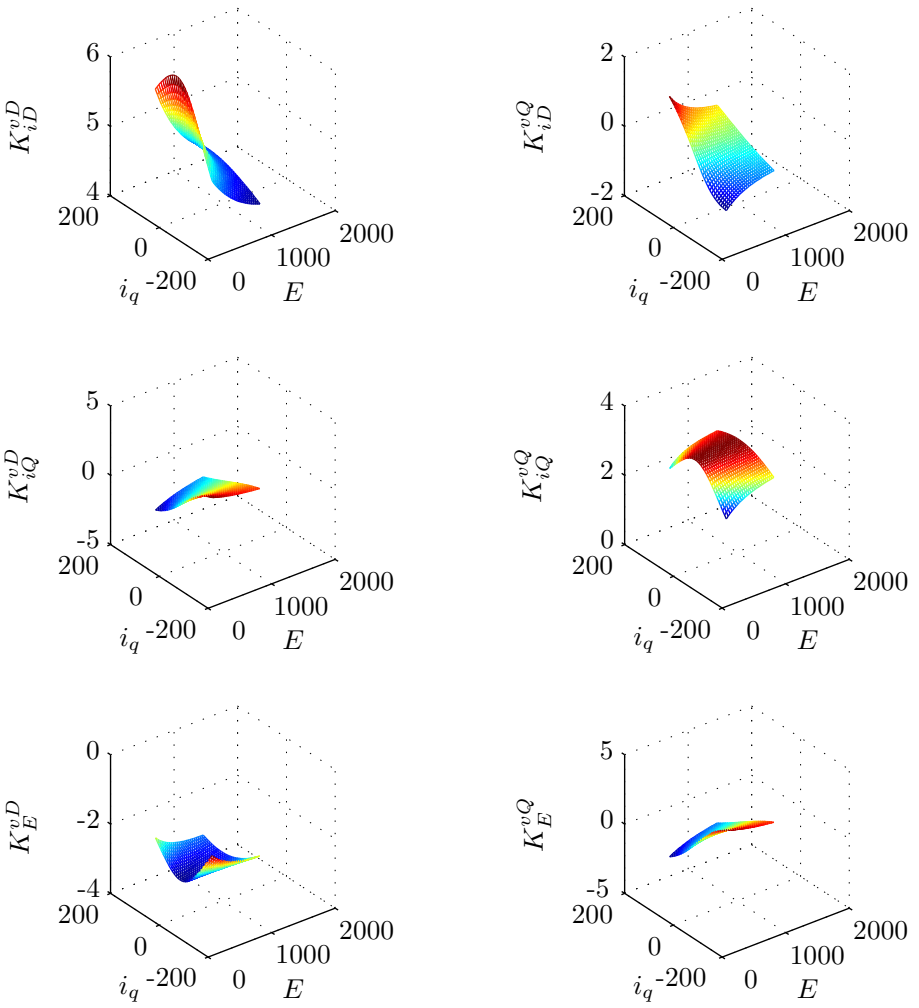

Figure 3.8: *Optimal gain matrix for varying i_Q and E*

now perturbations from the linearization point.

$$\boldsymbol{u} = \boldsymbol{u_0} + \boldsymbol{K}(x_0)\boldsymbol{x_0} - \boldsymbol{K}(x)\boldsymbol{x} \tag{3.23}$$

The optimal gain is found by minimizing the cost function,

$$J(u) = \int_0^\infty \delta\boldsymbol{x}^T\boldsymbol{Q}\delta\boldsymbol{x} + \delta\boldsymbol{u}^T\boldsymbol{R}\delta\boldsymbol{u} \tag{3.24}$$

where $\boldsymbol{Q}$ and $\boldsymbol{R}$ are weights on the state and input vectors, respectively. The variation of the operating points with respect to i_Q and E is shown in Figure 3.7 on page 18.

The weights used for this system were simply,

$$\boldsymbol{Q} = \begin{bmatrix} 1 & 0 & 0 \\ 0 & 1 & 0 \\ 0 & 0 & 1 \end{bmatrix} \quad \boldsymbol{R} = \begin{bmatrix} 0.1 & 0 \\ 0 & 0.1 \end{bmatrix} \tag{3.25}$$

This allows us to design a control system around the range of operating points. During operation, this "gain schedule" can be used to change the gain appropriately for the operating point in question, without using too much computing time. It can be seen in figure 3.8 on the preceding page, that the gain components vary in response to changes in i_Q and E.

It is important to note that some of the gains go from positive to negative, which could have an effect on the stability of the system. The dependence on E is not particularly strong in the normal operating range. It has most variation when E approaches zero, because of the inverse term in its differential equation. However, in actual operation, this is a time when the control is not really operating normally, as the modulation factor is saturated. The variation in E is included in the gain scheduling for this project, but may not be desirable in practice.

3.2.1 Simulation

The gain scheduling control is implemented in the grid model as shown in Figure 3.9. The control objective in this system is to minimize the reactive current flow in the grid. In this case, the objective is achieved by setting the reactive current output of the STATCOM to balance the demand from the load.

The output of the gain scheduling control is a inverter voltage which has been developed using an assumed grid voltage. In order to correct for any error in this assumption, or variation in the grid, the difference between the assumed voltage and measured voltage is added to the output voltages of the inverter.

For a step input the input states and output voltages are shown in Figures 3.10, 3.11, and 3.12. The variation of the gain is shown in Figure 3.13 on page 23. This system has no feedback, but the actual output is near to the actual required output. This shows that the model is correct, at least for the

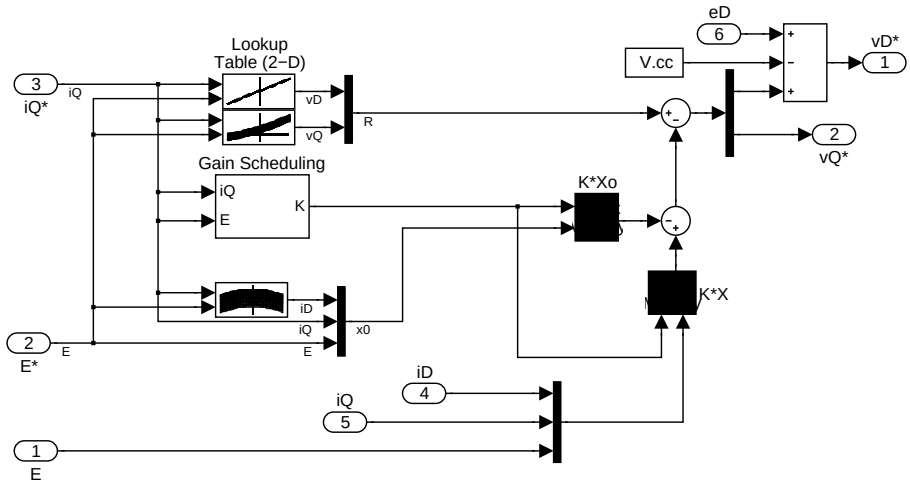

Figure 3.9: *Simulink gain scheduling control block*

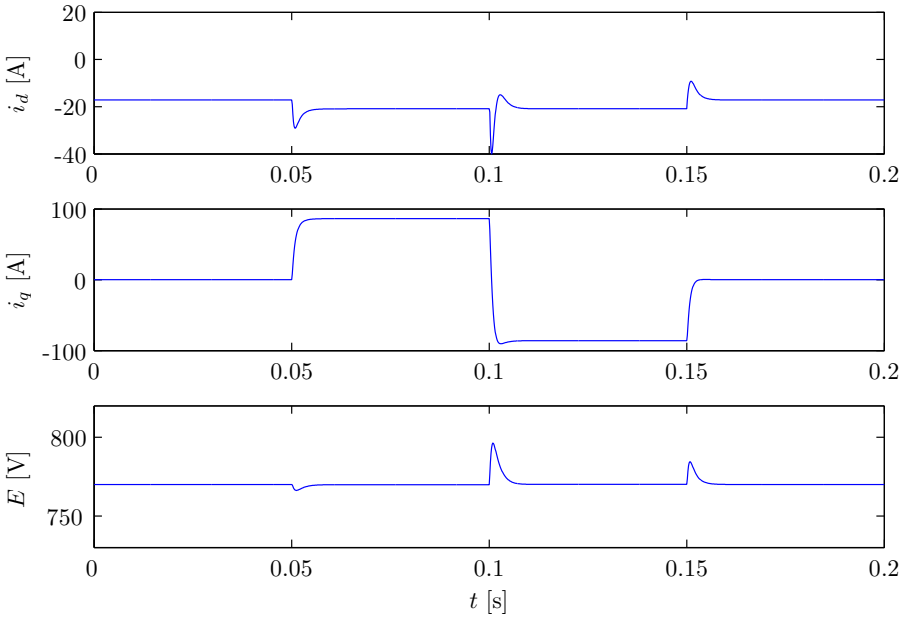

Figure 3.10: *State variation for state space control with gain scheduling*

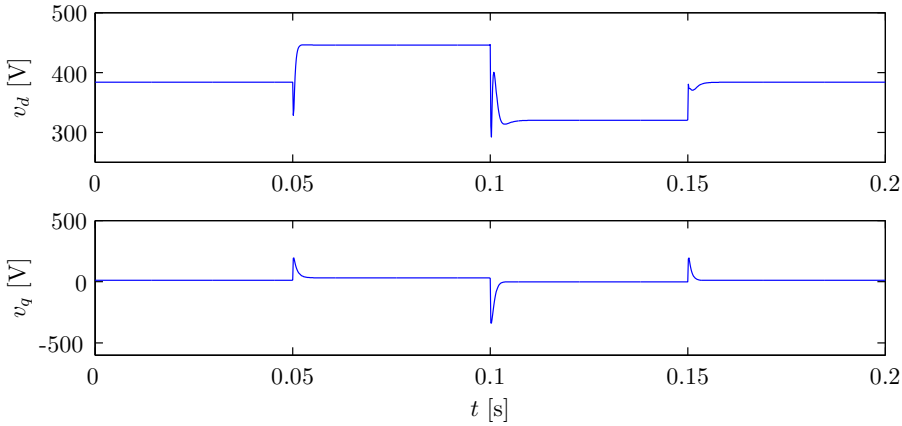

Figure 3.11: *Inverter voltages for state space control with gain scheduling*

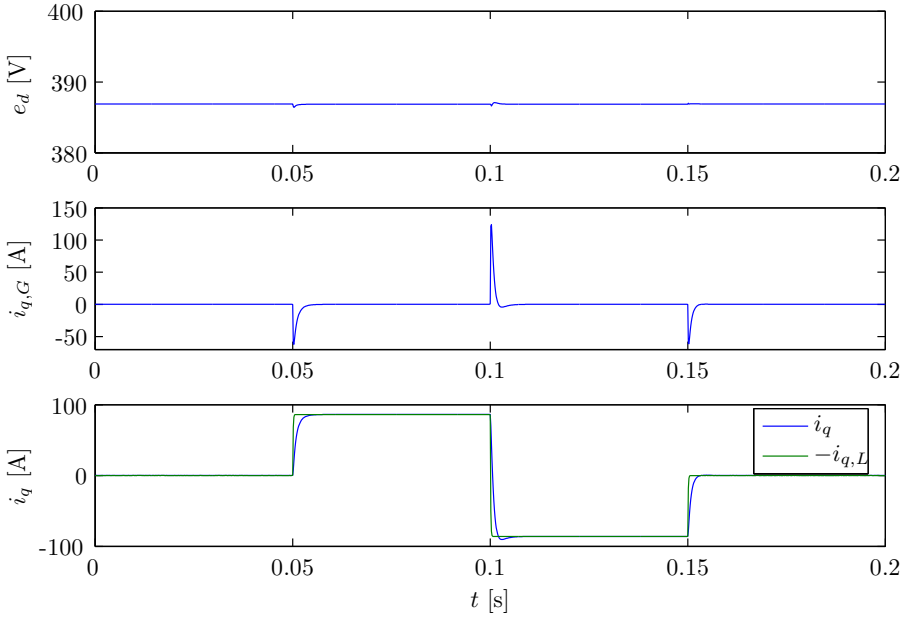

Figure 3.12: *Grid voltage and reactive currents for state space control with gain scheduling*

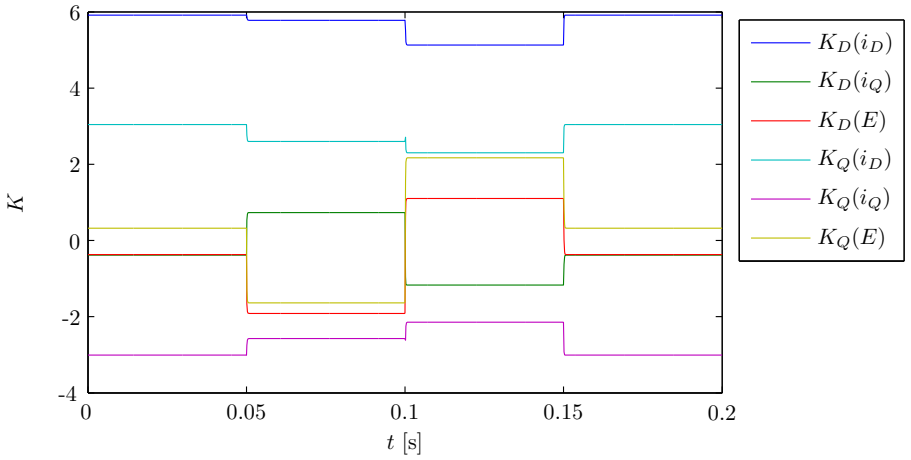

Figure 3.13: *Gain schedule for state space control with gain scheduling*

assumptions made for the mean model of the ASVC. However, in reality the model is never completely correct, so it is useful to have feedback in the control.

There is a spike in the change from positive to negative reactive power. This is due to the transition from positive to negative gains in the gain schedule, around $i_q = 0$.

3.3 Integral Control

Integral control is useful for removing steady state error. An additional state, $\boldsymbol{x}_I = \int^t \boldsymbol{C}x - r$ is augmented to the state matrix, resulting in the following state matrices.

$$\begin{bmatrix} \dot{\boldsymbol{x}} \\ \dot{\boldsymbol{x}}_I \end{bmatrix} = \begin{bmatrix} 0 & \boldsymbol{A} \\ 0 & \boldsymbol{C} \end{bmatrix} \begin{bmatrix} \boldsymbol{x} \\ \boldsymbol{x}_I \end{bmatrix} + \begin{bmatrix} \boldsymbol{B} \\ 0 \end{bmatrix} \boldsymbol{u} - \begin{bmatrix} 1 \\ 0 \end{bmatrix} r \tag{3.26}$$

and the feedback is,

$$u = -\begin{bmatrix} \boldsymbol{K}_0 & \boldsymbol{K}_I \end{bmatrix} \begin{bmatrix} \boldsymbol{x} \\ \boldsymbol{x}_I \end{bmatrix} \tag{3.27}$$

In the case of integral control, is is possible to use the reactive current into the transmission line as the control objective, rather than the load current. This automatically means that the ASVC matches the load reactive current, because they are the only three current branches in the system. However, because the purpose of this control is to be resistant to harmonics, it is better to keep the control objective as matching the load current.

For a step input, the input states and output voltages are shown in Figures 3.15, 3.16, and 3.17. The weight of the integral state is quite high in the control, but allows the system to become very fast, without too much overshoot.

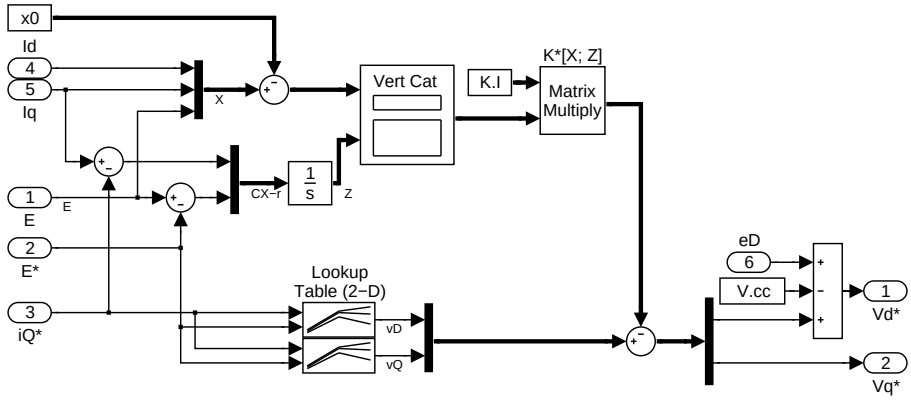

Figure 3.14: *Simulink integral control block*

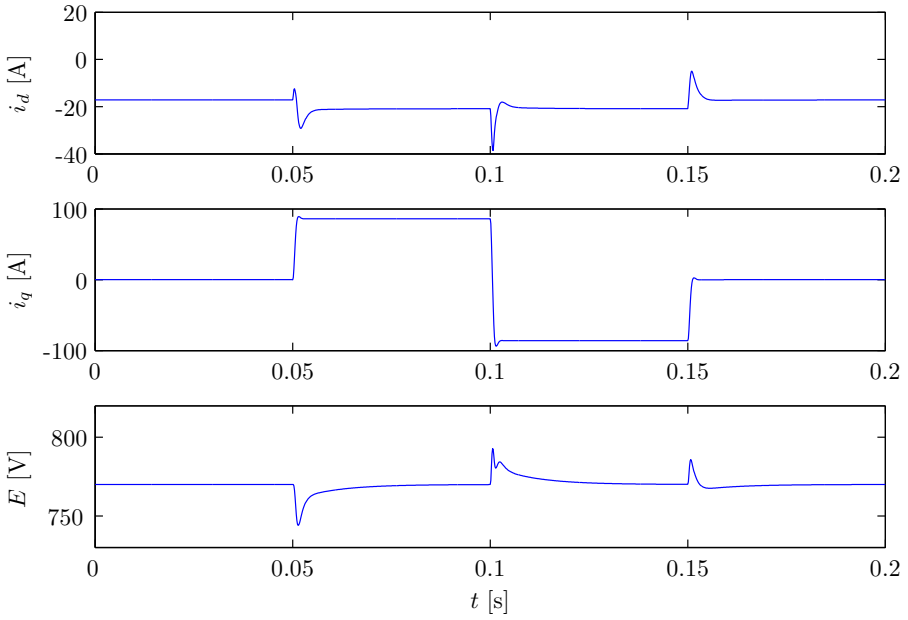

Figure 3.15: *State variation for integral state space control*

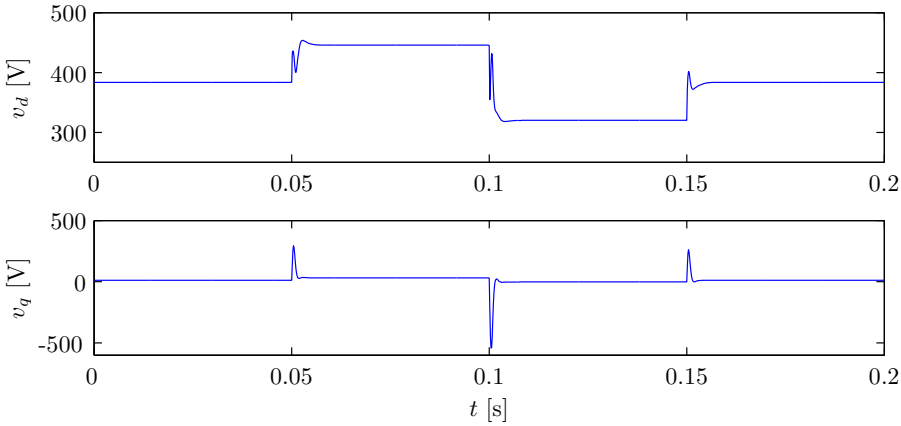

Figure 3.16: *Inverter voltages for integral state space control*

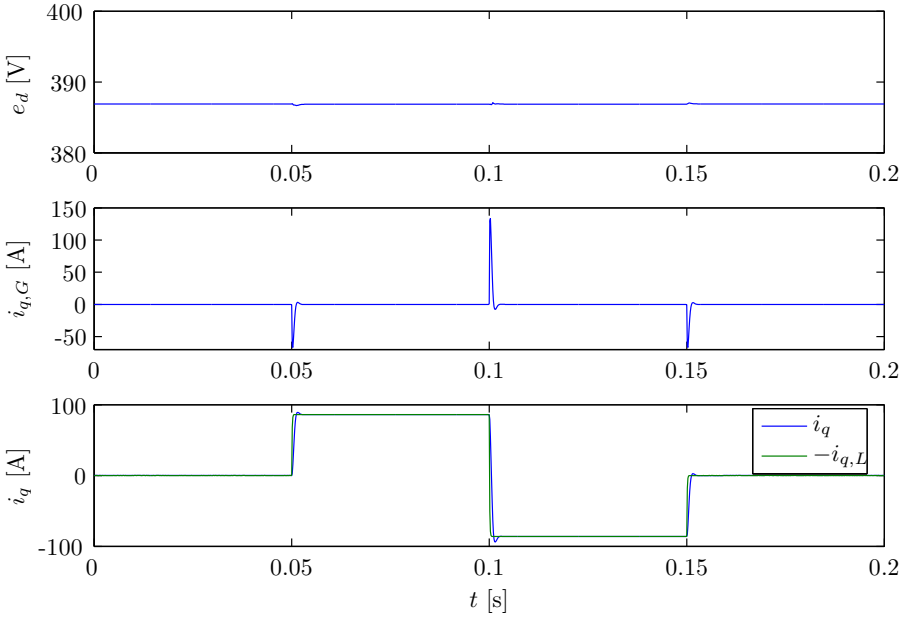

Figure 3.17: *Grid voltage and reactive currents using integral state space control in power simulation*

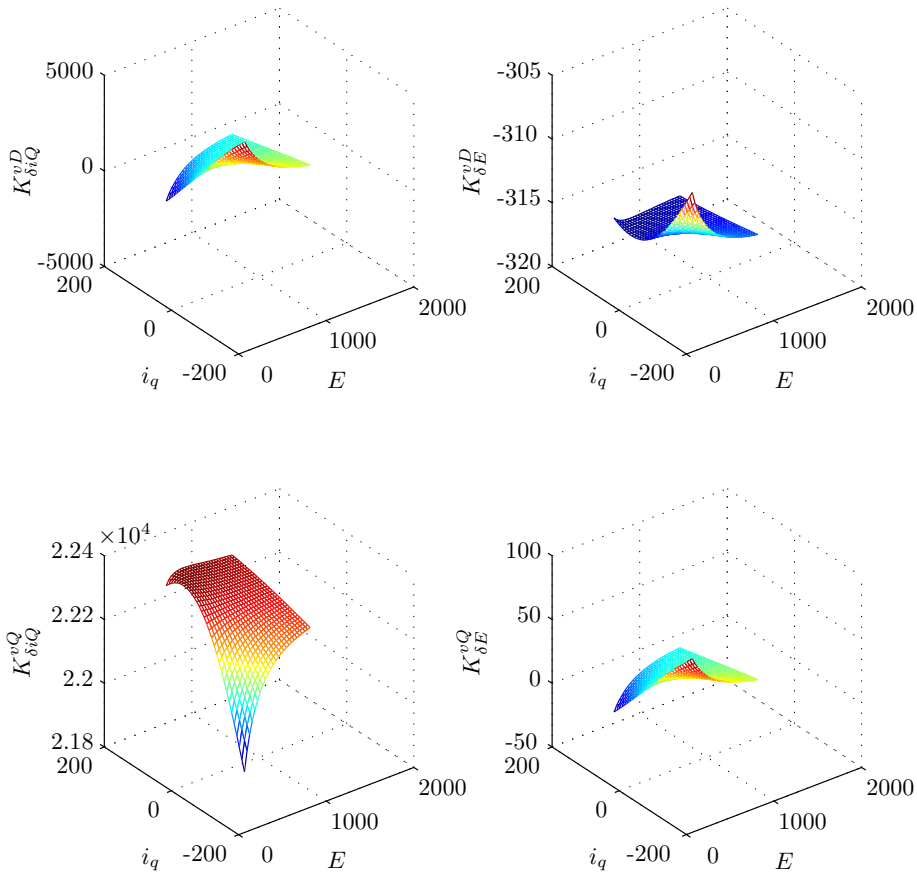

Figure 3.18: *Change in integral gain matrix with varying i_Q and E*

Though there is some feed forward in this system with the tables looking up the appropriate voltage set points, the current still reaches almost 50 amps, before the system reacts.

3.3.1 Integral control with gain scheduling

It is also possible to include feed forward in the integral control, so that the known dynamics are accounted for and the response can be more immediate. In this case, the gain becomes,

$$u = u_0 + \boldsymbol{K}_0\boldsymbol{x} - \boldsymbol{K}_I\boldsymbol{x}_I \tag{3.28}$$

The $\boldsymbol{R}$ weights are the same, but the weight for the states is now chosen as,

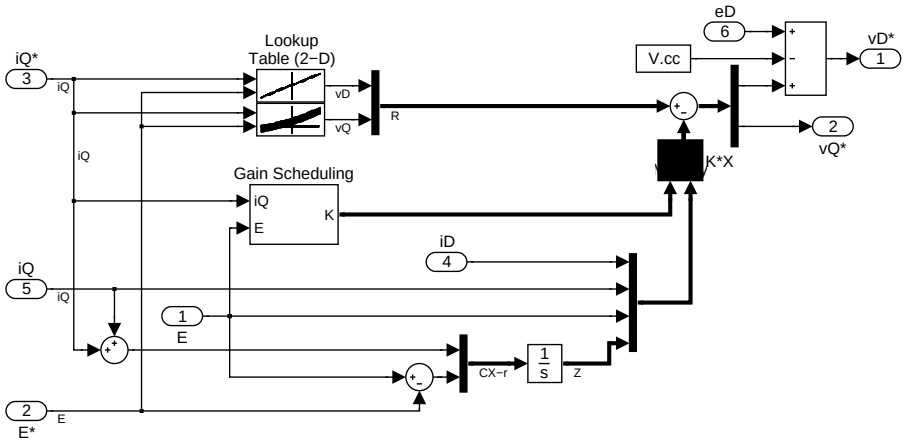

Figure 3.19: *Simulink gain scheduling with integral control block*

$$\boldsymbol{Q} = \begin{bmatrix} 1 & 0 & 0 & 0 & 0 \\ 0 & 1 & 0 & 0 & 0 \\ 0 & 0 & 1 & 0 & 0 \\ 0 & 0 & 0 & 50 \times 10^6 & 0 \\ 0 & 0 & 0 & 0 & 10 \times 10^3 \end{bmatrix} \tag{3.29}$$

In Figure 3.21, it could be seen that there are some unusual dynamics of integral control over the i_Q axis. The variation in the gain for the new integral states is shown in 3.18 on the facing page.

The two control strategies are be combined, resulting in the state variation shown in Figure 3.20 on the next page. The input variation is shown in Figure 3.21 on the following page. The grid voltages and currents are shown in 3.22 on page 29. This control shows reasonable response, it is very quick, without much overshoot, and no disturbances when crossing $i_Q = 0$.

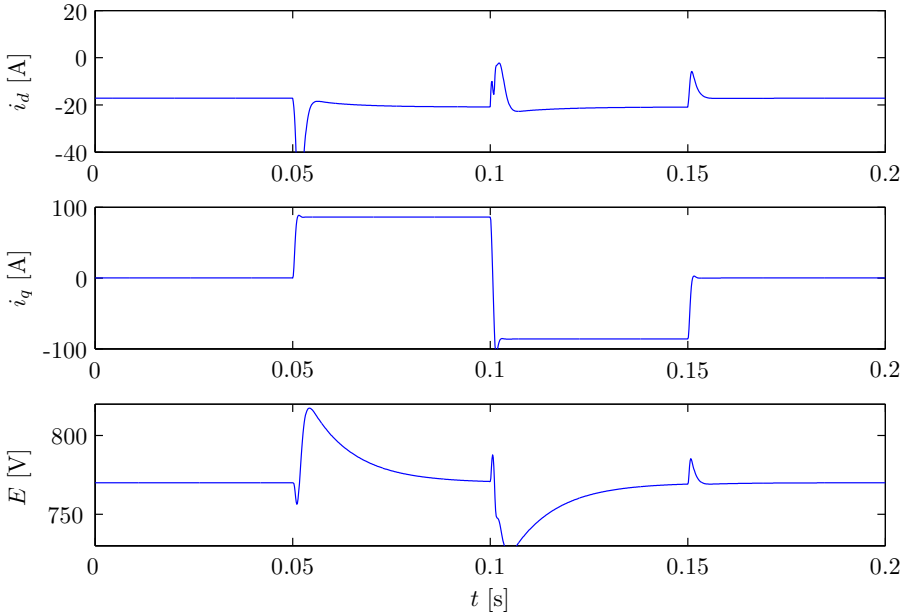

Figure 3.20: *State Variation for integral state space control with gain scheduling*

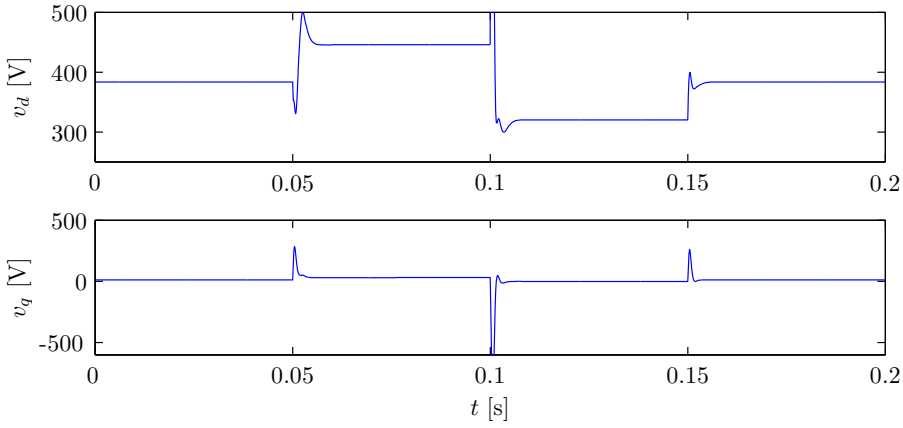

Figure 3.21: *Output variation for integral state space control with gain scheduling*

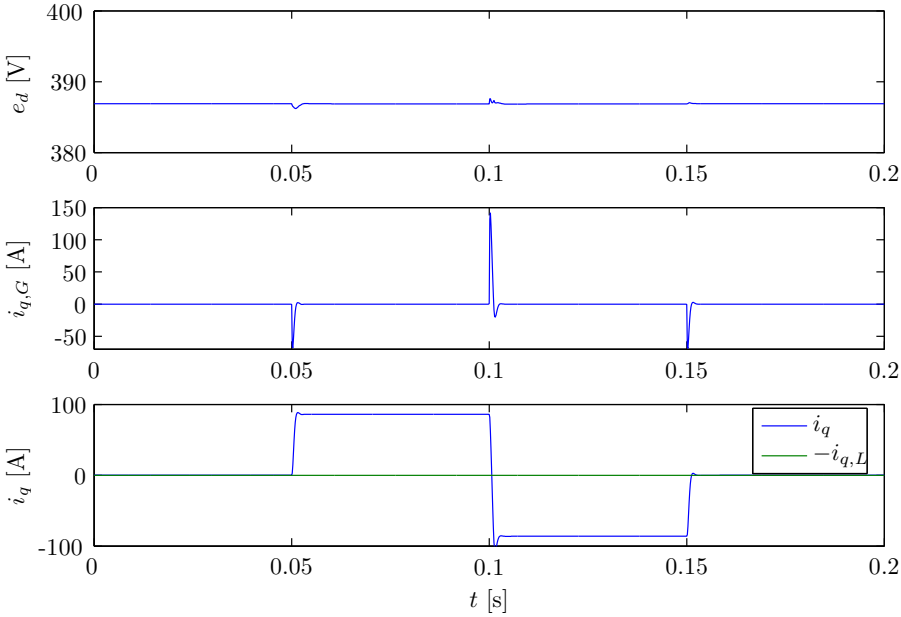

Figure 3.22: *Reactive current into grid using integral state space control with gain scheduling*

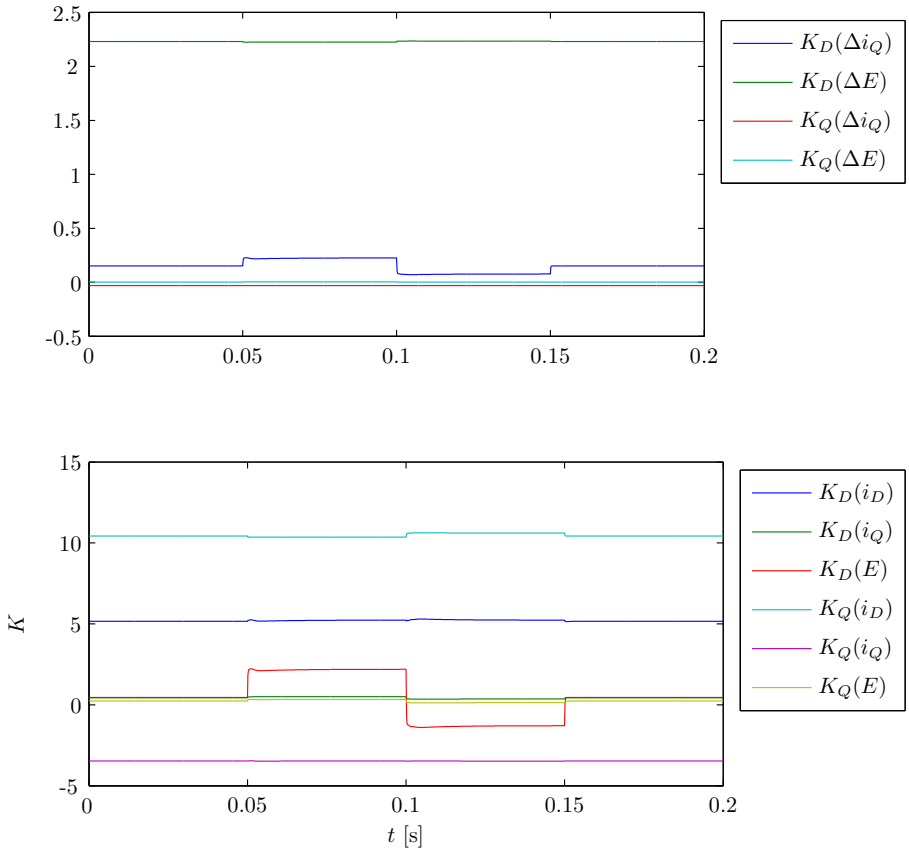

Figure 3.23: *State Variation for integral state space control with gain scheduling*

Chapter 4

Harmonic Estimation

4.1 Measurements

In order to describe the stochastic and harmonic components in the grid, measurements were taken in the lab at the the Ørsted department at the Technical University of Denmark. A weak grid was simulated by running the grid connection through a relatively large inductance. In order to initiate a phase shift, resistors were connected to ground with a switch. A nonlinear load was created by connecting an H-bridge rectifier and DC load. The phase jump was initiated when the nonlinear load was connected. An unbalanced grid was also created by quickly ramping up the motor-generator combination.

4.1.1 Equipment

The component values used in this experiment are noted in Table 4.1 on page 33. The measurements were taken using Labview with a PCI-6024E measurement card, which has a sample rate of up to 200 kS/s. Measurements of the three phase current and voltage were taken at 6400 Hz, allowing accurate measurement of harmonics up to the 64th, while still well within the capability of the card. The exceptions are the measurement of the generator startup, and the wind turbine cut-in and cut-out measurements which were sampled at 3200 Hz.

The sampling times were taken as power of two, to optimize for fourier analysis. Additionally, a hold and sample strategy was used to ensure that the data points were taken at the same time.

Measurements of the grid near the Nordtank wind turbine (NTK 550, 41) are taken using the measurement setup developed for the wind turbine measurements course at the Technical University of Denmark. The measurement point is at the 400V terminals of the generator. A series where the generator turns off is shown in Figure 4.2 on the next page, and the subsequent turn on period is shown in Figure 4.2 on the following page.

Measurements were also taken when the wind turbine was operating continuously, though in low winds, as shown in Figure 4.3 on page 33. The lab measurements of the nonlinear load, weak grid, and phase shift are not shown here explicitly, but are taken as test cases in the section on harmonic estimation. This data will be used to test a filter which will estimate the fundamental frequency, phase, and amplitude of the voltage, as well as the phase and amplitude of the harmonic components. The power spectral density of the data measured

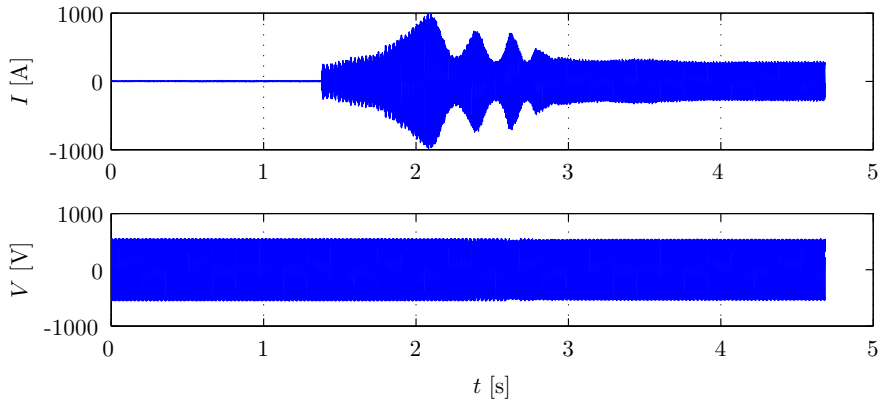

Figure 4.1: *Current and voltage during turbine cut-in*

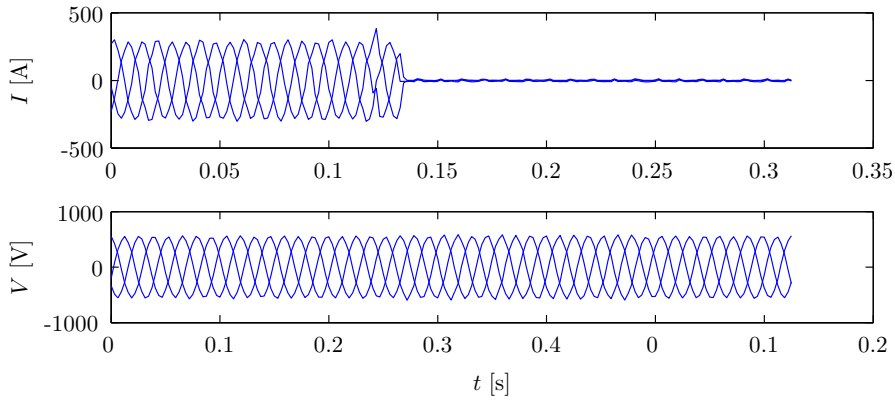

Figure 4.2: *Current and voltage during turbine cut-out*

from the Nordtank in normal operation is shown in Figure 4.4 on the facing page. All spectrums shown in this report use the Welch algorithm with a hamming window of length 128 and 50% overlap. The power spectral density for the lab measurements with a nonlinear load are shown in Figure 4.5 on page 34.

4.2 Estimation of grid dynamics

In order to estimate the frequency content of the grid, a state space maximum likelihood estimation is implemented. The Hartley transform is used to formu-

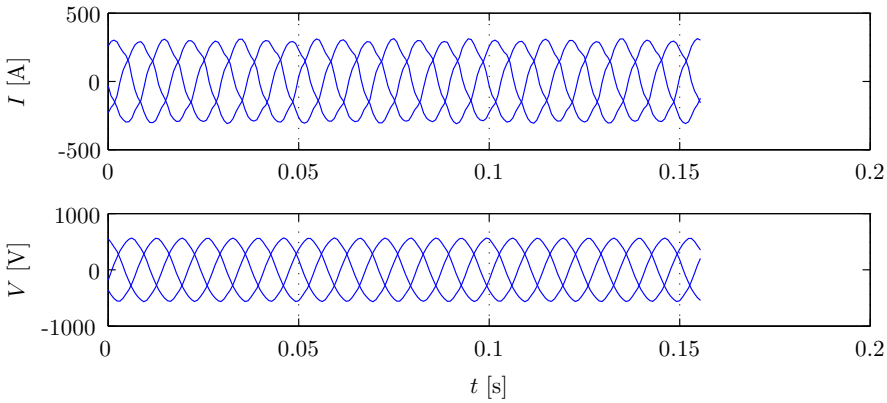

Figure 4.3: *Current and voltage during normal turbine operation*

L_m	R_P	R_{NL}	C_{NL}
22mH	10Ω	20Ω	4.4mF

Table 4.1: *Component values for weak disturbed grid*

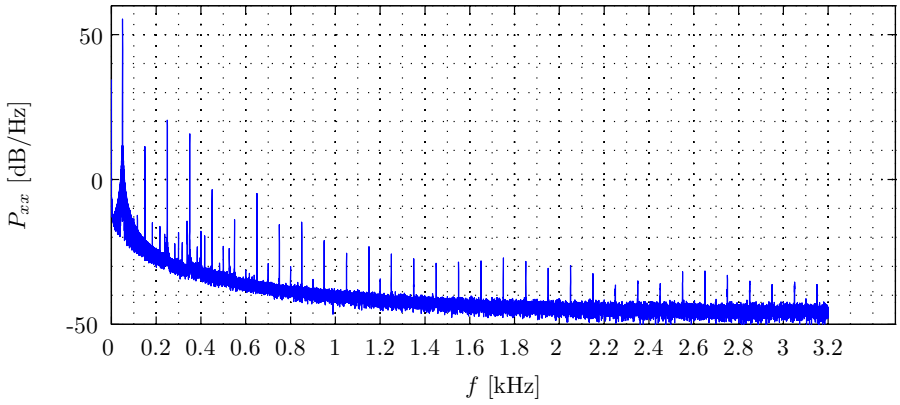

Figure 4.4: *Power spectral density of Nordtank voltage*

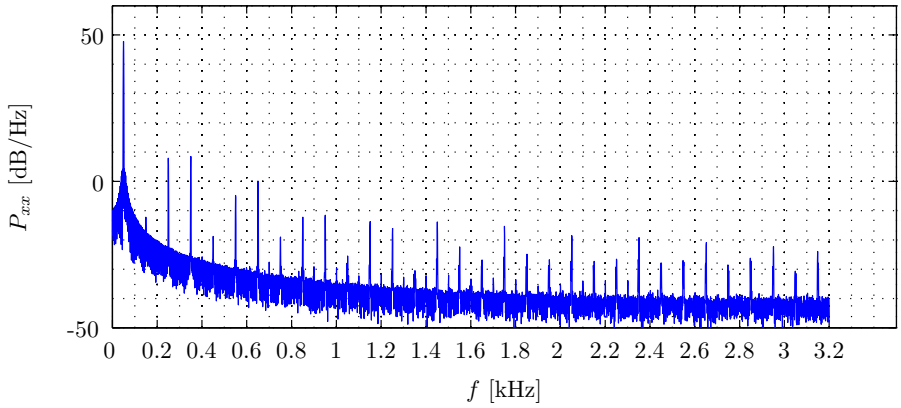

Figure 4.5: *Power spectral density of nonlinear load voltage*

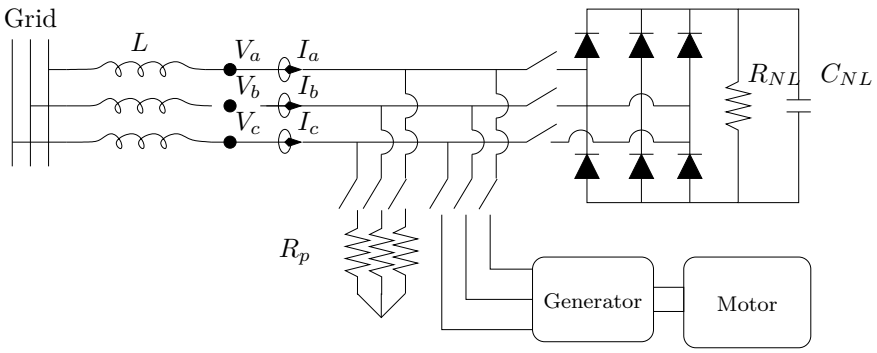

Figure 4.6: *Setup for measurements*

late the magnitude and phase in a linear manner.

$$y = A\cos(\omega t) + B\sin(\omega t) \tag{4.1}$$

If harmonics are included, the series can be described by,

$$y = \sum_{n}^{H} A_n \cos(\omega_n t) + \sum_{n=1}^{H} B_n \sin(\omega_n t) \tag{4.2}$$

where H is a vector of harmonic components to be estimated.

If the fundamental frequency of the system as well as the magnitude and phase of the harmonics are to be estimated, the state space formulation can be

found using linearization. The estimator is,

$$\theta = \begin{bmatrix} \omega_0 \\ A_1 \\ \vdots \\ A_H \\ B_1 \\ \vdots \\ B_H \end{bmatrix} \tag{4.3}$$

And the linearized state vector is:

$$\frac{\delta \hat{y}}{\delta \theta} \simeq \psi = \begin{bmatrix} \sum_{n=1}^{H} -ntA\sin(\omega_n t) + \sum_{n=1}^{H} ntB\cos(\omega_n t) \\ \cos(\omega_0 t) \\ \vdots \\ \cos(\omega_n t) \\ \sin(\omega_0 t) \\ \vdots \\ \sin(\omega_n t) \end{bmatrix} \tag{4.4}$$

The cost function becomes,

$$\epsilon = e - \sum_{n=1}^{H} \hat{A_n}\cos(\hat{\omega_n} t) + \sum_{n=1}^{H} \hat{B_n}\cos(\hat{\omega_n} t) \tag{4.5}$$

where,

$$\omega = \omega_0 \begin{bmatrix} 1 \\ \vdots \\ H \end{bmatrix} \tag{4.6}$$

The system is then plugged into a Recursive Prediction Error Method (RPEM) algorithm, with the addition of a forgetting factor, λ. In this case, the one-step prediction is written,

$$\hat{y}_{t|t-1}(\boldsymbol{\theta}) = f(\boldsymbol{\theta}) \tag{4.7}$$

Using only the first component of the Hessian, results in the following algorithm:

$$\epsilon_t(\hat{\boldsymbol{\theta}}_{t-1}) = y_t - \hat{y}_{t|t-1}(\hat{\boldsymbol{\theta}}_{t-1}) \tag{4.8}$$

$$\hat{\boldsymbol{\theta}}_t = \hat{\boldsymbol{\theta}}_{t-1} + R_t^{-1}(\hat{\boldsymbol{\theta}}_{t-1})\psi_t(\hat{\boldsymbol{\theta}}_{t-1})\epsilon_t(\hat{\boldsymbol{\theta}}_{t-1}) \tag{4.9}$$

$$R_t(\hat{\boldsymbol{\theta}}_{t-1}) = R_{t-1}(\hat{\boldsymbol{\theta}}_{t-1}) + \psi_t(\hat{\boldsymbol{\theta}}_{t-1})\psi_t^T(\hat{\boldsymbol{\theta}}_{t-1}) \tag{4.10}$$

where,

$$\psi = \nabla_\theta \hat{y}_{t|t-1}(\boldsymbol{\theta}) \tag{4.11}$$

However, if the second term in the Hessian matrix is maintained, the system can achieve faster convergence near the linearization point. Away from the linearization point, it carries a danger of leading to instability. Therefore the second derivative of the cost function is only included when the error in the estimate is small, e.g. $e \leq 10$. In this case, the covariance matrix becomes,

$$R_t(\hat{\boldsymbol{\theta}}_{t-1}) = R_{t-1}(\hat{\boldsymbol{\theta}}_{t-1}) + \psi_t(\hat{\boldsymbol{\theta}}_{t-1})\psi_t^T(\hat{\boldsymbol{\theta}}_{t-1}) - \nabla\psi_t(\hat{\boldsymbol{\theta}}_{t-1})e \tag{4.12}$$

In this implementation, all three residuals were required to be below the limit, before using the second term.

It is expected that the system parameters will vary in time. The fundamental frequency should have small variation, over a long time scale. The harmonic components should vary with changes in load, which will be expressed as small steps in the magnitude. The magnitude of the fundamental frequency will have slow changes, but during phase shifts, these components should be able to change very quickly. The forgetting factor is included as a weighted diagonal matrix, modifying the covariance matrix. The forgetting factor can be selective, such that the effective memory for each parameter can differ.

$$R_t = \sqrt{\lambda}^T R_{t-1}\sqrt{\lambda} + \psi_t\psi_t^T - \nabla\psi_t e \tag{4.13}$$

$$\lambda = \begin{bmatrix} \lambda_w & 0 & 0 & 0 & 0 & 0 & 0 \\ 0 & \lambda A_0 & 0 & 0 & 0 & 0 & 0 \\ 0 & 0 & \ddots & 0 & 0 & 0 & 0 \\ 0 & 0 & 0 & \lambda_{An} & 0 & 0 & 0 \\ 0 & 0 & 0 & 0 & \lambda B_0 & 0 & 0 \\ 0 & 0 & 0 & 0 & 0 & \ddots & 0 \\ 0 & 0 & 0 & 0 & 0 & 0 & \lambda_{Bn} \end{bmatrix} \tag{4.14}$$

For a given λ, the effective length of the parameter memory is given as,

$$T = \frac{Ts}{1-\lambda} \tag{4.15}$$

Through experimentation and common sense, the parameters are chosen such that the forgetting factor for the frequency is very close to 1, .995, while the harmonics have a shorter memory, with a forgetting factor near .99. A few harmonics which are characteristic of consumer loads are given a slightly lower forgetting factor, .985,to allow for step variation. Finally, the fundamental frequency components are weighted such that they have an effective memory of one tenth of a cycle. This allows them to change very quickly during power events.

Initially, an estimation of frequency, phase, and magnitude of the three phases was made separately. However, this turned out to be problematic, because in order to maintain sensitivity to changes in phase, the weighting of the magnitude vectors, A_n and B_n was decreased. This results in hysterical behavior within the estimator, if the frequency estimate is not given a more stable weighting, resulting in a tendency of the frequency to decrease, and the higher harmonic factors to take on the role of the fundamental. However, when the frequency is given more inertia, it has a tendency to settle in a slightly wrong location, while the magnitude vectors track the phase error actively. For a three phase system, it is even more problematic, because the three frequency estimates tend to settle in different places.

A solution to this is to estimate the frequency of the grid using all three phases. This alone causes the estimate to be more stable. In essence, the component magnitude is estimated on a phase by phase basis, while the frequency is estimated with the effect of all three phases. This uses the same algorithm as outlined above, but adds the requirement that the frequency estimate should be the same for all phases. This assumption is fulfilled in practice.

$$\hat{\omega} = \frac{1}{3}\left(\hat{\omega}_a + \hat{\omega}_b + \hat{\omega}_c\right) \tag{4.16}$$

The output of the filter is now the predicted value of the voltage for a given time, using the estimated frequency, magnitude and phase of the fundamental component of the signal.

$$y_0 = A_0 \cos(\omega t) + B_0 \sin(\omega t) \tag{4.17}$$

4.2.1 Simulated data

In order to test the algorithm on data of known parameters, a three phase grid with harmonics was simulated. The equation for the simulated grid is,

$$\begin{aligned}
e_a &= \sum_H I_a \left[m_H A \cos(\theta_a + \phi + H\omega t) + m_H B \sin(\theta_a + \phi + H\omega t)\right] + \epsilon \\
e_b &= \sum_H I_b \left[m_H A \cos(\theta_b + \phi + H\omega t) + m_H B \sin(\theta_b + \phi + H\omega t)\right] + \epsilon \\
e_c &= \sum_H I_c \left[m_H A \cos(\theta_c + \phi + H\omega t) + m_H B \sin(\theta_c + \phi + H\omega t)\right] + \epsilon
\end{aligned} \tag{4.18}$$

where I is the relative intensity of each phase, θ is the relative angle of the phases, and ϕ is the angle offset of all three phases. The values used for the

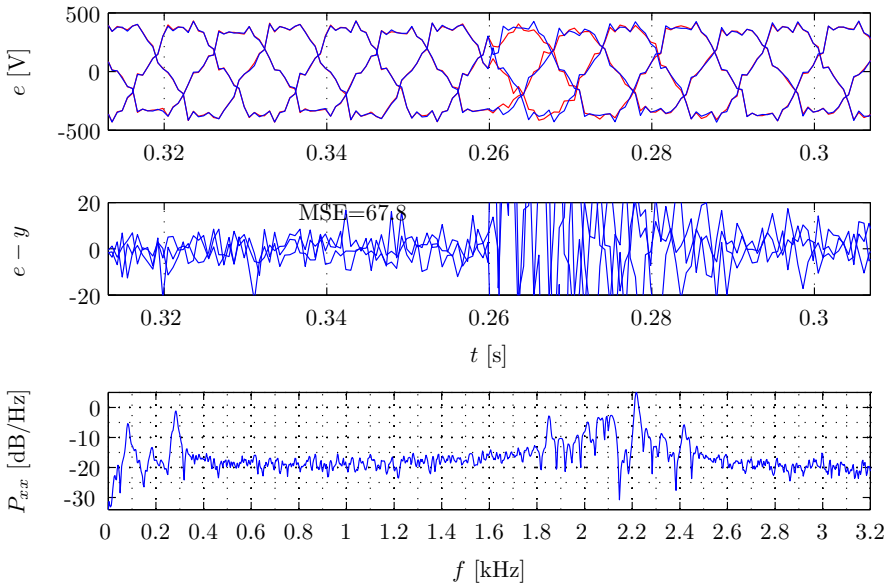

Figure 4.7: *Estimate, residual, and residual spectrum for simulated voltage*

simulation are,

$$A = 400\sqrt{2}, \quad B = 400\sqrt{2}, \quad \omega = 2\pi 50$$
$$\sigma^2 = 20, \quad \epsilon = N(0, \sigma^2)$$
$$H = \begin{bmatrix} 1 \\ 5 \\ 7 \\ 11 \\ 13 \\ 17 \end{bmatrix}, \quad I = \begin{bmatrix} 1.0 \\ 0.9 \\ 1.0 \end{bmatrix}, \quad \theta = \begin{bmatrix} 0 \\ -\frac{2\pi}{3} \\ \frac{2\pi}{3} + \frac{5\pi}{180} \end{bmatrix}$$
$$\phi = \begin{cases} 0, & t < 0.6; \\ -30^0, & t \geq 0.6. \end{cases}$$
$$m_H = \begin{cases} \begin{pmatrix} 1.0 & 0.10 & 0.05 & 0.07 & 0.09 & 0.06 \end{pmatrix}^T, & t < 0.3; \\ \begin{pmatrix} 1.0 & 0.05 & 0.05 & 0.07 & 0.09 & 0.06 \end{pmatrix}^T, & t \geq 0.3. \end{cases}$$

This simulates many of the challenges that the estimator might encounter, namely and unbalanced, nonsymmetric grid with noise, with a phase shift of 30^0 at $t = 0.3$ and a -50% step in the magnitude of the 5th harmonic at $t = 0.6$. The amount of noise is also considerable, with a variance of 5% of the fundamental amplitude.

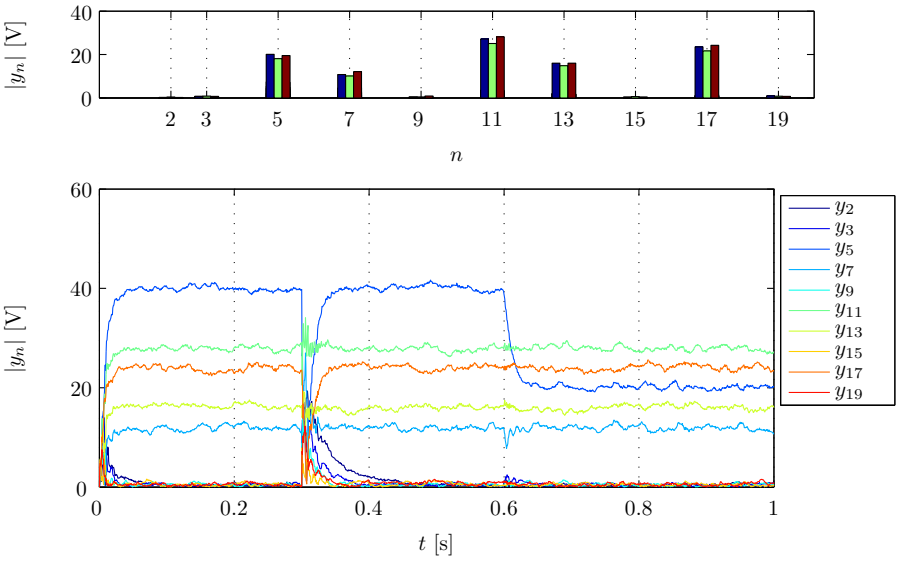

Figure 4.8: *Harmonic estimates for simulated voltage*

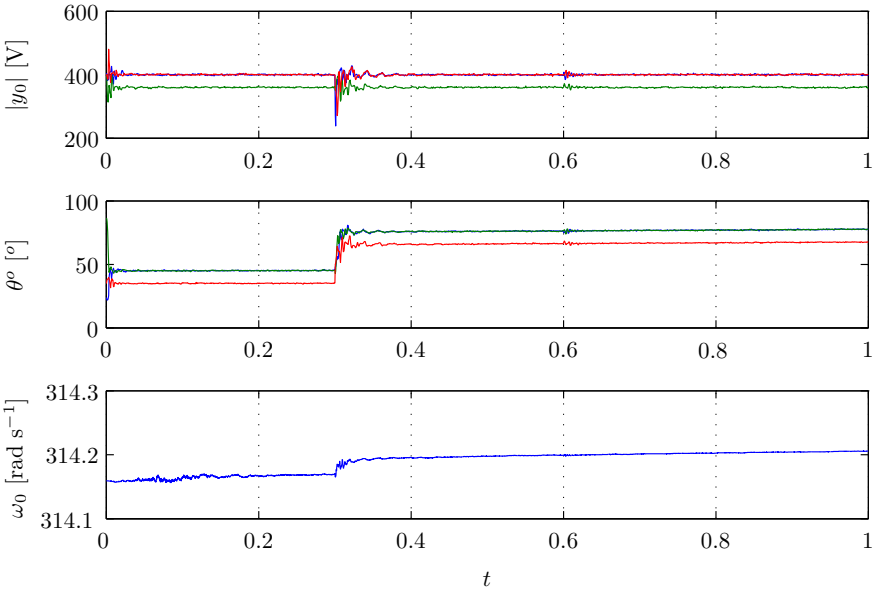

Figure 4.9: *Parameter Estimates for simulated voltage*

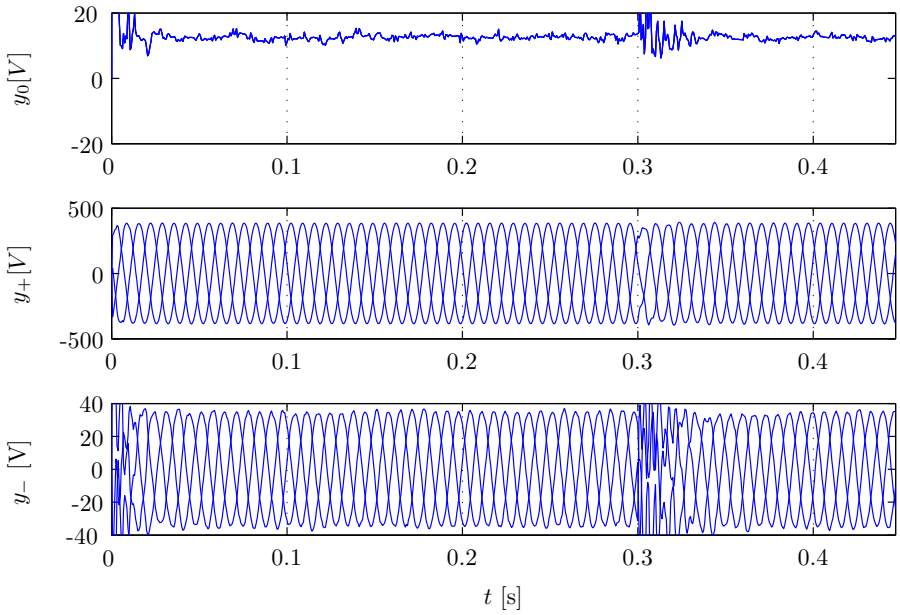

Figure 4.10: *Sequence decomposition for simulated voltage*

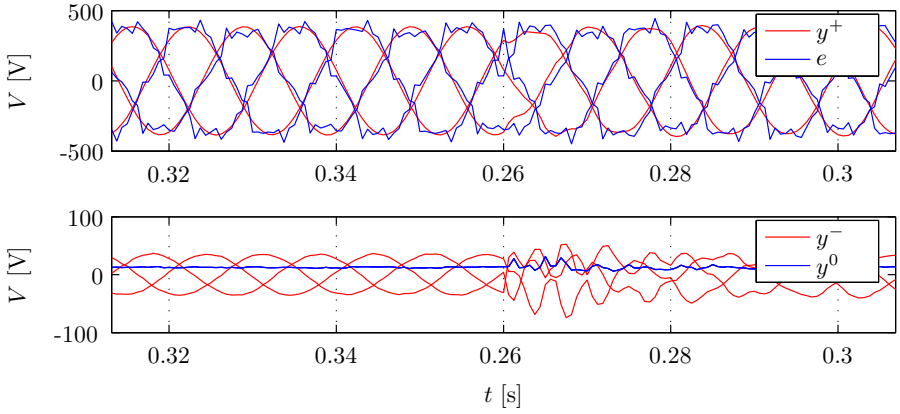

Figure 4.11: *Sequences near disturbance for simulated voltage*

The comparison between the measured and filtered simulated voltage, as well as the residual and power spectral density of the residuals are shown in 4.7 on page 38. The estimates of the phase magnitude, phase angle [1] , and fundamental frequency are shown in 4.9 on page 39. The estimates of the final harmonic magnitude of one phase and the evolution of the estimates are shown in 4.8 on page 39.

The estimate of the 5th harmonic registers the step at 0.6s. The phase shift at 0.3s is also registered quickly by the fundamental estimator. It should be noted that phase jumps cause the harmonic estimates to go way off for a short time, they also cause a step in the estimate of the frequency.

It can be seen that the estimate of the fundamental frequency is not very accurate, causing the fundamental amplitude estimates to actively track the phase error. This is not problematic, because the resulting filtered estimate has the correct phase. It is preferable to have this effect, rather than having large steps in the frequency estimates during phase shifts. However, the forgetting factor on the frequency should not be too stiff, or the stability of the estimator becomes jeopardized.

The loss of tracking in the harmonics during phase jumps is not problematic, because they are not used in the output. In fact, though the overall residuals do go up during phase shifts, the fundamental frequency converges to the new phase very quickly. However, it can be seen that estimates of harmonics which are not present are not exactly zero. Though not catastrophic, these false parameters degrade the estimate, and should be removed if possible.

In the classical control method, the filtered data would be fed into the Clark and Park transformation, but this filter is actually perfect for using symmetrical components, as described in Appendix A. This has several benefits; the transformation removes any imbalance and non-symmetries in the actual measured data, additionally, any non-symmetries introduced by the estimator during convergence are also removed.

The positive negative and zero sequences are shown in 4.10 on the preceding page. A closer look at the positive sequence during the phase shift is shown in 4.11 on the facing page, where it can be seen that the phase shift is still registered, though the harmonic components are removed.

4.2.2 Selecting harmonics

In order to determine which harmonic estimates are necessary to track changes on the real electrical grid, the estimator has been run using all harmonic components. The components whose standard deviation is larger than their mean will be removed from the estimator. This test was performed on three sets of data, the nonlinear load and the unbalanced grid from the laboratory, and the wind turbine in normal operation. The smallest number of harmonics from

[1] The angles plotted here are the angle of phase a, and the angles of phase c and c, offset by -120^0 and 120^0, respectively

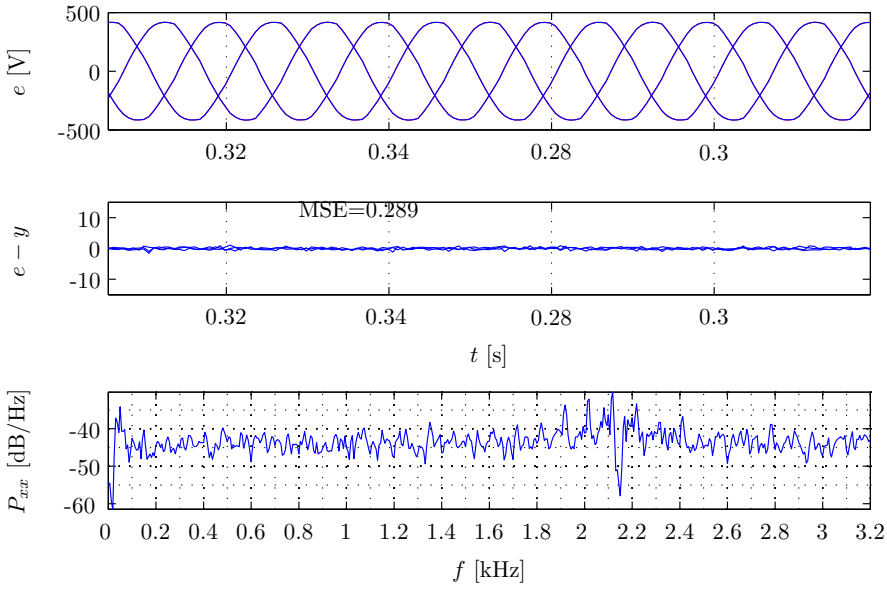

Figure 4.12: *Estimate, residual, and residual spectrum for weak grid with nonlinear load, using all harmonics*

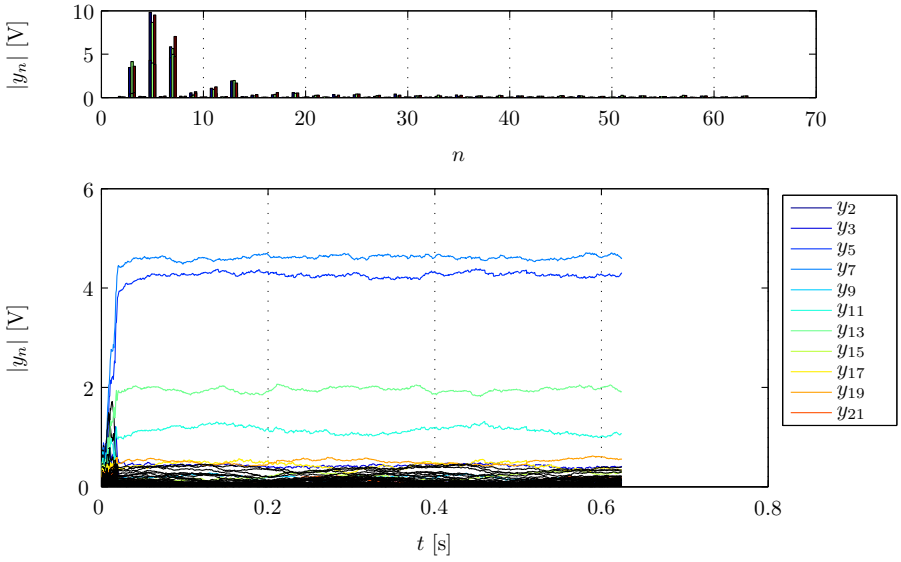

Figure 4.13: *Harmonic estimates for weak grid with nonlinear load, using all harmonics*

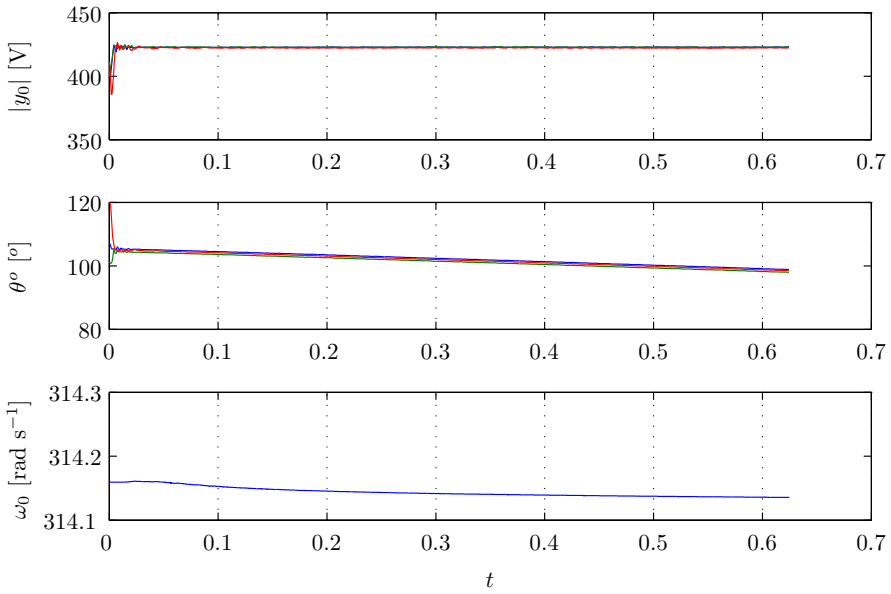

Figure 4.14: *Parameter Estimates for weak grid with nonlinear load, using all harmonics*

these three sets came from the unbalance grid, thus these are the harmonics which have been chosen. The weak grid is a special case because it has been measured at 3200 Hz, but also because it is one of the most difficult to track. When attempting to use additional parameters when estimating the unbalanced grid, it often diverged.

The harmonic estimates for all harmonics for the wind turbine are shown in Figure 4.16 on the next page. The harmonic estimates for all harmonics for the unbalanced grid are shown in Figure 4.17 on page 45. The harmonics which have passed the standard deviation test are shown in the legend, and printed in color.

There are three phases, and two amplitude estimates for each frequency, so the variance and amplitude are averaged across the phases, and both amplitude estimates are tested. The harmonic components which are finally selected are shown in Table 4.2 on page 45.

The estimate, residuals and residual spectrum for the estimate of all harmonics for the nonlinear grid are shown in Figure 4.12 on the facing page. It can be seen that there is very little periodic content in the residual, so the estimate has done a good job of absorbing the nonlinear component. The harmonic magnitudes and estimates are shown in Figure 4.13 on the preceding page. The test of the standard deviation of all harmonics in the nonlinear grid has removed all of the even harmonics, except for the 2nd. It has also determined that odd

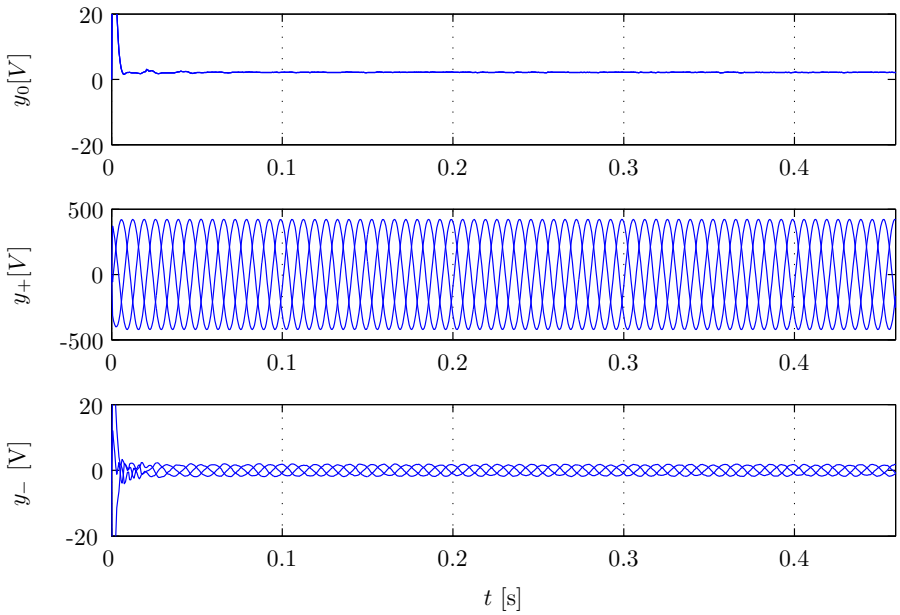

Figure 4.15: *Sequence decomposition for weak grid with nonlinear load, using all harmonics*

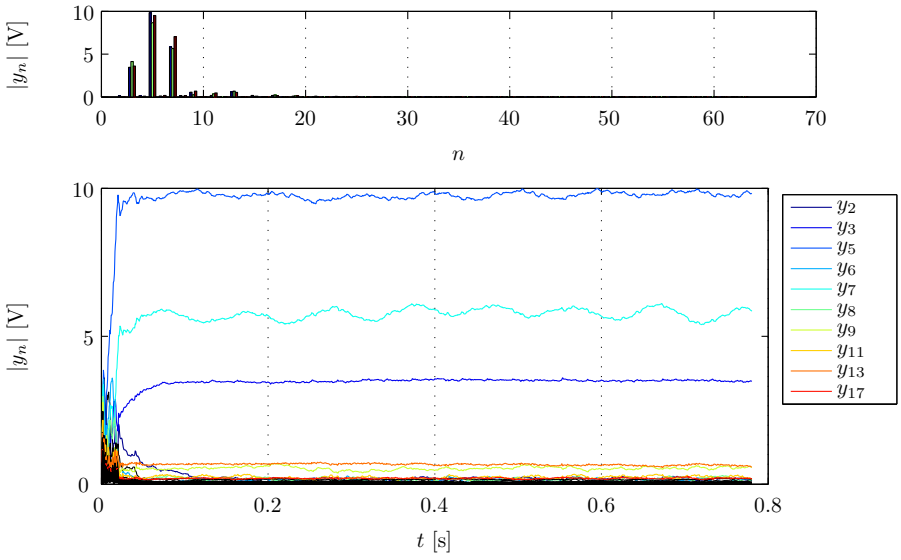

Figure 4.16: *Harmonic magnitude for wind turbine with all harmonics*

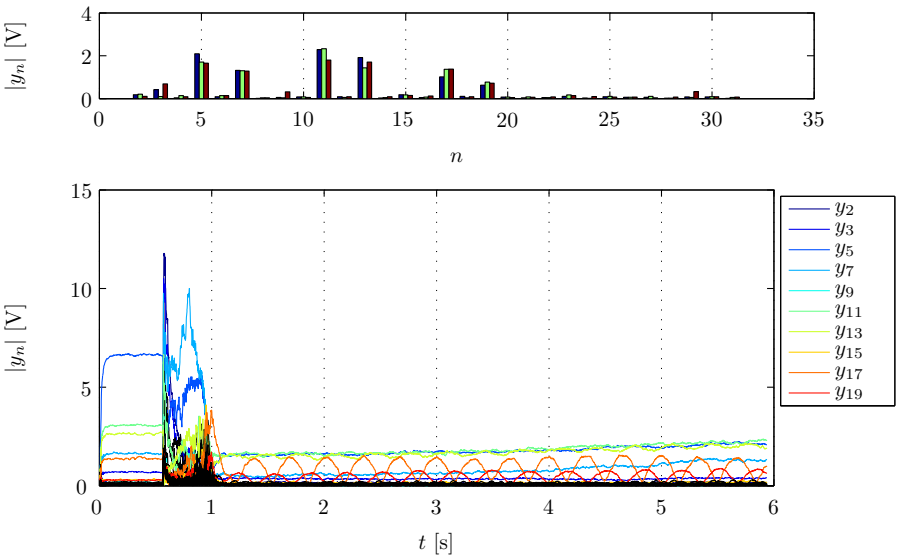

Figure 4.17: *Harmonic magnitude for unbalanced grid with all harmonics*

1	2	3	4	5	7	9	11	13	15	17	19

Table 4.2: *Relevant Harmonics*

harmonics above the 37th are negligible. For the wind turbine, and unbalanced grid, this cutoff occurs after the 21st harmonic. This may give some clue as to the the sampling speed which is required to accomplish the estimation, but that would require further investigation, as it may be a result of the convergence speed of the estimator. It may also be that the additional harmonics are useful for dynamically covering the nonlinearities in the voltage, but are not estimating complete harmonics.

Selected Harmonics

The filtering has been performed on measured data, as described in 4.1 on page 31, where a rectified load has been added to a grid weakened by an impedance. The nonlinear load presents a challenge to the estimator, because it is not covered by the model which the estimator is using. It is also an increasingly common feature of consumer loads.

In general, even harmonics are not expected to occur in the electrical grid. This a result of cancelling of the even harmonics due to the inherent symmetry of sine waves. For currents, harmonic factors of three should sum to zero because of the three phase symmetry in the electrical grid. Both of these assumptions may

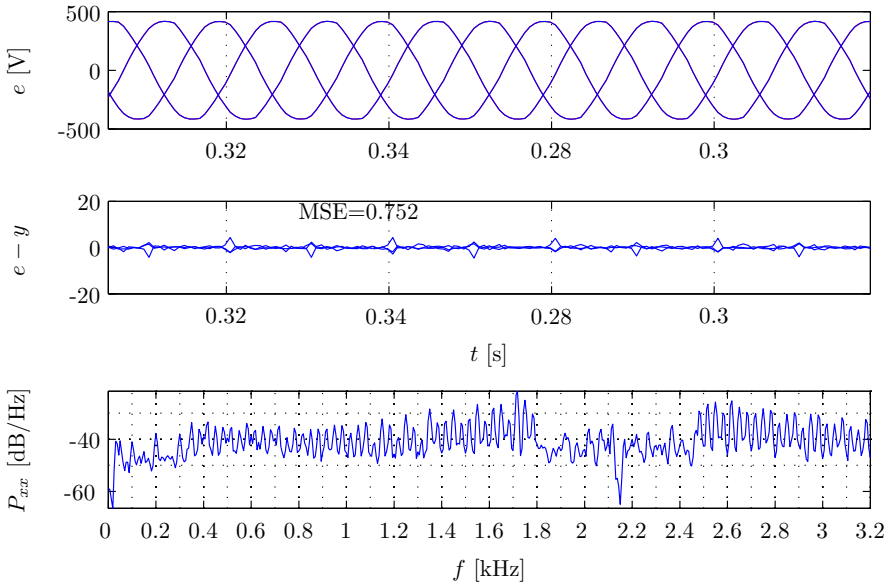

Figure 4.18: *Estimate, residual, and residual spectrum for weak grid with nonlinear load*

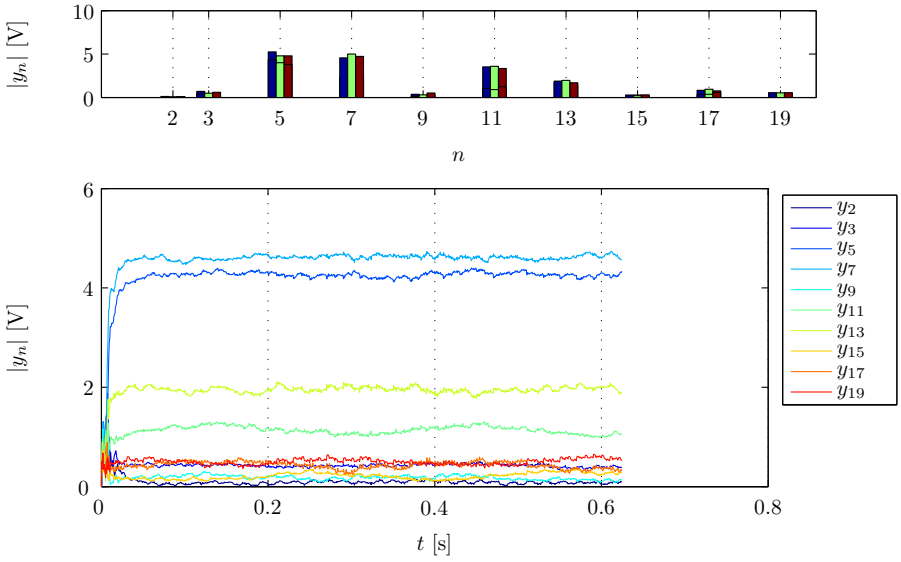

Figure 4.19: *Harmonic estimates for weak grid with nonlinear load*

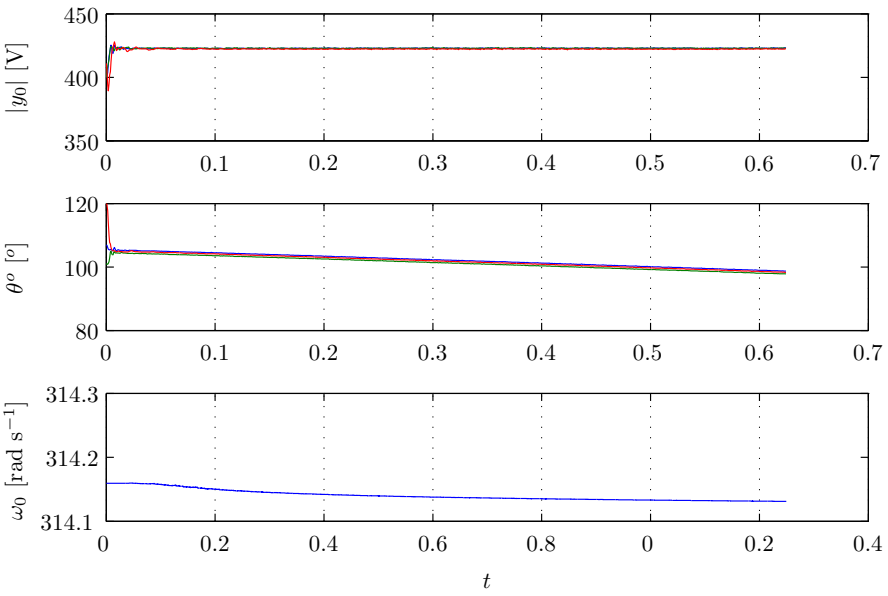

Figure 4.20: *Parameter Estimates for weak grid with nonlinear load*

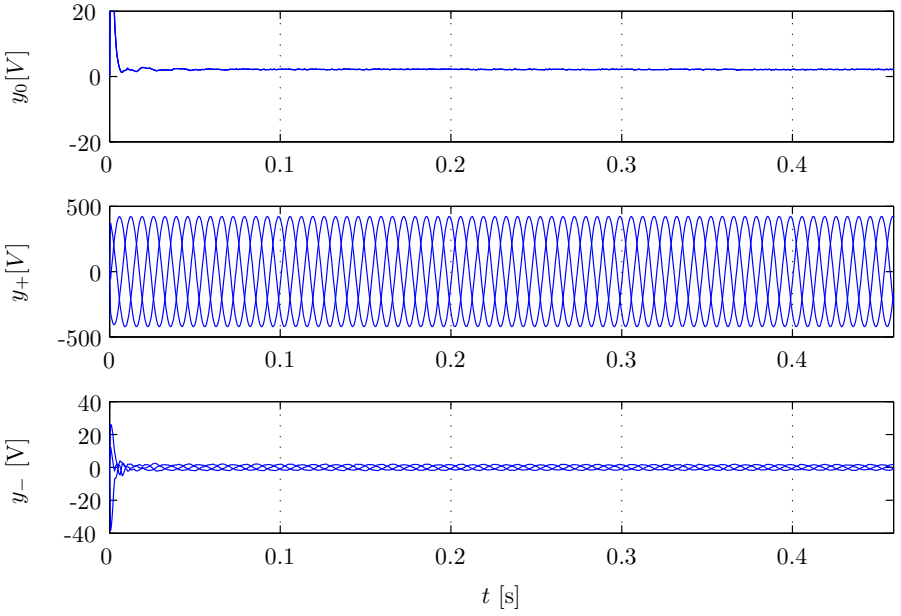

Figure 4.21: *Sequence decomposition for weak grid with nonlinear load*

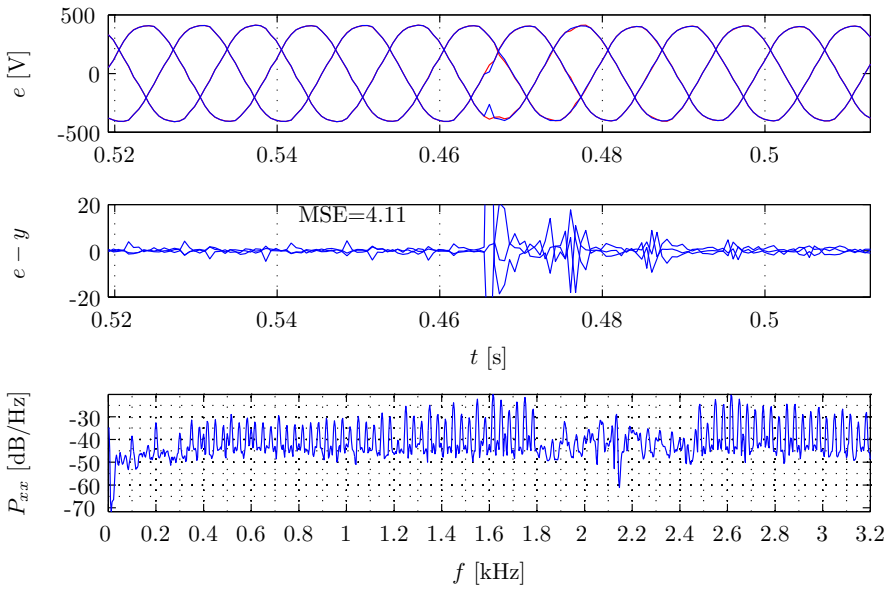

Figure 4.22: *Estimate, residual, and residual spectrum for nonlinear grid with phase shift*

be false in certain cases, particularly in the case of unbalanced, unsymmetrical grids. The ASVC control system is only operating on the balanced symmetric component of the grid, so it is not necessary to track these cases. However, in each of the standard deviation test, the 2nd, 3rd and 9th harmonics were found to be relevant parameters.

The nonlinear load has been estimated using only the harmonics deemed relevant in the previous section, shown in Figure 4.18 on page 46. More of the nonlinear load can now be seen in the residual, but still within reasonable limits. The harmonic estimates are shown in Figure 4.19 on page 46, and the positive sequence in Figure 4.21 on the previous page.

4.2.3 Phase Jump

Phase jumps occur when large active elements are switched onto the grid. These occurrences are problematic for ASVC, because the voltage reference changes quite suddenly. If an normal filter is being used, this change is not detected immediately, because of the phase delay due to the filter. The phase shift in analog filters tends to be quite large, because it has to filter the 5^{th} harmonic, which is relatively close to the fundamental.

In theory, the RPEM filter does not have a phase shift, because the output is actually a prediction of the phase at the next time step. In the case of phase

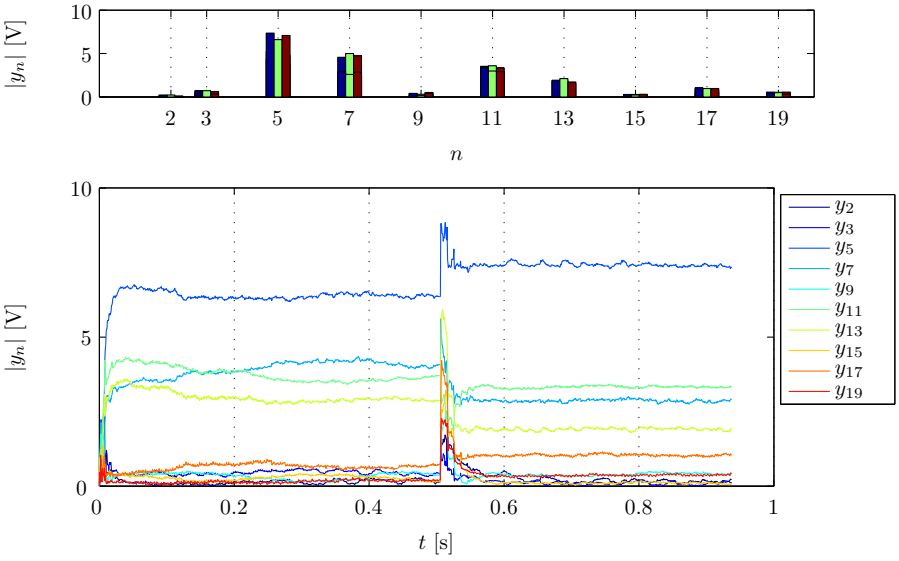

Figure 4.23: *Harmonic estimates for nonlinear grid with phase shift*

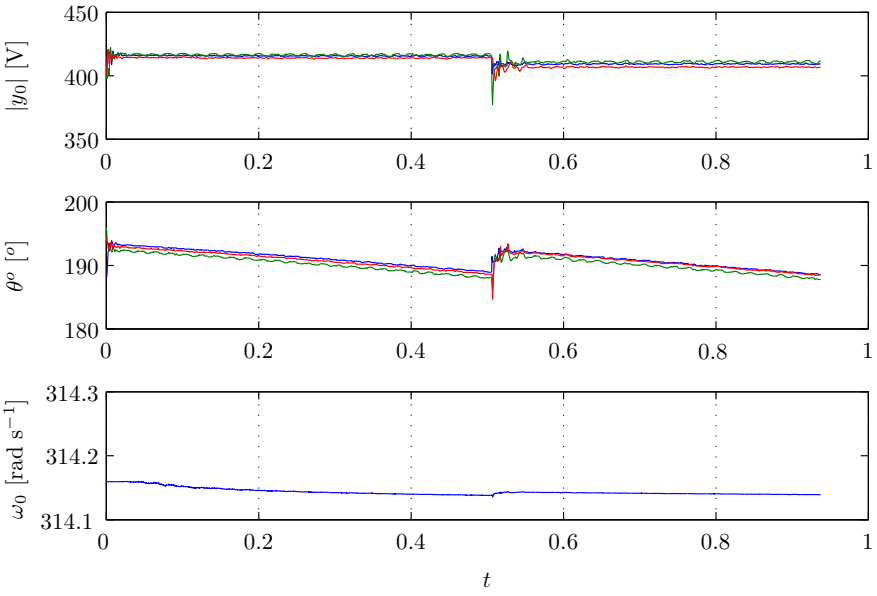

Figure 4.24: *Parameter Estimates for nonlinear grid with phase shift*

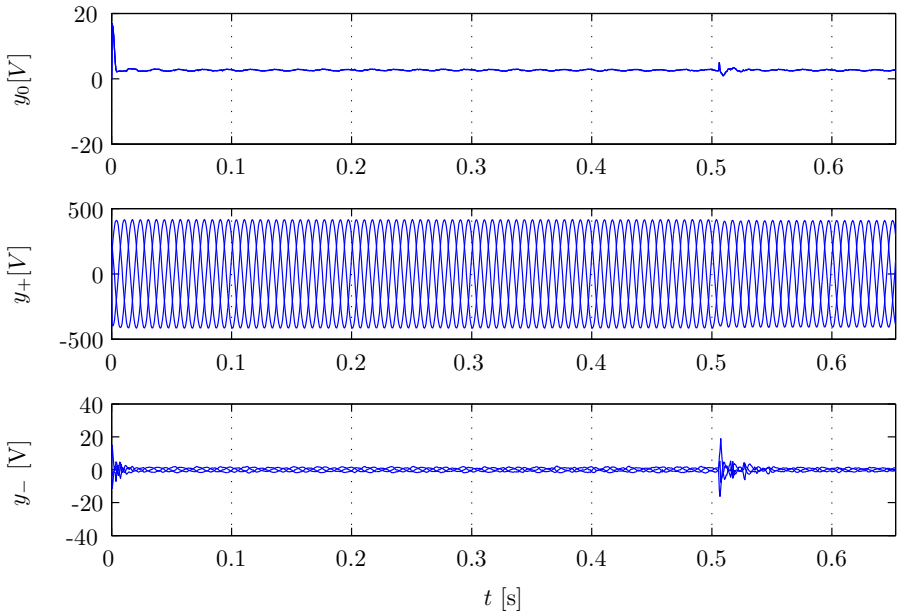

Figure 4.25: *Sequence decomposition for nonlinear grid with phase shift*

shifts, the time constraint is the convergence of the parameter values to the new values, in particular the fundamental amplitude estimates, A_0 and B_0. The forgetting factor for this parameter has been set to 1/10th of a cycle, so, if it does converge, it will converge within that time. This has been shown to be fairly resilient and resistant to noise in the simulated case. For measured data, the estimate and residuals are shown in Figure 4.22 on page 48. The harmonics are shown in Figure 4.23 on the previous page. The sequence filtering near the phase shift is shown in Figure 4.26 on the facing page is useful in this case as well, because the estimates have some overshoot when the phase jump occurs. The sequence remove some of this error, while spreading the correct information across the phases.

4.2.4 Unbalanced Grid

An unbalanced grid is an extremely difficult situation for the estimator to handle. The optimal reaction is for the estimator to register the voltage change as quickly as possible, in a symmetrical way. This is what the estimator does, as can be seen in Figure 4.27 on the next page, Figure 4.30 on page 53, and Figure 4.31 on page 53. The sequence extraction actually slows the convergence down in this case, but in this kind of situation, it is better to be conservative. It is interesting to note that two of the higher harmonics pick up a lower frequency

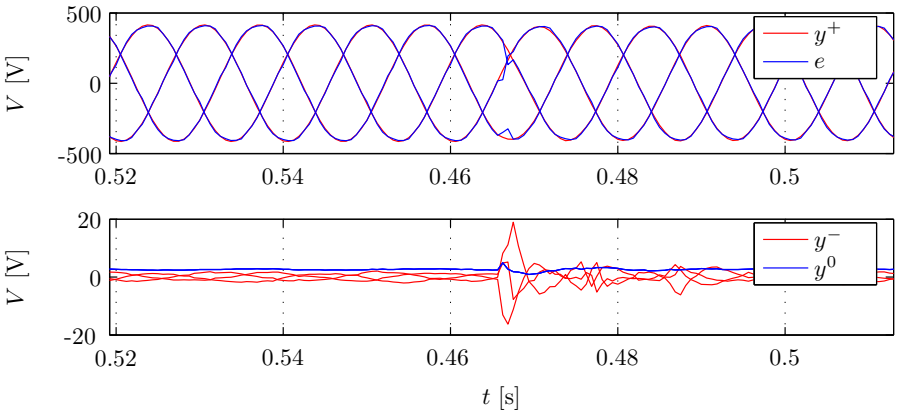

Figure 4.26: *Sequences near disturbance for nonlinear grid with phase shift*

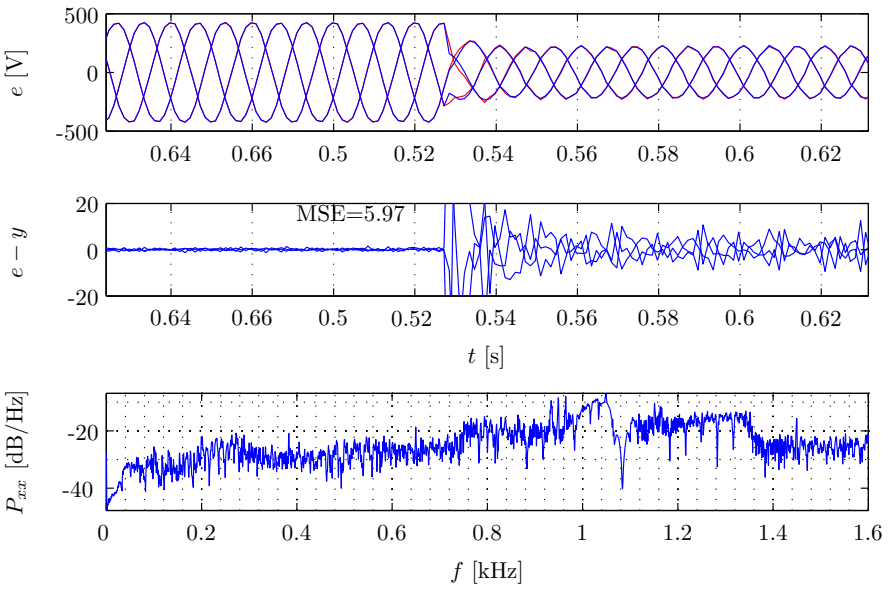

Figure 4.27: *Estimate, residual, and residual spectrum for unbalanced grid*

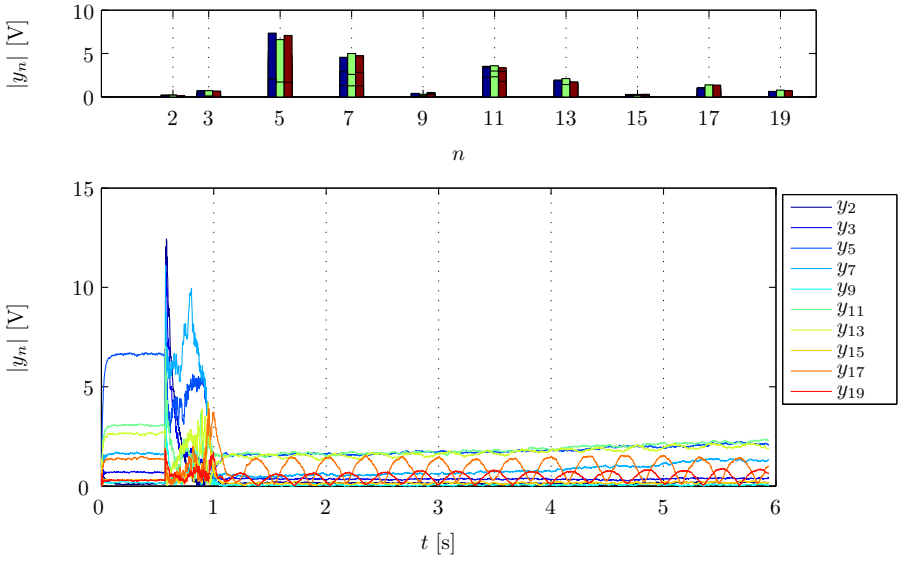

Figure 4.28: *Harmonic estimates for unbalanced grid*

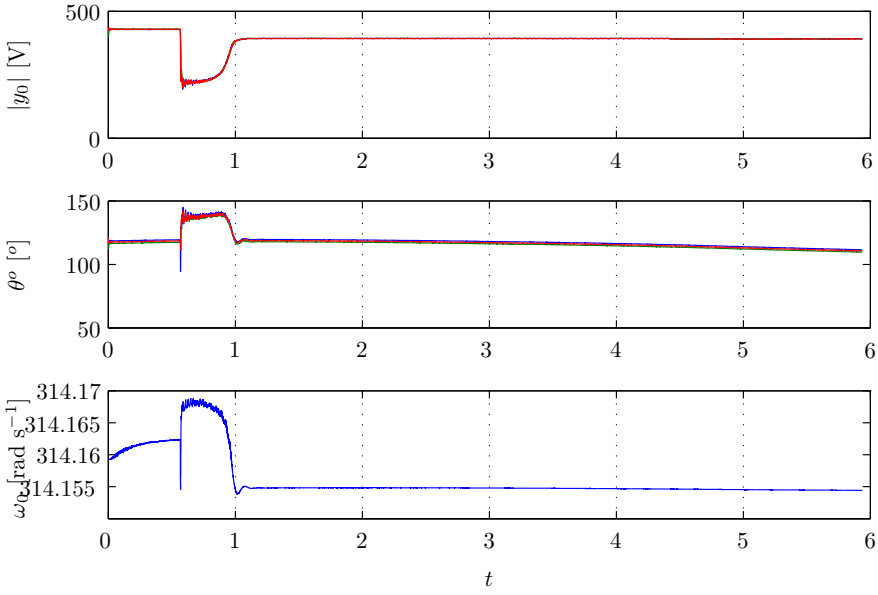

Figure 4.29: *Parameter Estimates for unbalanced grid*

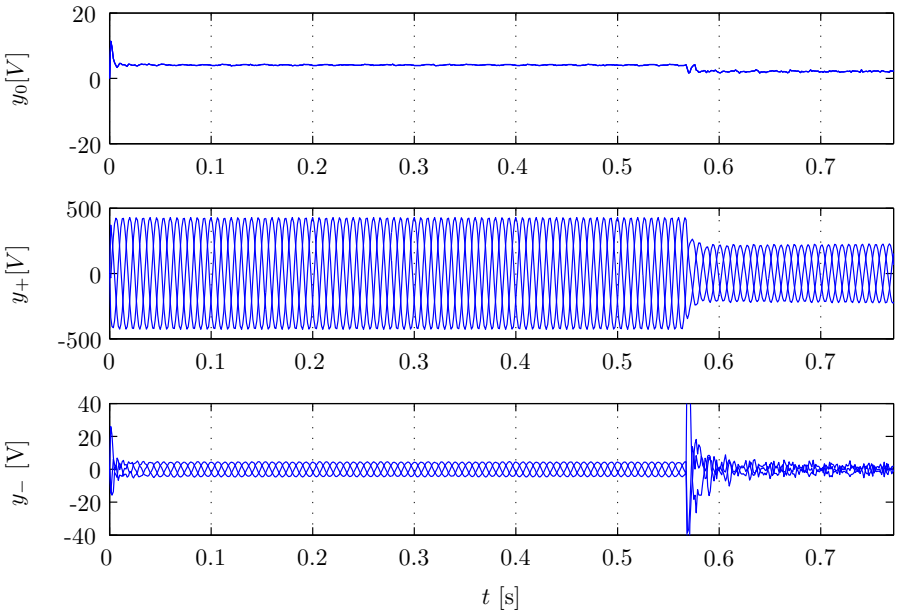

Figure 4.30: *Sequence decomposition for unbalanced grid*

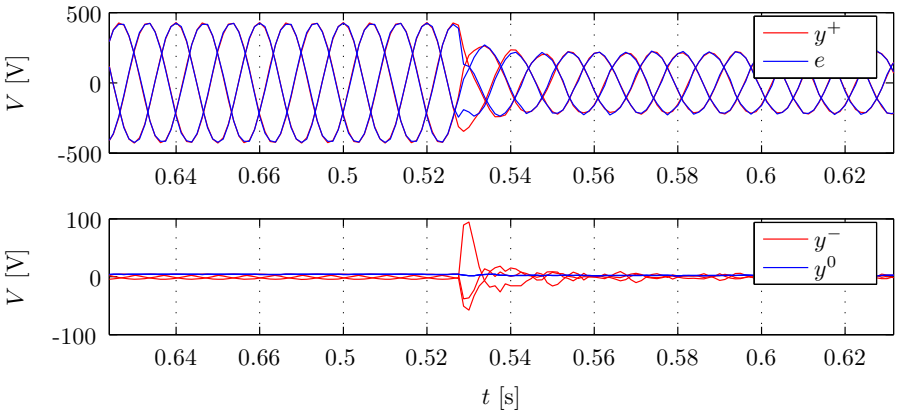

Figure 4.31: *Sequences near disturbance for unbalanced grid*

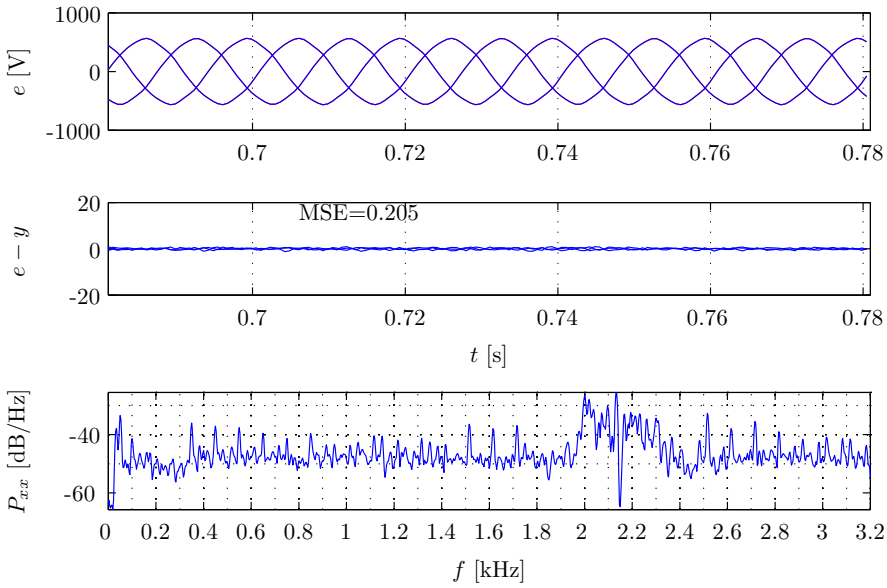

Figure 4.32: *Estimate, residual, and residual spectrum for wind turbine voltage*

after the power event, in Figure 4.28 on page 52. This may not be an actual phenomena, but a result of the convergence of the parameters. It can also be seen in the residuals. It does not appear to effect the final filtered estimate, and should eventually dissipate. Unfortunately, this could not be ascertained because the measurements end quickly.

4.2.5 Wind Turbine

The estimate of the voltage at the terminals of the wind turbine generator during normal operation is shown in 4.32. The harmonic estimate is shown in 4.33 on the facing page, where the third harmonic is seen to be much larger than would be expected. This is also seen in the power spectral density in Figure 4.4 on page 33. The residual spectrum for this estimate has a lot of sharp harmonic components. These are probably harmonics which occur during the connection, and as long as the fundamental is not disturbed, it is not important to follow them. However, if more dynamic information was desired about the cut in harmonics, it would be necessary to include additional harmonics in the estimate.

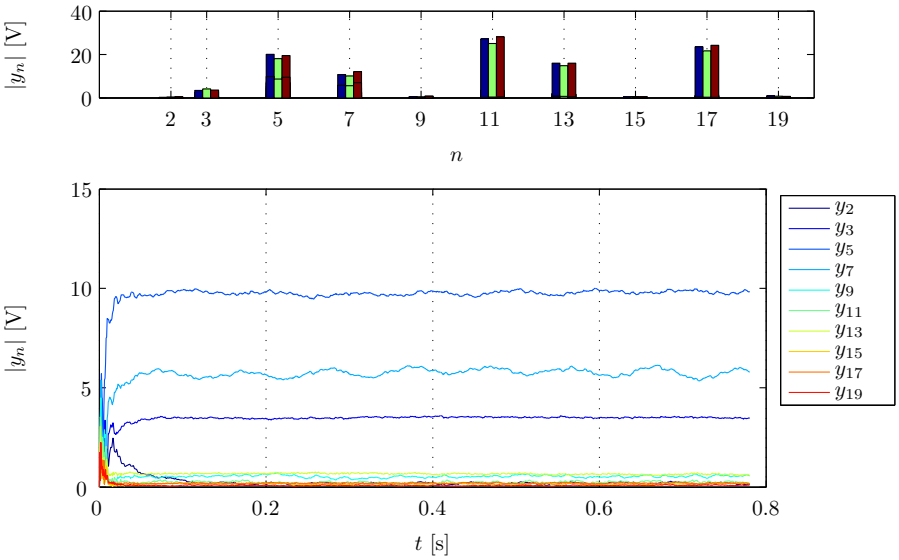

Figure 4.33: *Harmonic estimates for wind turbine voltage*

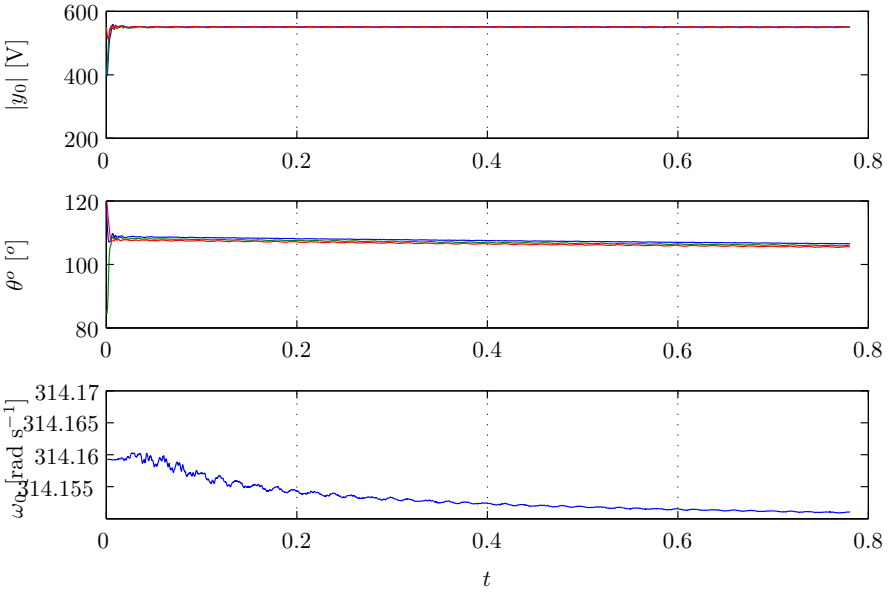

Figure 4.34: *Parameter Estimates for wind turbine voltage*

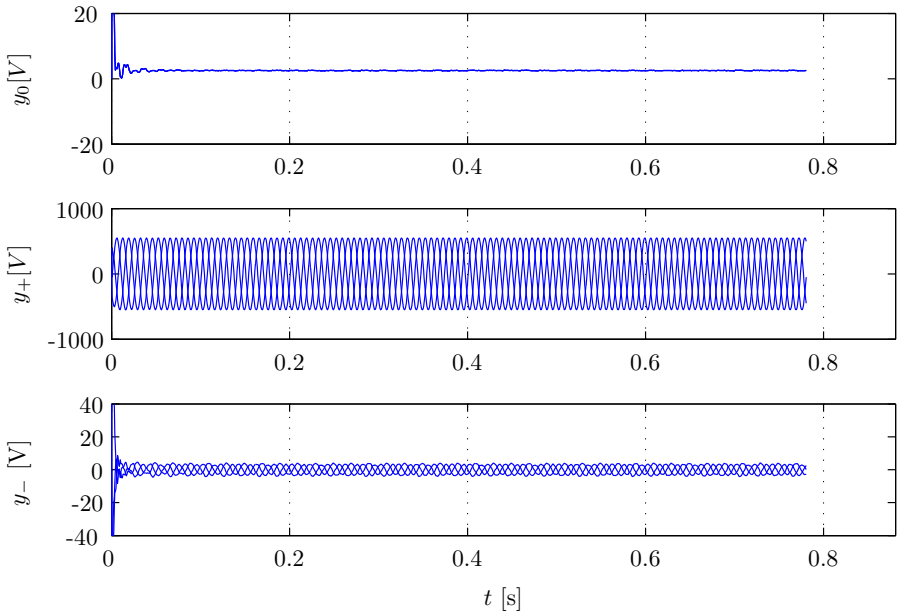

Figure 4.35: *Sequence decomposition for wind turbine voltage*

4.2.6 Wind Turbine Cut-in

The measurements for this situation have been taken at the RisøNordtank wind turbine, on a day with light wind. Therefore, it has been possible to catch a cut-in and cut-out event.[2] The measurements for this data have been taken with a sampling frequency of 3200 Hz.

The estimation results for the case of a wind turbine connecting to the grid is shown in 4.36 on the facing page. It can be seen in Figure 4.37 on the next page that there are a lot of harmonics during the cut in, which are picked up in the estimates of A and B. However, the positive sequence removes most of these variations, as shown in Figures, 4.39 and 4.40.

It is noted that there appear to be some nonlinear components in the voltage after cut-in, but not during normal operation. This may be the presence of a test SVC, which was installed at Risøseveral years ago, and may still be operating. The cut off series was not analysed because it is not very disruptive.

[2]This is quite an old turbine, so it's electrical performance should not be taken as an indication of the performance of all turbines!

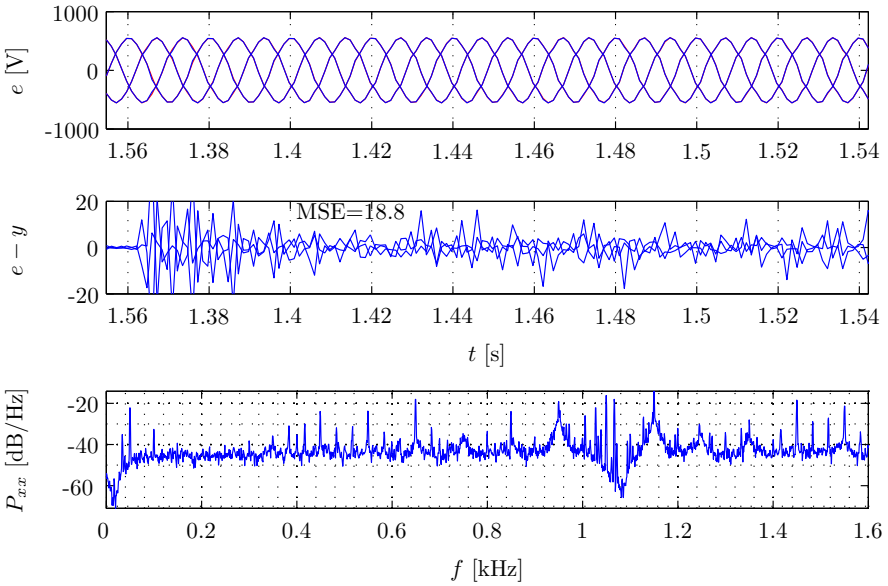

Figure 4.36: *Estimate, residual, and residual spectrum for wind turbine cut-in voltage*

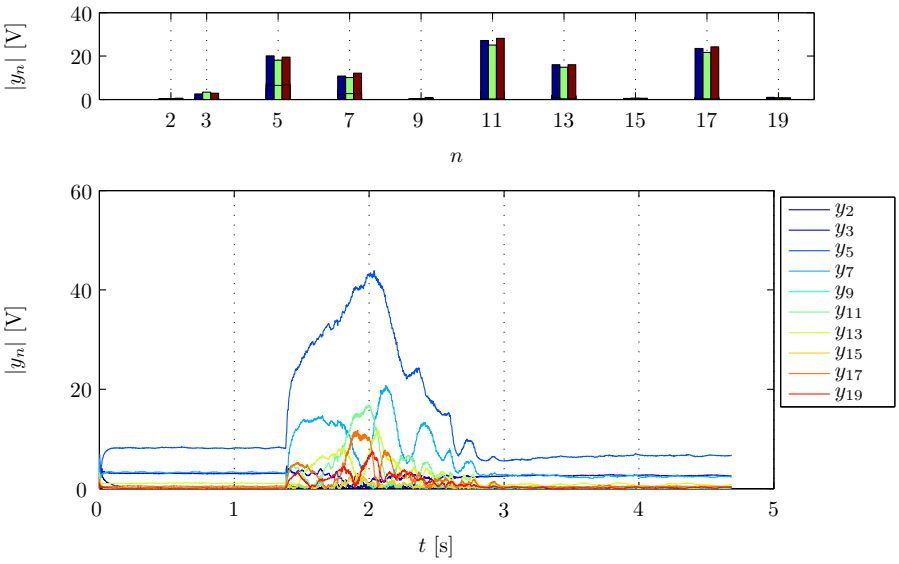

Figure 4.37: *Harmonic estimates for wind turbine cut-in voltage*

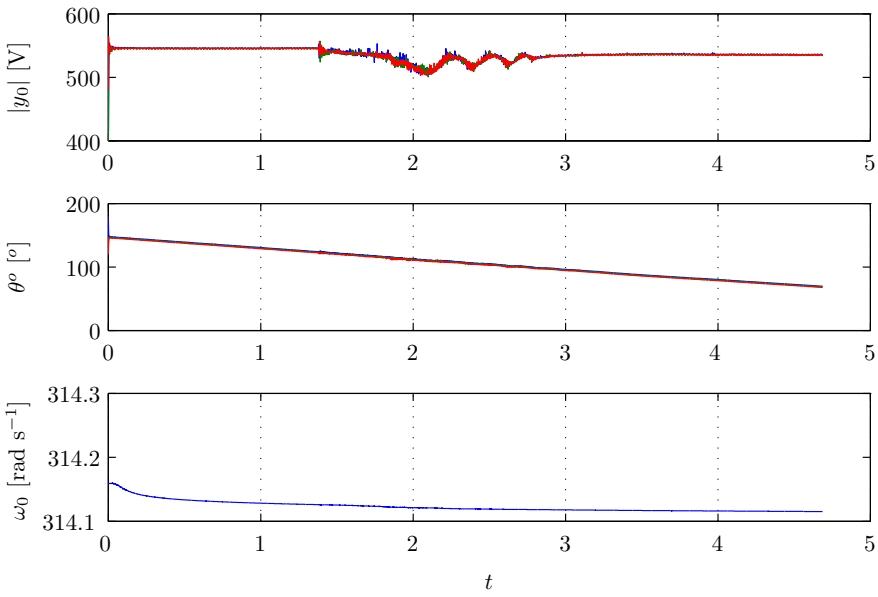

Figure 4.38: *Parameter Estimates for wind turbine cut-in voltage*

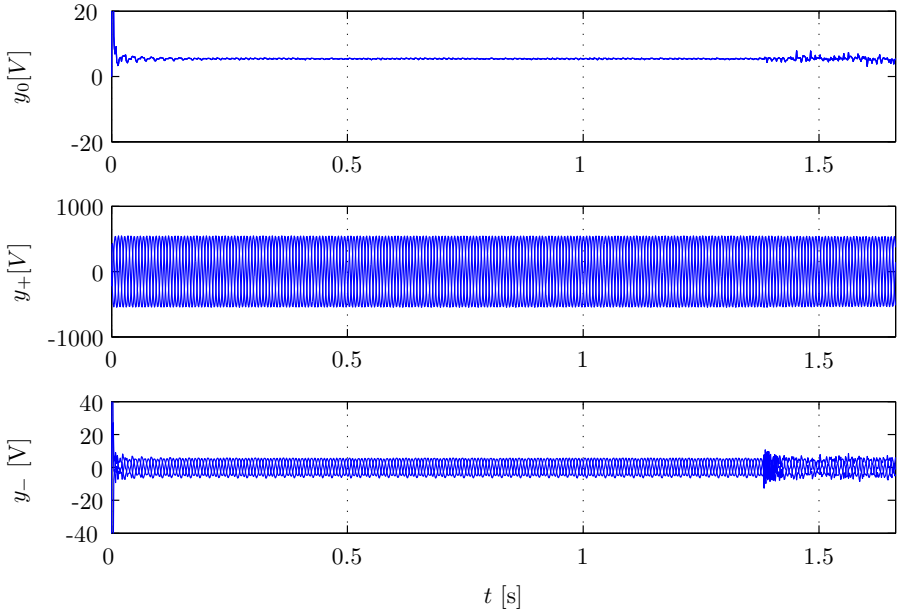

Figure 4.39: *Sequence decomposition for wind turbine cut-in voltage*

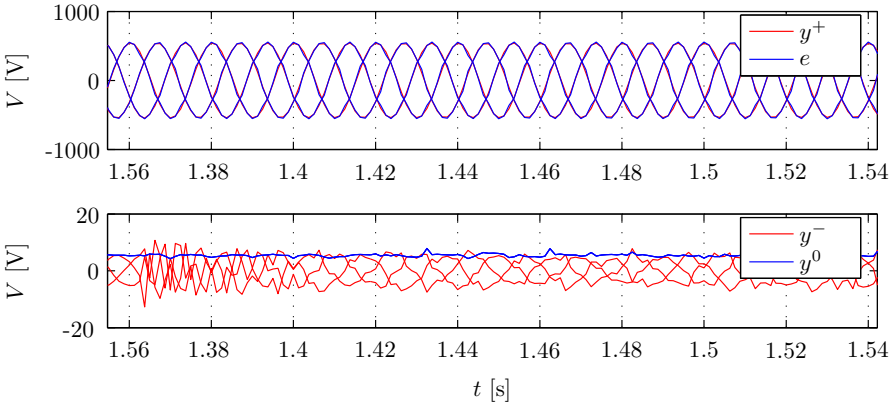

Figure 4.40: *Sequences near disturbance for wind turbine cut-in voltage*

Chapter 5

Adaptive filtering in control

5.1 Harmonics in Transformations

When discussing harmonics in the context of reactive power compensation, it should be understood that the goal of the ASVC has historically been to compensate only for the RMS value of the reactive current, as reactive power is not really defined as an instantaneous value. There is further discussion of this topic in [14] and [5].

Therefore, the goal of an ASVC is to compensate for the current which is out of phase with the fundamental voltage, while remaining insensitive to harmonics in the grid voltage. Though active components tend to have a larger harmonic component, it is possible for harmonics to occur in reactive current. However, when there are harmonics in the grid voltage, they will initiate harmonic fluctuation in the active current of a constant load (or vice versa). Though the same thing may occur with reactive current, it is assumed that the magnitude of the effect of reactive current harmonics on voltage is small enough to neglect.

In order to explore this a little bit more in a real system, the $\alpha\beta$ and pq components of the wind turbine in normal operation are shown in Figures 5.1 and Figure 5.2 on the next page. The values for a filtered system are also

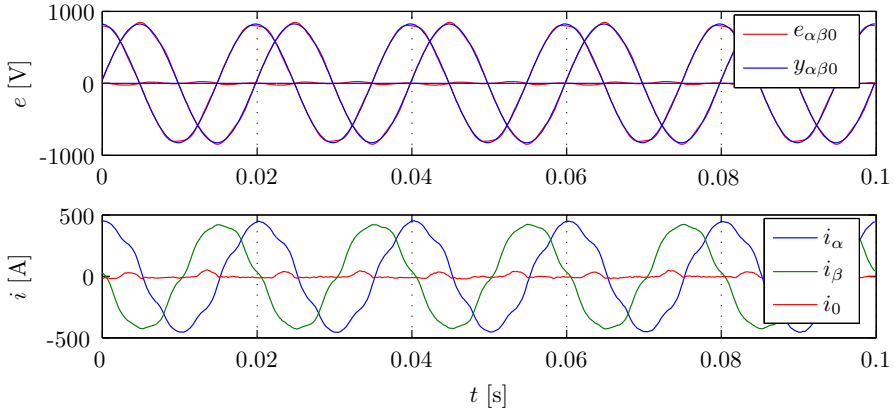

Figure 5.1: *$\alpha\beta$ components of wind turbine voltage and current*

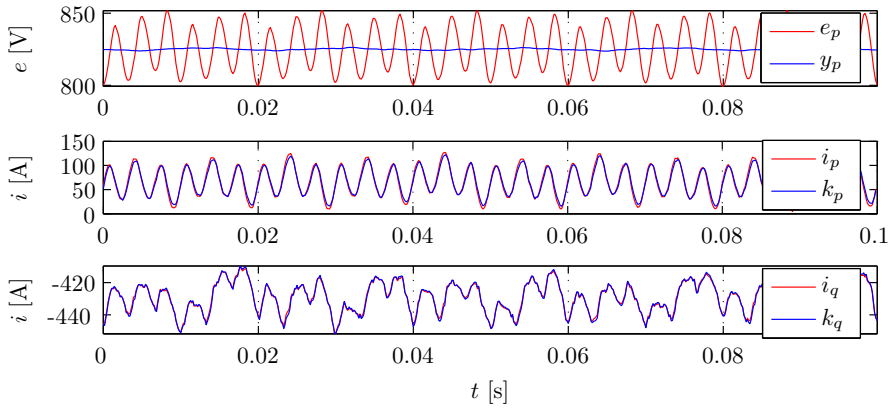

Figure 5.2: *pq components of wind turbine voltage and current*

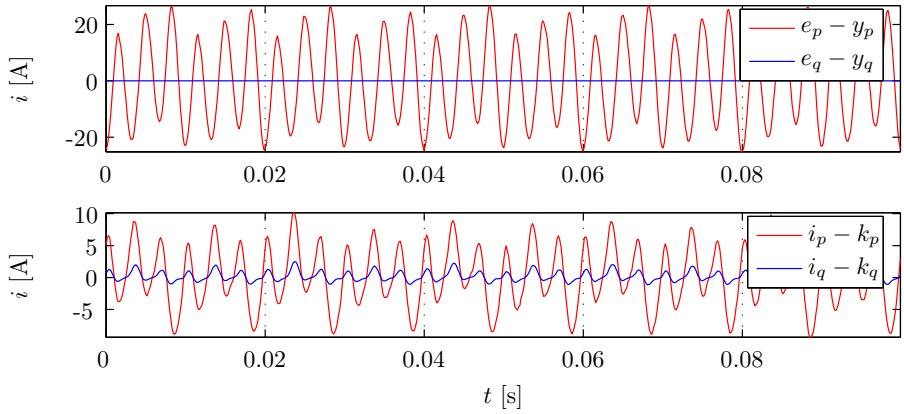

Figure 5.3: *pq components of wind turbine voltage and current*

included in these plots, where y_0 is the RPEM filtered voltage, and k is the current calculated using the filtered voltage as a reference. It can be seen that there is a large difference between the two, with some harmonic components appearing the k values. This occurs because the harmonic components of the active current are not in phase with the fundamental component of the voltage. Therefore, they are included in the computed value of the reactive current, yielding an incorrect value.

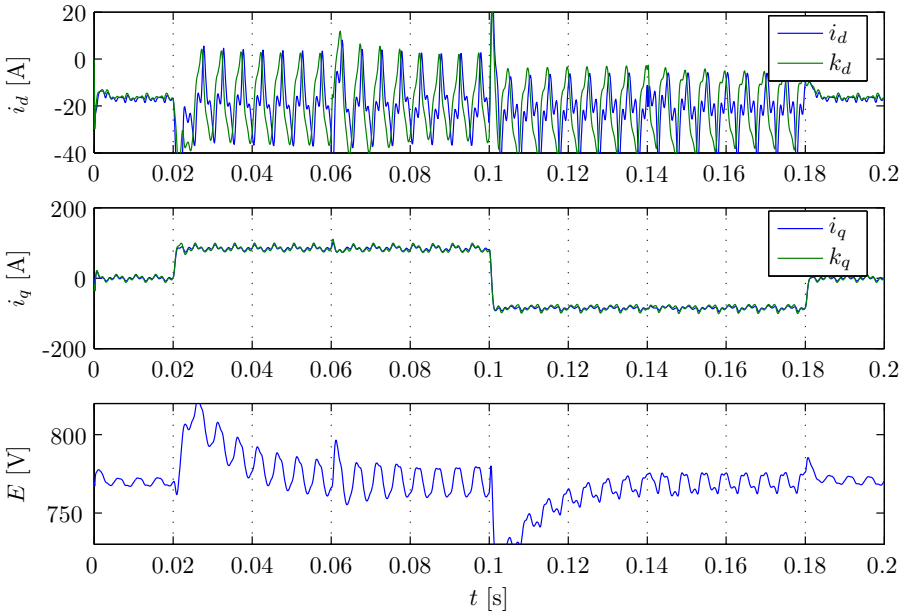

Figure 5.4: *States for gain scheduled integral state space control with harmonics*

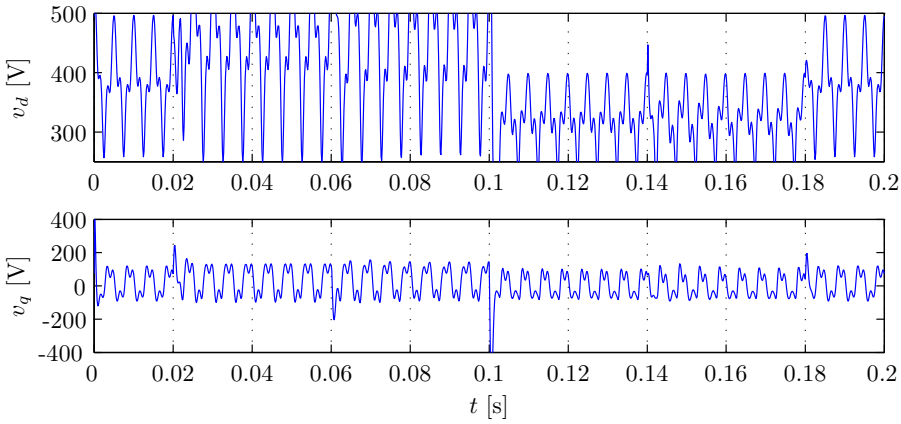

Figure 5.5: *Inverter voltages for gain scheduled integral state space control with harmonics*

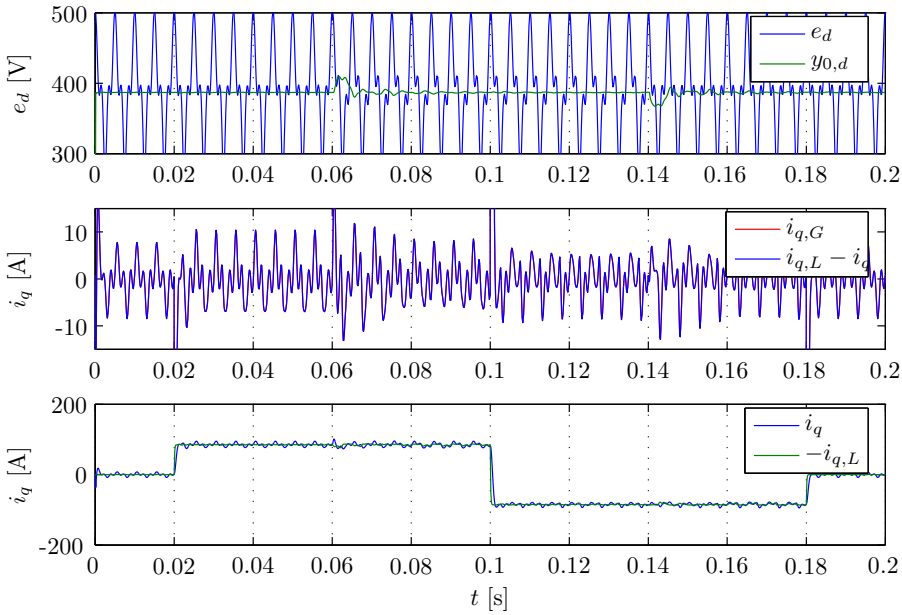

Figure 5.6: *Grid voltage and reactive currents for gain scheduled integral state space control with harmonics*

5.2 Effect of harmonic distortion on Control

When harmonics are present in the voltage, the control system attempts to react to them. For lower harmonics, this may be possible, but at some point the harmonics are changing the voltage faster than the system can control it, leading to a degradation of the quality of the output. When there are harmonics in the grid voltage, the control of the capacitor is also adversely affected, and even less able to track the variation because of the relatively slow time constant on the DC voltage control.

Generally, harmonics are removed by filtering the input voltage, but because lower harmonics are relatively close to the fundamental, this creates a significant phase delay in the measurement data, in effect creating a lag in the control. It is possible to compensate for this lag, but with changing grid frequency, and phase jumps, this is not always possible. The effect of a phase jump is also problematic, because it changes both the direct and quadrature reference voltages at the same time, magnifying the cross coupling in the system.

The effect of harmonics and phase shifts on the control system have been simulated in Matlab, as shown in Figure 5.4 on the preceding page, Figure 5.5 and Figure 5.6. The same reactive power variation as used in the previous simulations is used, a step of 50 kVar at $t = 0.05$s, -100 kvar at $t = 0.1$s, and

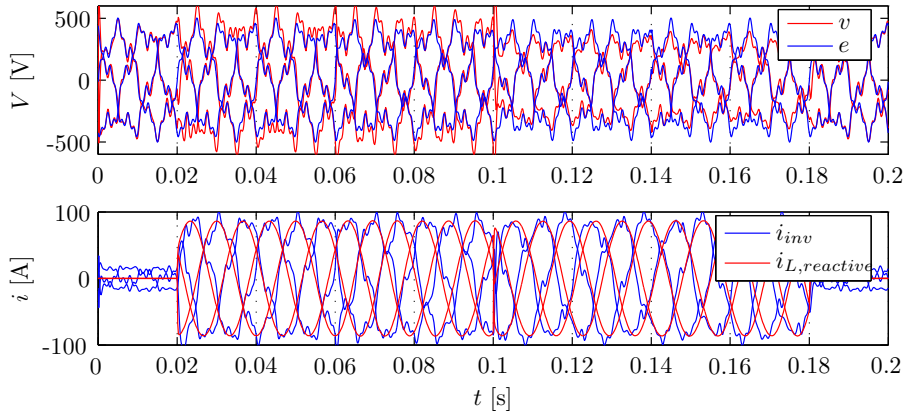

Figure 5.7: *AC voltage and inductor current for gain scheduled integral state space control with harmonics*

50kVar at $t = 0.15$s. In addition, the grid voltage source is given a phase shift of 15^0 at $t = 0.075$s, and back to the original phase at $t = 0.125$s. The harmonic content is constant, with the 5th and 13th harmonic having a relative magnitude to the fundamental of 15% and 10% respectively. The harmonics are generated by the voltage source. All of the following simulations include these disturbances.

It can be seen that all of the state variables in the system have become distorted by harmonics. In particular, the direct voltage and current of the inverter oscillate wildly, in an attempt to keep the capacitor voltage stable. The current flowing into the reactive load in this simulation, has no harmonics, however, it can be seen in Figure 5.7, that the ASVC is actually injecting harmonics into the grid.

5.3 Implementation of Estimator in Simulink Model

Clearly, filtering the grid voltage is necessary to improve the operation of the control system during harmonic distortion. However, when the voltage has been filtered, it is useful to consider the currents in the inverter in reference to the filtered voltage, so that the control system is operating as if on a nonharmonic system. However, this takes care when transforming the currents, as will be seen in the simulations.

The purpose of this thesis has been to design a filter which will improve the control of an ASVC. Thus the estimator must not be disturbed by the actions of the ASVC. The estimator has been implemented as a Matlab block, and placed into the ASVC simulation with the measurement of the grid voltage as input. The fundamental components are estimated and their positive sequence is taken. This is then fed into the Clark transform, and the Park transform. The reference

phase for the park transformation of the grid voltage is then found using the $\alpha\beta$ terms from the filtered voltage. The control is the combined integral and gain scheduling method.

The output of the estimator is the frequency estimate, ω_t, the fundamental cosine amplitude, $A_{0,t}$, and the fundamental sin amplitude, $B_{0,t}$. The positive sequence of the $A_{0,t}$ and $B_{0,t}$ components are extracted using,

$$y_{012} = \frac{1}{3}\begin{bmatrix} 1 & \beta^2 & \beta \\ 1 & \beta & \beta^2 \\ 1 & 1 & 1 \end{bmatrix} (A_0 + \imath B_0) \tag{5.1}$$

$$y_{0,abc} = \begin{bmatrix} 1 \\ \beta^2 \\ \beta \end{bmatrix} y_1$$

$$y_{abc} = \Re\left(y_{0,abc}\right)\cos\left(\omega t\right) + \Im\left(y_{0,abc}\right)\imath\sin\left(\omega t\right)$$

Where β is $\exp\frac{2\pi\imath}{3}$.

The phase angle used in the PLL to convert the load and grid current measurements to the d-q frame is not the filtered one, but rather the arctangent of the unfiltered[1] grid voltage, as was used in the mean model. The inverter currents are transformed using the filtered phase. The sampling period of the estimator is 6400 Hz.

One has to be a little careful here, because now the load and inverter currents do not sum to the grid current, because they are in different reference frames. In order to prevent the active harmonics from polluting the reactive current reference, the harmonic phase must be used, however, if this is used on the grid current, the non-harmonic active current into the inverter will pollute the calculation of the grid reactive current. This affects the choice of control objective, as it is no longer feasible to use zero reactive current into the grid as the objective.

The voltage output of the control system is now the control as if there were no harmonics in the grid. However, there are harmonics at the grid side, and if ignored, they will cause a harmonic current through the transformer. Therefore, it is necessary to offset the harmonics and any estimate error by adding the difference between the filtered and measured grid voltage to the output of the inverter.

The control response for the integral control with gain scheduling and filtering of the grid voltage and inverter current is shown in Figure 5.8 on the next page. It can be seen that the converter is providing a relatively constant reactive current, and that there is much less variation in the capacitor voltage and direct current.

The inverter output voltages are shown in Figure 5.9. The output voltage is clearly smoothed. Note that this measurement was taken before the measure-

[1] A filter could be used to remove much higher frequencies

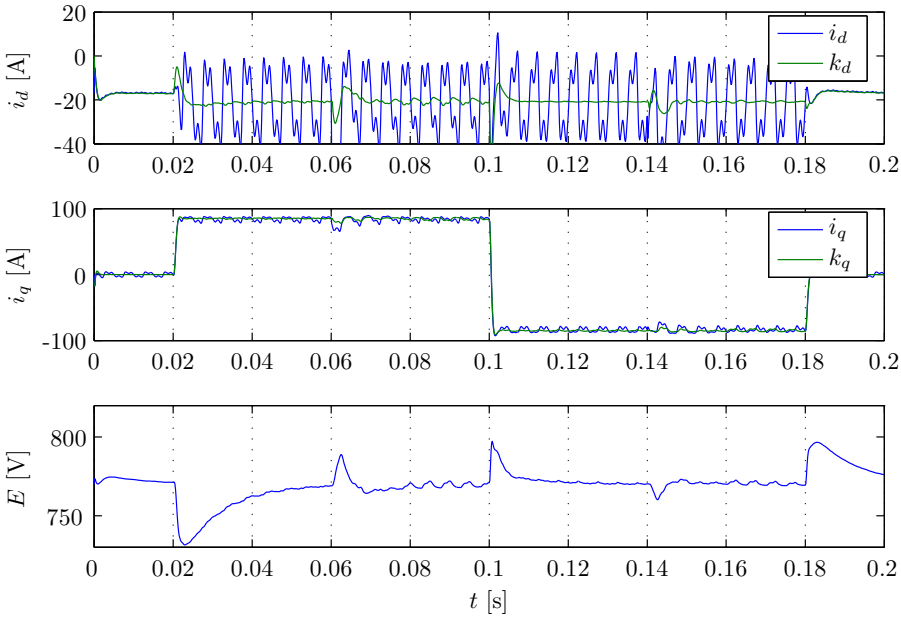

Figure 5.8: *State Variation for estimator control*

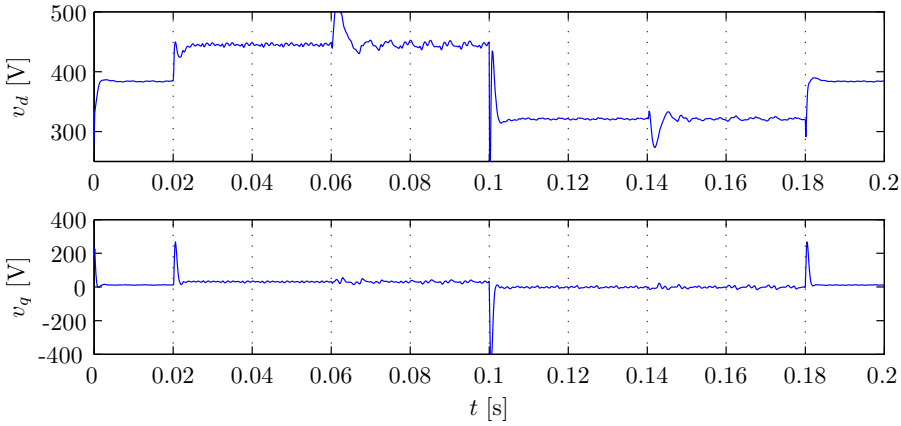

Figure 5.9: *Output variation for estimator control*

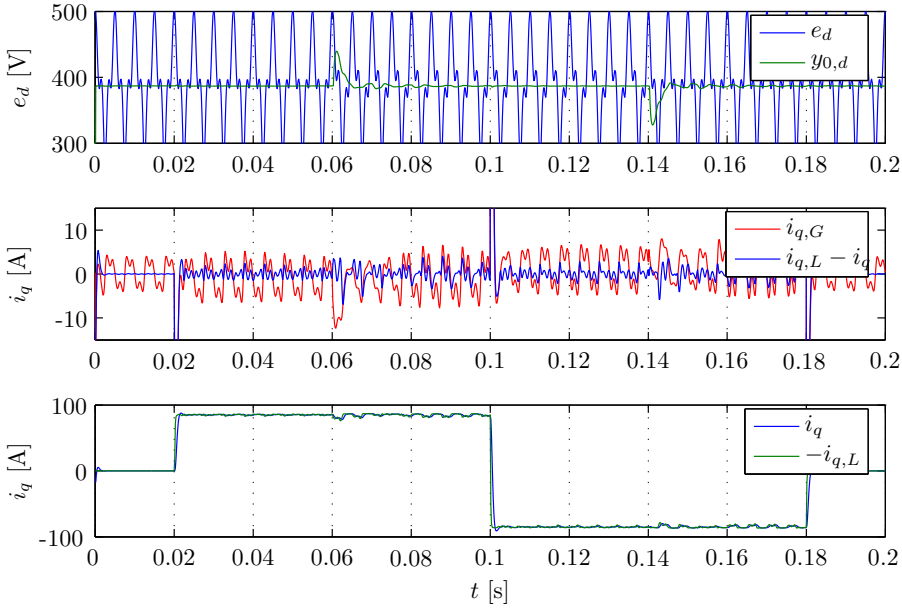

Figure 5.10: *Output voltage and current for estimator control*

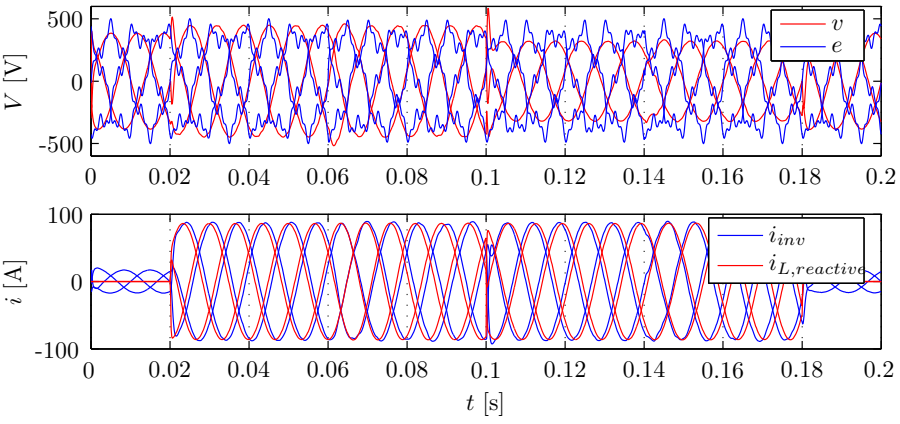

Figure 5.11: *Output voltage and current for estimator control*

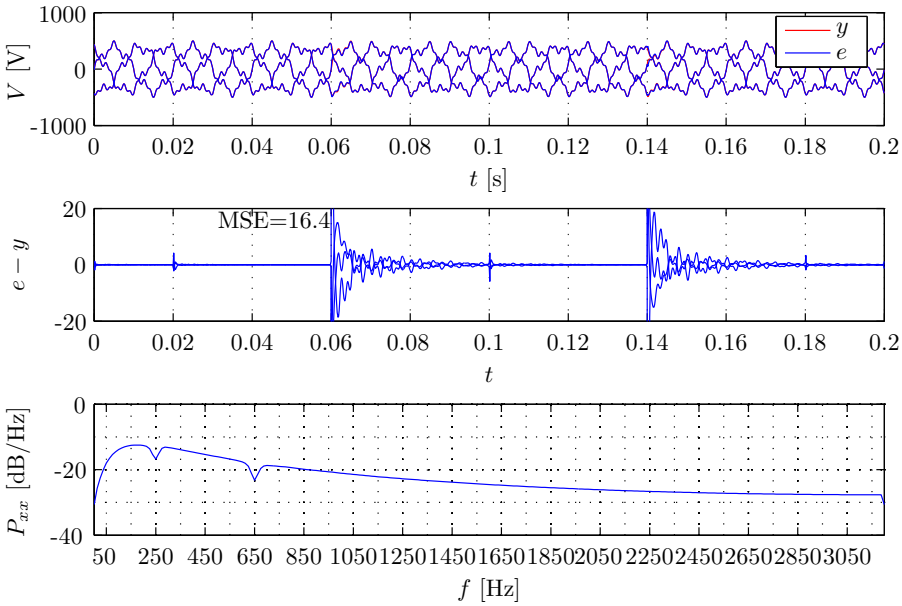

Figure 5.12: *Estimate, residual, and residual spectrum for mean model with estimator control*

ment offset was added back to the voltage, so the actual inverter output would be much more distorted.

The currents in the inductor are shown along with the reactive load current in Figure 5.11 on the facing page. The AC current through the inverter in the lower plot clearly has very few harmonics. This is shown with the load, in order to prove that both the load reactive current and the inverter reactive current are without harmonic distortion. The fact that the the difference between the load and inverter current no longer equals the grid current is also apparent, in Figure 5.10(b). This occurs because the ASVC is now drawing active and reactive current with no harmonics, and in the reference of the harmonic voltage, these are not incorporated correctly.

The results from the estimator are shown in Figure 5.12. It can be seen that the large variation in reactive load does not seem to affect the estimate much. The phase shifts are a notable disturbance, but the estimate recovers quickly, and the control system recovers within a quarter of a cycle, and simply compensates the harmonic component of the current until the estimate settles again.

The fundamental parameter and harmonic estimates are shown in Figure 5.14 on the following page and Figure 5.13 on the next page. The magnitude of the estimates of the harmonics seem to be correct. Though the mean squared error

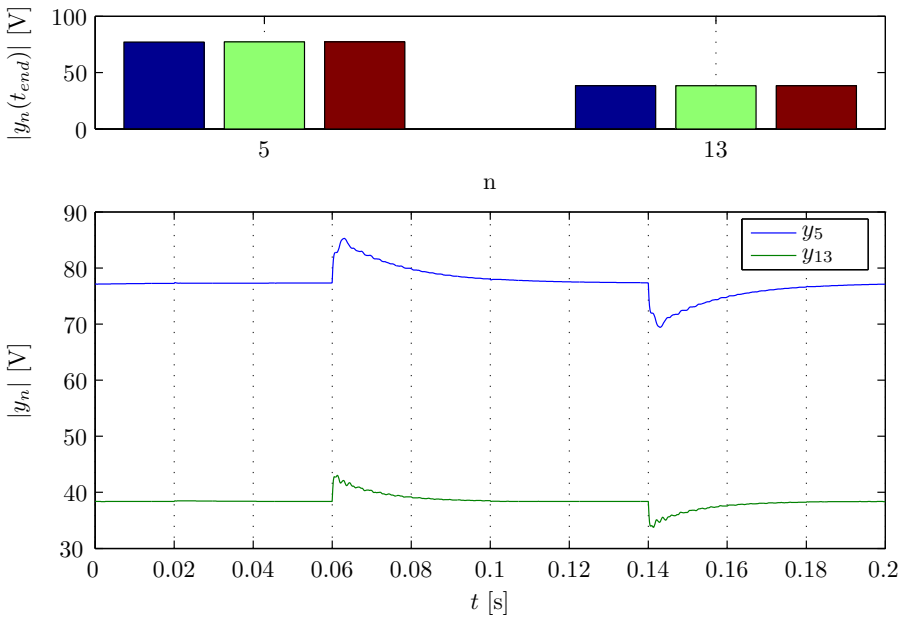

Figure 5.13: *Harmonic estimates for mean model with estimator control*

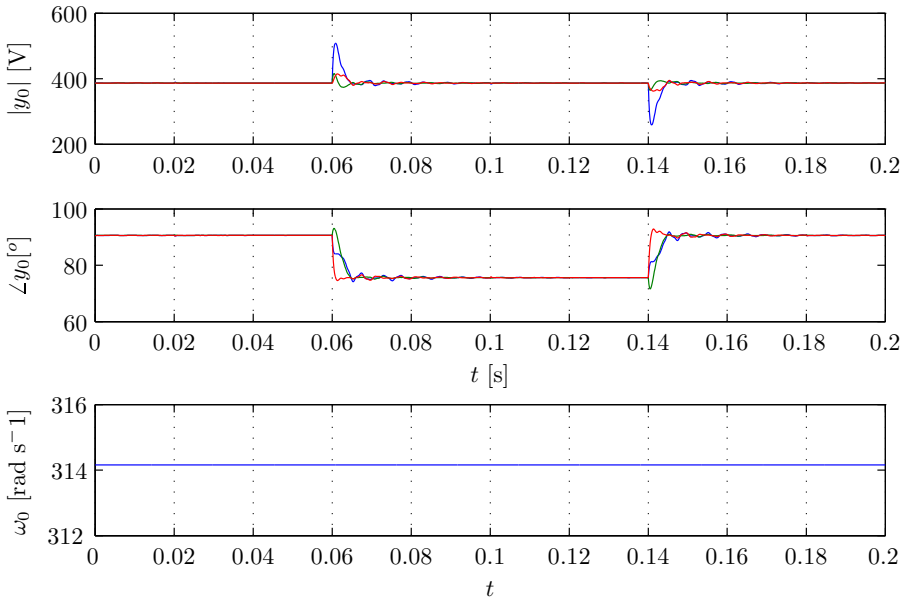

Figure 5.14: *Parameter estimates for mean model with estimator control*

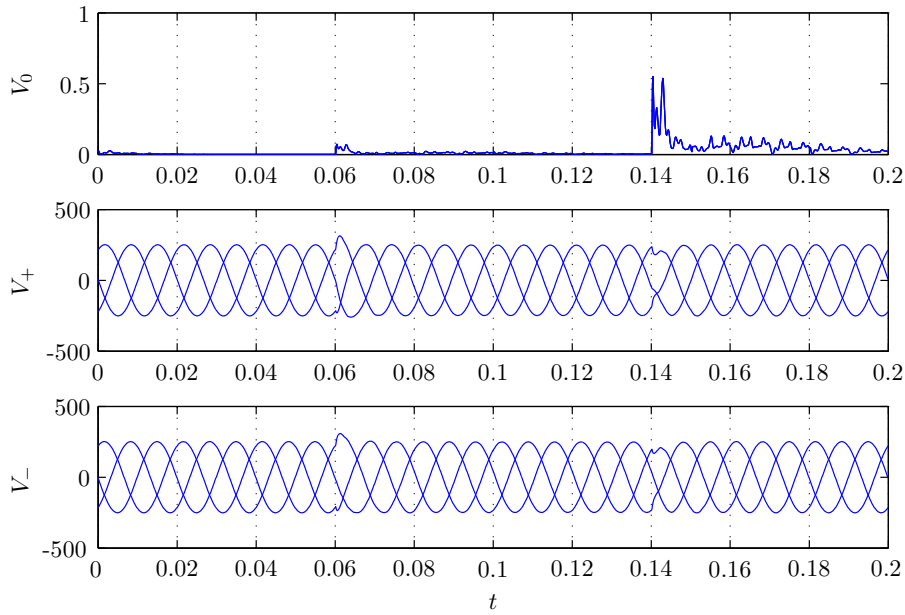

Figure 5.15: *Sequence decomposition for mean model with estimator control*

is a little high, it should be remembered that there are two large phase jumps within a very short period. Finally, the symmetrical three phase voltage which is used for the control system is shown in 5.15.

Chapter 6

Switching Simulation

The simulation is now performed on a Simulink power-systems model which includes pulse width modulation and a Simulink Power Library model of a universal bridge, with IGBT's and diodes. The model for the ASVC is shown in Figure 6.1. The parameters for the switching simulation are shown in Table 6.1. Pulse width modulation has been used for this simulation. It is not the state of the art, but is quick and easy for demonstrating the viability of this system. The state of the art approach would be some sort of space vector modulation, however, this has not been attempted in this project.

The snubber sizes, and component resistance were determined for a ±100 kVar inverter. The t_T and t_f are said to be the rise and fall time in the Matlab documentation, but the name along switching problems suggest that t_T is actually the tail time, and this is what has been used. The switching frequency

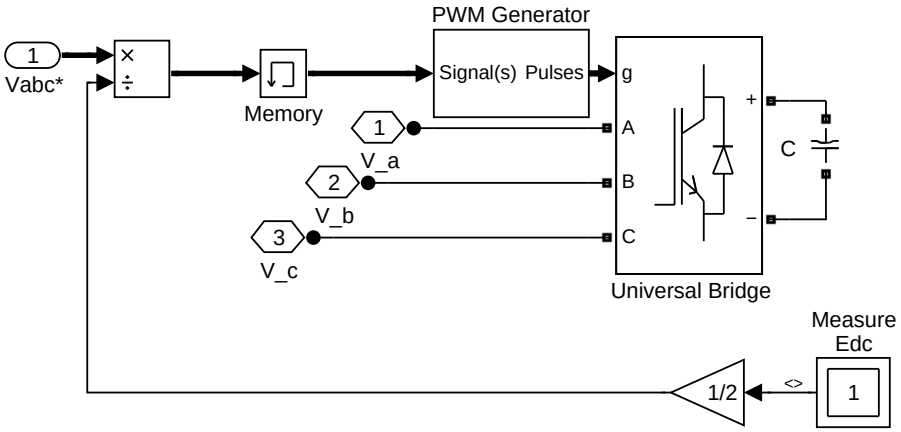

Figure 6.1: *Simulink Power Systems model of switching ASVC*

R_{snub}	C_{snub}	R_{on}	t_f	t_T	f_s
1.8Ω	86nF	10 mΩ	100ns	39 nS	10 kHz

Table 6.1: *Parameters used for PWM ASVC simulation*

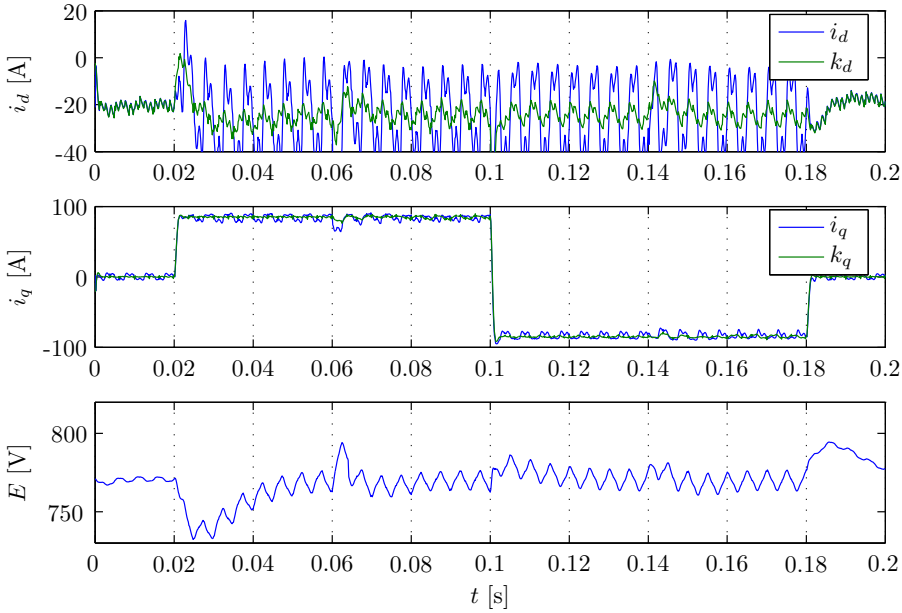

Figure 6.2: *States for switching model filter*

is a reasonable value for PWM in practice, though it may be a little higher than normal. Because there were no analog filters used in this project, it was beneficial to have a higher switching frequency.

6.0.1 Switched Model Controlled With Adaptive Filter

Finally, the control is implemented in the switching model, including the adaptive filtering. The input parameters are shown in Figure 6.3 on the next page. The state variation is shown in Figure 6.2. The capacitor voltage has quite a bit more variation, which may be due to some inverter dynamics which have not been modelled. However, the oscillation is not nearly as much as in the non filtered system in Figure 5.4.

It can be seen in Figures 6.4 and 6.5, that the output reactive current of the inverter is approximately constant, even though its reference current, $i_{q,L}$ actually has harmonic components. This is exactly what the goal of this control has been. There is clearly some noise in the system, and some high frequency filters would certainly be helpful to clean up the operation.

The comparison of the filter estimate with the actual measurement is shown in Figure 6.6 on page 76, along with the residuals and residual spectrum. The fundamental parameter estimates are shown in Figure 6.8 on page 77. The harmonic estimates are shown in Figure 6.7 on page 77. Finally, the sequence

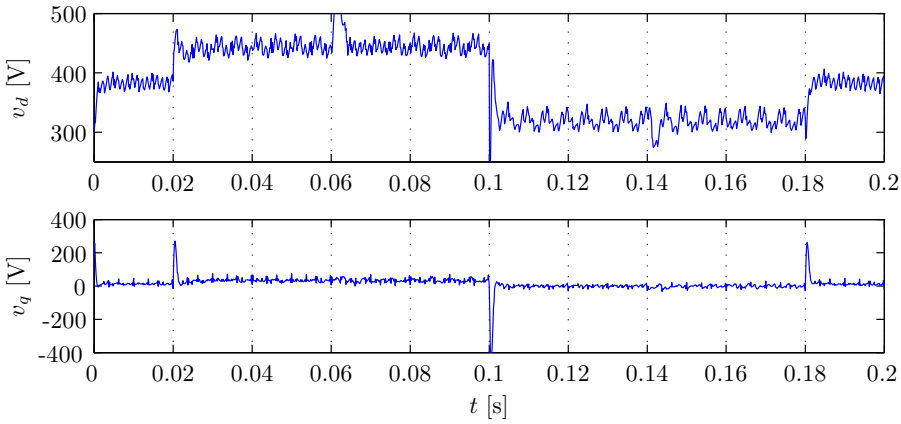

Figure 6.3: *Inverter voltages for switching model filter*

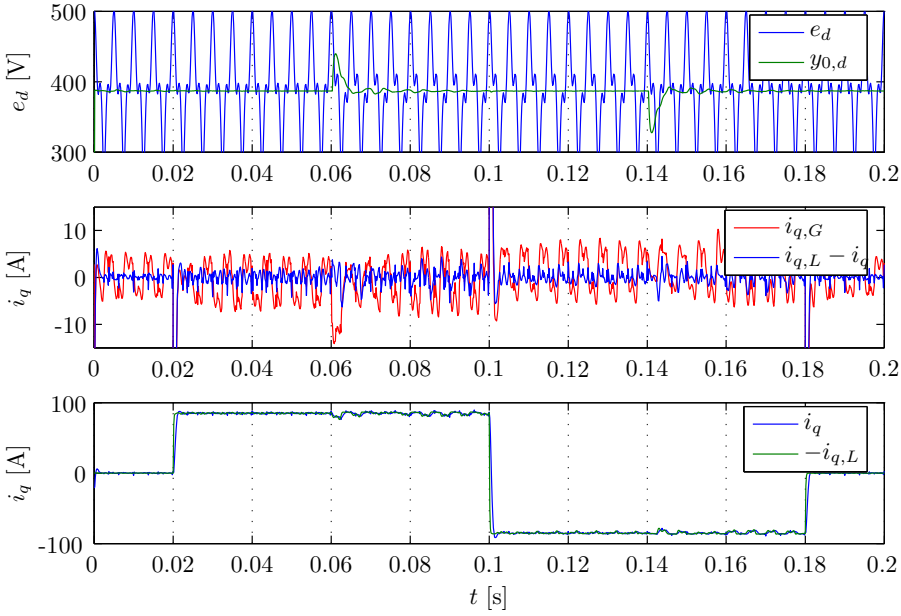

Figure 6.4: *Grid voltage and reactive currents for switching model filter*

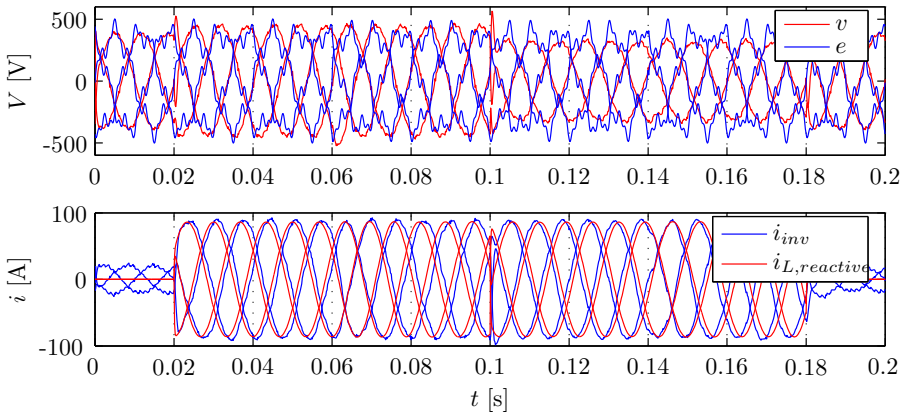

Figure 6.5: *Output voltage and current for switching model with filter*

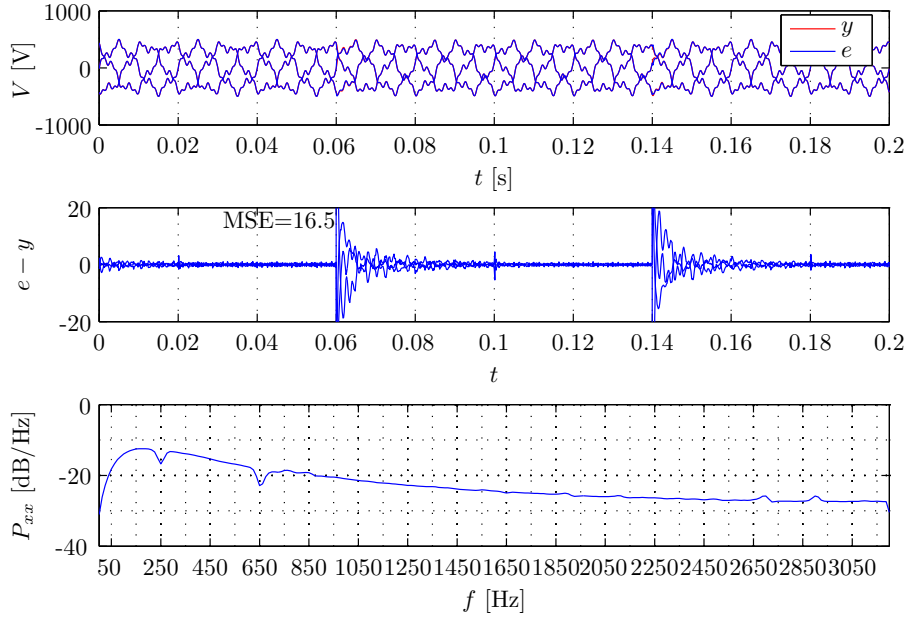

Figure 6.6: *Estimate, residual, and residual spectrum for switching model with filter*

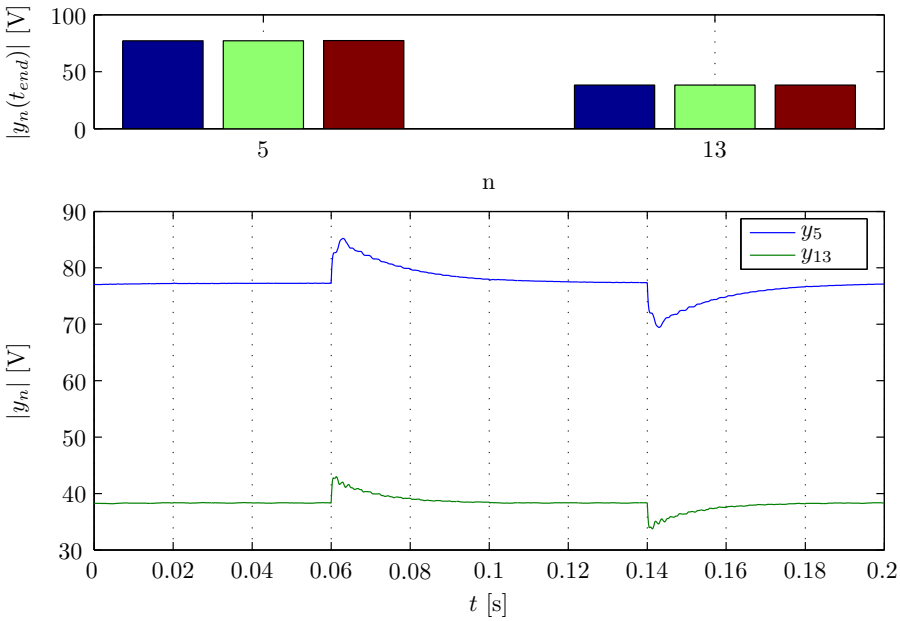

Figure 6.7: *Harmonic estimates for switching model with filter*

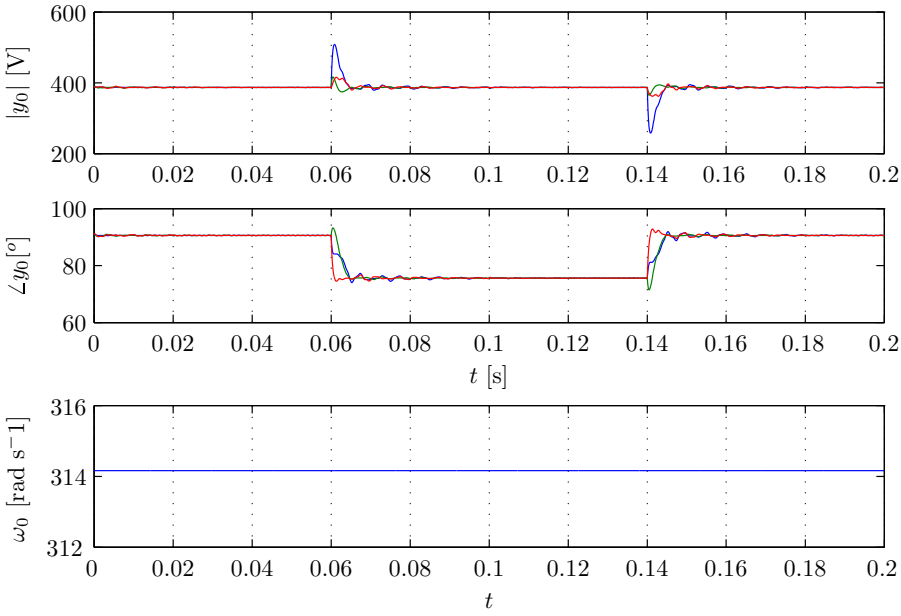

Figure 6.8: *Parameter estimates for switching model with filter*

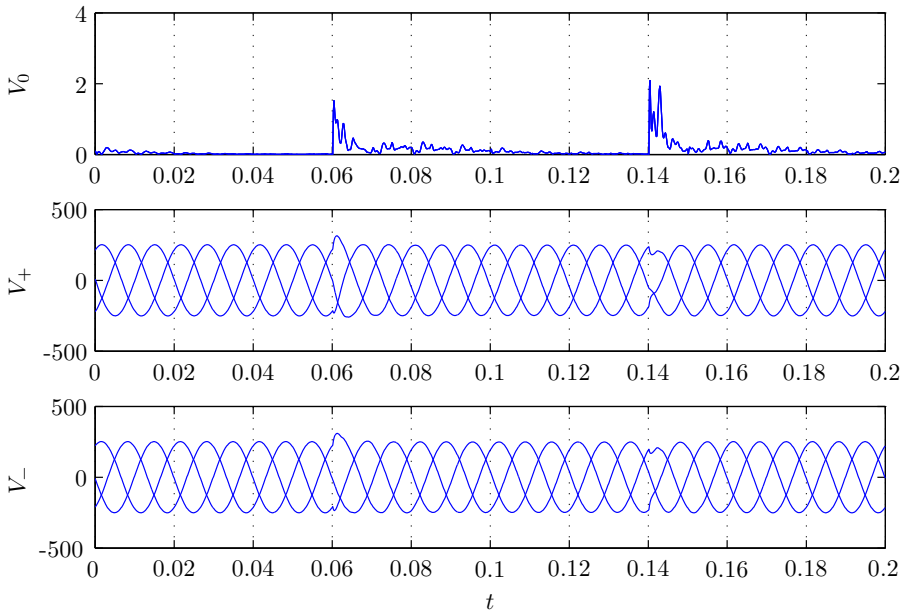

Figure 6.9: *Sequence decomposition for switching model with filter*

extraction is shown in Figure 6.9. The estimation during the switching simulation seems to be as good as the one where there is no switching. The only harmonics estimated in the Simulink implementation are the ones which have been injected into the voltage, which had a limit of two, but the previous tests should show that the filter can withstand quite large disturbances.

The estimating system is able to handle phase jumps, with the largest change occurring in the capacitor voltage, and returning to normal within less than a quarter of a cycle. The positive sequence clearly does a good job of filtering out the convergence of the estimator.

Chapter 7

Conclusion

An adaptive phase estimator has been developed for use in the context of ASVC control. The harmonic distortion of the 400 V grid has been determined by taking measurements from the consumer grid in the lab, as well as at a operating wind turbine. The ability of the phase estimator to estimate the full range of measured harmonics has been evaluated, and the significant harmonics for practical purposes have been selected, as shown in 4.2 on page 45.

A basic state space control system with integral action and gain scheduling has been implemented, and simulated in Simulink using the power systems library. Initially, a mean model has been used to develop the control and implement the filtering system. The control system is by no means the most advanced, but it is simple, and improves the operation of the ASVC in comparison to vector control.

It has been shown that by using the filtered phase in the park transformation of the grid voltage and inverter current while leaving the harmonic components in the phase reference for the park transformation of the load current, the ASVC can be made insensitive to harmonic distortion.

The system has been implemented in a switching model, and has performed as expected, suggesting that the assumptions made in this project are acceptable.

7.0.2 Future Work

Future work could involve implementing this control system in a laboratory demonstration. Also, it may be possible to get a better calculation of the reactive currents in the system by subtracting the active currents from the three phase measurements, by using an unfiltered transformation and then using the filtered transformation to find the quadrature value. However, the gains from this operation may not be worth the extra calculations.

Additionally, though processor speed is a moving target, it would be important to compare the time required to calculate the voltage estimate with the frequency used in this simulation. If not feasible, the sensitivity of the estimation to sampling period should be explored.

Chapter A

Appendices

A.1 Three phase transformations

In the analysis of active and reactive power in the three phase electrical system, there are several transformations which are useful for extracting information about the system. These transformations, and the assumptions that are made are integral to the control of reactive power, and can be used on both voltage and current. For this project, because of the use of the Matlab Powerlib, the American standard for phase naming has been used, with $\theta_b = \theta_a - 2pi/3$ and $\theta_c = \theta_a + 2\pi/3$. However, all transformations will be kept in a general form here to avoid confusion.

A.2 Clark Transformation

The Clark transformation is used to allow interpretation of the three phase system as a single phase. The transformation is simply the sum of the projections of the three phases on a two dimensional cartesian axis, as shown in figure A.1 on the following page.

$$\begin{bmatrix} \hat{x}_\alpha \\ \hat{x}_\beta \end{bmatrix} = c \begin{bmatrix} \cos(\theta_a) & \cos(\theta_b) & \cos(\theta_c) \\ \sin(\theta_a) & \sin(\theta_b) & \sin(\theta_c) \end{bmatrix} \begin{bmatrix} \hat{x}_a \\ \hat{x}_b \\ \hat{x}_c \end{bmatrix} \tag{A.1}$$

where c is a constant. When c is chosen as $\frac{2}{3}$, then the length of the voltage and current vectors remain the same. If the constant is chosen as $c = \sqrt{\frac{2}{3}}$, then the power calculated in the $\alpha\beta$ is the same as in the abc frame. Then the system is said to be power invariant. For this project, the non-power invariant system will generally be used.

Clearly, this transformation is only invertible if the actual system is centered on zero, or balanced, and has symmetry between the phases, by having the angles correctly described by θ_a, θ_b, and θ_c. It is possible to include information about the zero phase of the system by finding the resultant of the three phases in the cartesian frame,

$$\begin{bmatrix} \hat{x}_\alpha \\ \hat{x}_\beta \\ \hat{x}_0 \end{bmatrix} = \begin{bmatrix} \cos(\theta_a) & \cos(\theta_b) & \cos(\theta_c) \\ \sin(\theta_a) & \sin(\theta_b) & \sin(\theta_c) \\ \frac{\sqrt{2}}{2} & \frac{\sqrt{2}}{2} & \frac{\sqrt{2}}{2} \end{bmatrix} \begin{bmatrix} \hat{x}_a \\ \hat{x}_b \\ \hat{x}_c \end{bmatrix} \tag{A.2}$$

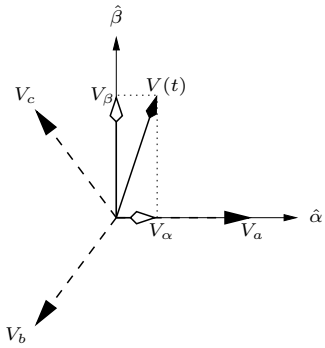

Figure A.1: *Clark Transformation*

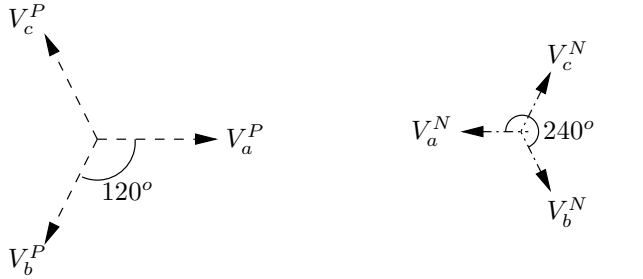

(a)Positive Sequence (b)Negative Sequence

(c) Zero Sequence

Figure A.2: *Symmetrical Components*

A.3 Positive Sequence

In the power system, symmetric balanced conditions are not a good assumption. In fact, in the situations where the control system is most stressed, they are almost certainly not the case. Thus, it is useful to separate the measurements into positive, negative, and zero sequences. The positive sequence is composed of three vectors which are equal in magnitude, 120^o apart, with the sequence, $a \rightarrow b \rightarrow c$. The negative sequence is also symmetric and balanced, but has the sequence, $a \rightarrow c \rightarrow b$. The zero sequence is a measure of the imbalance in the system, and is composed of three vectors which are equal in magnitude, and have the same direction. The algorithm for accomplishing this transformation

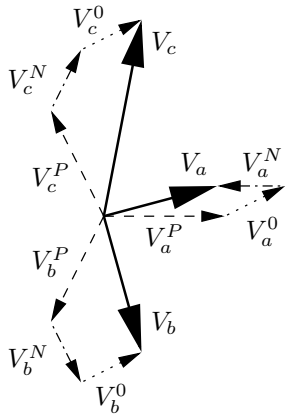

Figure A.3: *Symmetrical Components of an Voltage*

Sequence	Series		Examples
Positive	$h = 6k + 1$,	k=1,2,...	7, 13, 19
Negative	$h = 6k - 1$,	k=1,2,...	5, 11, 17
Zero	$h = 3k$,	k=1,2,...	3, 9 , 15

Table A.1: *Sequences of harmonics*

uses the rotational operator, $e^{\frac{2\pi j}{3}}$, which will be replaced by β in the following equation [16].

$$\begin{bmatrix} \hat{x}_p \\ \hat{x}_n \\ \hat{x}_0 \end{bmatrix} = \frac{1}{3} \begin{bmatrix} 1 & \beta^2 & \beta \\ 1 & \beta & \beta^2 \\ 1 & 1 & 1 \end{bmatrix} \begin{bmatrix} \hat{x}_a \\ \hat{x}_b \\ \hat{x}_c \end{bmatrix} \tag{A.3}$$

An example of a nonsymmetric, nonzero, three phase voltage is shown in Figure A.3. The voltage is actually composed of the same components shown in Figure A.2 on the facing page[9]. It should be understood that the signal which is being transformed must be a complex number in order for this transformation to work properly.

Harmonics of a voltage also have a sequence, as shown in Table A.1. This means that if the positive sequence of a a signal is taken, the 5th harmonic will be removed, but the 7th will pass through.

A.4 Park Transformation

Finally, if the rotational speed of the system is known, it is convenient to observe the system from a reference frame which is rotating at the same speed, thereby causing the steady state to appear as a constant vector. This is known as the

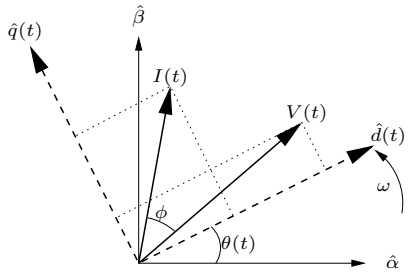

Figure A.4: *Park Transformation*

park transform, and consists of a frame dq, which rotates with speed ω with respect to the stationary frame, $\alpha\beta$. At any given moment, the transformation is determined by the variable, θ_t, which can be calculated from atan($\frac{v_\beta}{v_\alpha}$).

$$\begin{bmatrix} \hat{x}_d \\ \hat{x}_q \end{bmatrix} = \begin{bmatrix} \cos\theta_t & \sin\theta_t \\ -\sin\theta_t & \cos\theta_t \end{bmatrix} \begin{bmatrix} \hat{x}_\alpha \\ \hat{x}_\beta \end{bmatrix} \tag{A.4}$$

Note that this is the opposite direction what is used in most literature, as a result of the American standard used in Matlab. Also note that when a differentiation is performed on a variable which has been transformed in such a manner, the time dependent term, θ_t must be included, introducing an ω term into the transformation.

Bibliography

[1] D. Abramovitch. Phase-locked loops: a control centric tutorial. In *American Control Conference, 2002. Proceedings of the 2002*, volume 1, pages 1–15 vol.1. American Automatic Control Council, 2002.

[2] A.Draou, M. Benghanem, and A. Tahri. Control and dynamic analysis of a static var compensator using a three level inverter topolopgy. In *The 12th International Conference on Microelectronics*, pages 353–356, Tehran, Nov. 2000.

[3] Roland E. Best. *Phase-locked Loops : Design, Simulation, and Applications*. McGraw-Hill, Oberwil, Switzerland, 3 edition, 1997.

[4] Su Chen and G. Joos. A novel dsp-based adaptive line synchronization system for three-phase utility interface power converters. In *Power Electronics Specialists Conference, 2001. PESC. 2001 IEEE 32nd Annual*, volume 2, pages 528–532 vol.2. IEEE, 2001.

[5] Leszek S. Czarnecki. On some misinterpretations of the instantaneous reactive power *p-q* theory. *IEEE Transactions on Power Electronics*, 19(3):828–836, May 2004.

[6] R. Davalos M., J.M. Ramirez, and R. Tapia O. Three-phase multi-pulse converter statcom analysis. *International Journal of Electrical Power and Energy Systems*, 27(1):39–51, 2005.

[7] R. Grunbaum, P. Halvarsson, D. Larsson, and P.R. Jones. Conditioning of power grids serving offshore wind farms based on asynchronous generators. *Power Electronics, Machines and Drives, 2004. (PEMD 2004). Second International Conference on (Conf. Publ. No. 498)*, pages 34–39 Vol.1, 2004.

[8] V. Kaura and V. Blasko. Operation of a phase locked loop system under distorted utility conditions. *Industry Applications, IEEE Transactions on*, 33(1):58–63, 1997.

[9] Prabha Kundur. *Power System Stability and Control*. Electric Power Research Institute: Power System Engineering Series. McGraw-Hill, Inc., 1993.

[10] Sang-Joon Lee, Jun-Koo Kang, and Seung-Ki Sul. A new phase detecting method for power conversion systems considering distorted conditions in power system. In *Proceedings of 34th Annual Meeting of the IEEE Industry Applications*, volume 4, pages 2167 –2172. IEEE, 1999.

[11] S. Mohagheghi, R.G. Harley, and G.K.Venayagamoorthy. Intelligent control schemes for a static compensator connected to a power network. In *Power Electronics, Machines and Drives. Second International Conference on*, volume 2 of *Conf. Publ. No. 498*, pages 594–599. IEE, IEE, 2004.

[12] Knud Ole Helgesen Pedersen, Jørgen Kaas Pedersen, and Arne Hejde Nielsen. Monitoring a dc-connected wind farm. *2001 Proc. On European Wind Energy Conference and Exhibition*, pages 1191–1195, 2001.

[13] R. Pena, J.C. Clare, and G.M. Asher. A doubly fed induction generator using back-to-back pwm converters supplying an isolated load from a variable speed wind turbine. In *Electric Power Applications, IEE Proceedings-*, volume 143, pages 380–387. IEE, 1996.

[14] Fang Zheng Peng, George W. Ott, and Donald J. Adams. Harmonic and reactive power compensation based on the generalized instantaneous reactive power theory for three-phase four-wire systems. *IEEE Transactions on Power Electronics*, 13(6):1174–81, November 2998.

[15] P. Petitclair, S. Bacha, and J.P. Rognon. Averaged modelling and nonlinear control of an asvc (advanced static var compensator). In *Power Electronics Specialists Conference*, volume 1, pages 753–758, Baveno , Italy, 1996. IEEE.

[16] F. Ronchi and A. Tilli. Three-phase positive and negative sequences estimator to generate current reference for selective active filters. In *Proceedings of the 10th Mediterranean Conference on Control and Automation*, Lisbon, Portugal, 2002. MED2002.

[17] C. Schauder and H. Mehta. Vector analysis and control of advanced static var compensators. *IEE Proceedings-C*, 140:299–306, July 1993.